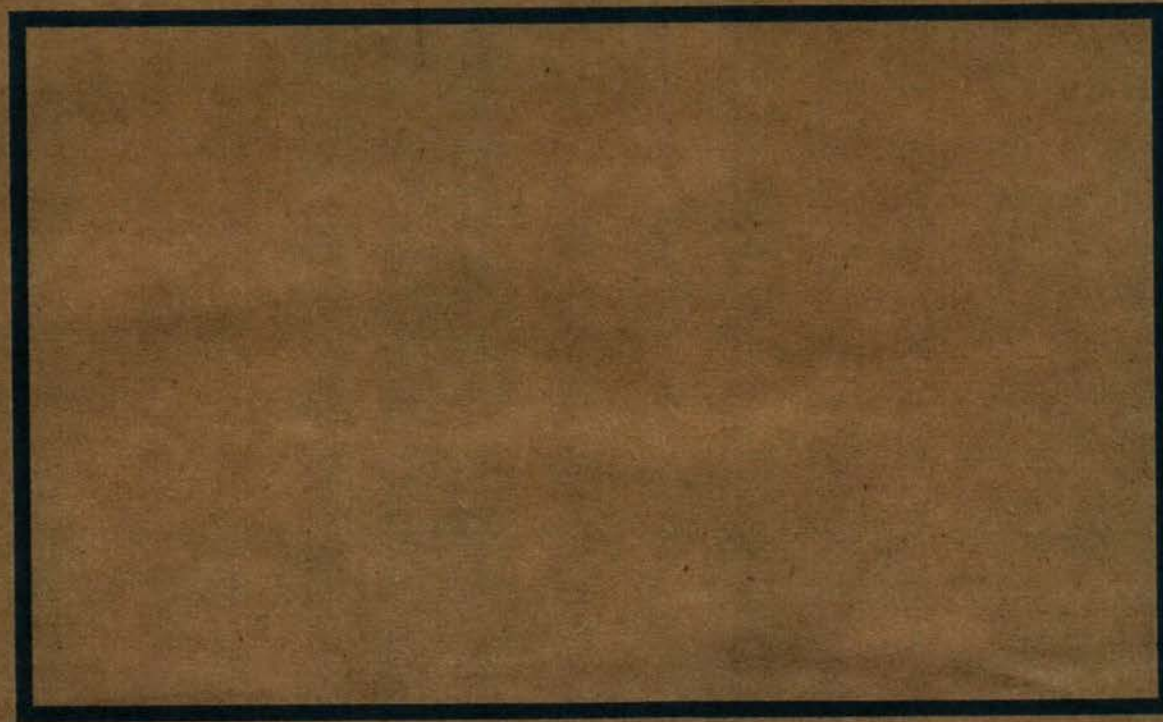


ENG 263-(EQC 1991/10)

Performance of Steel Brace Members

*L Sukendro Leowardi, Warren R Walpole, University of
Canterbury Dept of Civil Engineering*



RESEARCH REPORT

Performance of Steel Brace Members

**L. Sukendro Leowardi
and
Warren R. Walpole**

March 1996

96-3

Department of Civil Engineering

**University of Canterbury
Christchurch New Zealand**

ISSN 0110-3326

Research Report

PERFORMANCE OF STEEL BRACE MEMBERS

L. Sukendro Leowardi

and

Warren R. Walpole

November 1996

96-3

Department of Civil Engineering
University of Canterbury
New Zealand

ABSTRACT

Analytical and experimental studies have been conducted in this research to study the inelastic steel brace member behaviour under cyclic load.

In the analytical study, three types of steel brace model were reviewed. They were the purely theoretical model, the phenomenological model, and the refined physical theory model. Their advantages and disadvantages were also identified.

A 150 UC 30 was chosen as a representative universal column section. Three 150 UC 30 brace specimens were tested with slenderness ratios of 40, 60, and 80. The overall and inelastic behaviour of the specimens under cyclic load were studied.

The refined physical theory brace model from Ikeda was used to predict the axial force versus axial displacement relationships of the test specimens. The analytical results showed good agreement with the test results for relatively low axial displacement amplitudes. The need to include the effect of tangent modulus history degradation and strain hardening into the available model were emphasised for large axial displacement amplitudes.

ACKNOWLEDGMENTS

The research presented in this report was carried out in the Department of Civil Engineering, University of Canterbury, Christchurch, New Zealand, by Sukendro Leowardi as part of his Master of Engineering degree under the supervision of Dr Warren R Walpole. We extend our gratitude to Dr. Nigel Cooke, Head of the Civil Engineering Department, and to his predecessor, Professor R. Park, for the use of departmental facilities.

We wish to thank Senior Technical Officer Mr Geoff. Hill, Technical Officers Messrs George Clarke and Ray Allen, Technical Staff Messrs John Maley and Gary Harvey for their contribution toward the design, construction, and testing of the steel brace specimens.

Further thanks to Mr Brandon Hutchison and Mr Peter Coursey for assistance with computing activities, and to Mr Martin Roestenburg for photographic work.

Sukendro Leowardi wishes to thank all his fellow graduate students, especially Messrs Jose Restrepo, Juan C. Mejia, Li Xinrong, S. Hakuto, and Widodo, for their friendship, assistance and advice.

Finally, the scholarship funded by the Ministry of External Relations and Trade and the financial support for this project provided by the Earthquake and War Damage Commission are greatly appreciated.

CONTENTS

ABSTRACT.....	iii
ACKNOWLEDGEMENTS	v
CONTENTS.....	vii
LIST OF FIGURES	xi
NOTATION.....	xv
1. INTRODUCTION.....	1
1.1 OBJECTIVE AND SCOPE OF RESEARCH	1
1.2 REVIEW OF PREVIOUS RESEARCH.....	2
1.2.1 Experimental Studies.....	2
1.2.2 Theoretical Brace Model.....	3
1.2.3 Phenomenological Modelling	4
1.2.4 Refined Physical Theory Brace Model	5
2. MODELLING OF HYSTERESIS LOOP	7
2.1 GENERAL CHARACTERISTICS OF HYSTERESIS LOOP.....	7
2.2 PHENOMENOLOGICAL MODEL.....	8
2.3 REFINED PHYSICAL THEORY BRACE MODEL (Ikeda, Mahin (1984) ⁽⁷⁾).....	11
2.3.1 Empirical Formulas Employed in the Model.....	13
2.3.2 Method for Calculation from Zone to Zone.....	15
2.3.3 Integration Procedure for Plastic Hinge Axial Displacement	17
3. EXPERIMENTAL PROGRAMME	23
3.1 TEST SET-UP	23
3.1.1 Testing Equipment	23
3.1.2 Instrumentation.....	23

3.2 SPECIMEN.....	24
3.2.1 Specimen Selection.....	24
3.2.2 Initial Crookedness	25
3.2.3 Loading History and Test Procedure.....	25
3.2.4 Connection Details.....	26
4. EXPERIMENTAL RESULTS	43
4.1 GENERAL.....	43
4.2 MATERIAL PROPERTIES.....	43
4.2.1 Monotonic Test.....	43
4.2.2 Stub Column Cyclic Test.....	44
4.3 OVERALL BEHAVIOUR OF BRACE SPECIMEN UNDER CYCLIC LOADING.....	44
4.3.1 Deflected Shape and Lateral Displacement.....	44
4.3.2 Yield Lines	45
4.3.3 Hysteresis Loops.....	45
4.3.4 Maximum and Minimum Axial Loads.....	46
4.3.5 Maximum and Minimum Axial Displacements.....	46
4.3.6 Hinge Moment Versus Axial Force.....	46
4.4 INELASTIC BEHAVIOUR OF BRACE SPECIMEN UNDER CYCLIC LOADING.....	47
4.4.1 General Shape of Cyclic Strain Curves	47
4.4.2 Curvature in Plastic Hinge Regions	47
4.4.3 Local Buckling.....	48
5. DISCUSSION	81
5.1 INTRODUCTION	81
5.2 INPUT DATA FOR ANALYSIS	81
5.2.1 Axial Force - Plastic Hinge Moment Relationship	81
5.2.2 Hysteresis Behaviour of Tangent Modulus of Elasticity	82
5.2.3 Axial Force Plastic Hinge Rotation Curve.....	82

5.2.4 Effect of Boundary Condition.....	83
5.3 COMPARISON OF ANALYTICAL RESULTS WITH EXPERIMENTAL RESULTS	83
5.3.1 Axial Force - Axial Displacement Curves.....	83
5.3.2 Axial Force - Plastic Hinge Moment Curves.....	84
5.3.3 Axial Force - Plastic Hinge Rotation Curves.....	85
5.3.4 Buckling Loads and Maximum Tensile Loads.....	85
6. SUMMARY, CONCLUSIONS, AND RECOMMENDATION.....	107
6.1 SUMMARY	107
6.2 CONCLUSIONS.....	107
6.3 RECOMMENDATION FOR FUTURE RESEARCH.....	108
REFERENCES	109
APPENDIX A Point Hinge Model.....	111

LIST OF FIGURES

Figure	Page
2.1 Definition of different zones ⁽⁷⁾	18
2.2 Physical explanation of zones used in the refined phenomenological model ⁽⁶⁾	19
2.3 Input parameters ⁽⁶⁾	19
2.4 Hysteresis phenomenological model proposed by Ikeda, Mahin and Dermitzakis ⁽⁶⁾	20
2.5 Phenomenological model proposed by Jain, Goel and Hanson ⁽²⁾	21
2.6 Linear idealization curves for tangent modulus history ⁽⁷⁾	22
2.7 Analytical axial force - plastic hinge rotation curve model ⁽⁷⁾	22
3.1 Position of strain gauges and linear potentiometers on specimen 1	28
3.2 Position of strain gauges and linear potentiometers on specimen 2	29
3.3 Position of strain gauges and linear potentiometers on specimen 3	30
3.4 Corrected standard deviation versus section type with 150 UC 30.0 as a standard of comparison	31
3.5 Corrected standard deviation versus section type with 200 UC 52.2 as a standard of comparison	33
3.6 Initial crookedness of specimen 1	35
3.7 Initial crookedness of specimen 2	36
3.8 Initial crookedness of specimen 3	37
3.9 Loading history used by Jain, Goel, and Hanson ⁽²⁾	38

Figure	Page
3.10 Imposed displacements used by Gugerli ⁽¹¹⁾	40
3.11 Imposed displacements for the specimens in this report	40
3.12 End connection details	42
4.1(a) Tensile test coupon	50
4.1(b) Maximum and minimum axial loads per cycle	51
4.1(c) Maximum and minimum axial ductilities per cycle	52
4.2 Stub column cyclic test set-up	53
4.3 Experimental and calculated stress - strain relationship	55
4.4 Experimental and calculated tangent modulus history	56
4.5 Deflected shape of specimen with fixed-fixed end condition	57
4.6 Yield line patterns under compression and tension	59
4.7 Hysteresis loops of specimen 1, 2, and 3	61
4.8 Axial force - plastic hinge moment interaction curves of specimen 1	63
4.9 Axial force - plastic hinge moment interaction curves of specimen 3	63
4.10 Strain history of specimen 1 and 3 at the centre	64
4.11 Curvature distribution at load condition C of specimen 1	65
4.12 Curvature distribution at load condition C of specimen 3	66
4.13 Curvature distribution at load condition H of specimen 1	67
4.14 Curvature distribution at load condition H of specimen 3	68
4.15 Local buckling of specimen 1	69

Figure	Page
4.16 Local buckling of specimen 2	71
4.17 Local buckling of specimen 3	75
5.1 Comparison of analytical and experimental axial force - axial displacement curves for specimen 1	96
5.2 Comparison of analytical and experimental axial force - axial displacement curves for specimen 2	97
5.3 Comparison of analytical and experimental axial force - axial displacement curves for specimen 3	98
5.4 Comparison of analytical and experimental axial force - plastic hinge moment interaction curves for specimen 1	99
5.5 Comparison of analytical and experimental axial force - plastic hinge moment interaction curves for specimen 3	100
5.6 Comparison of analytical and experimental axial force - plastic hinge rotation curves for specimen 1	101
5.7 Comparison of analytical and experimental axial force - plastic hinge rotation curves for specimen 3	102
5.8 Analytical axial force - plastic hinge moment curves for specimen 2	103
5.9 Analytical axial force - plastic hinge rotation curves for specimen 2	103
5.10 Comparisons of analytical and experimental buckling loads	104
5.11 Comparisons of analytical and experimental maximum tensile loads	105
A.1 Point hinge model	114
A.2 Flow rule associated with the yield surface	114

NOTATION

a_2	Constant defining theoretical interaction curve
A	Cross sectional area
b_1, b_2	Constants defining theoretical interaction curve
c_1, c_2	Constants defining theoretical interaction curve
$e_1, e_2,$ e_3, e_4	Constants defining history of tangent modulus of elasticity
E	Initial modulus of elasticity
E_t	Tangent modulus of elasticity
E_t^+	Tangent modulus value just after a displacement history reversal
E_t^-	Tangent modulus value before a displacement history reversal
f	Function for nonlinearity of deflected shape as function of x
g	Function for geometric nonlinearity of relation between plastic hinge moment and plastic hinge rotation as a function of κ
h_1	Function for geometric shortening as function of κ
I	Cross-sectional moment of inertia
k	Effective length factor
kL	Effective member length
kL/r	Effective slenderness ratio
L	Member length of a strut
m	Normalized plastic hinge moment
M	Plastic hinge moment
\bar{M}	Bending moment at x
\underline{M}	Function for theoretical interaction curve as a function of axial force
\underline{M}^*	Function for empirical interaction curve as function of axial force
M_p	Plastic moment of cross section
p	Normalized applied axial force
p_{12}	Constant defining theoretical interaction curve
P	Applied axial force
P_{cr}	Euler buckling load
P_y	Tensile yield load

P_o	Axial force at which plastic hinge initially become plastic
r	Radius of gyration
R	Strain hardening ratio as a proportion to E
x,y	Coordinates
y_n	Location of instantaneous neutral axis
α_p, α_c	Magnification factors for interaction curve on tension side and that in compression side
β	Parameters defining plastic hinge rotation degradation in Zone EL2
Δ	Lateral deflection at midspan
$\bar{\Delta}$	Lateral deflection along strut as function of x
δ	Axial displacement of strut
δ_e	Elastic axial displacement
δ_g	Geometric shortening
δ_m	Residual displacement due to material nonlinearities in the nominal elastic range
δ_{mo}	Cumulative value of residual displacement due to material nonlinearities
δ_p	Plastic hinge displacement
δ_{po}	Cumulative value of plastic hinge displacement
δ_{ty}	Tensile yield displacement
δ_y	Axial displacement at yield load
θ	Plastic hinge rotation
$(\theta)_{min}$	Minimum plastic hinge rotation
κ	Parameter for geometric nonlinearity
Φ	Formula for interaction curve as a function of both P and M
$\Phi_{,P}, \Phi_{,M}$	Derivatives of Φ regarding P and regarding M
σ_y	Axial yield stress

CHAPTER 1

INTRODUCTION

Concentrically-braced steel frames are frequently used in order to increase the strength and stiffness of a structure. Such frames generally rely on inelastic deformations in the braces as the main source of earthquake energy dissipation. This cyclic behaviour involves several complex physical phenomena, including yielding by tensile loads, buckling by compressive loads, post-buckling deterioration of compressive load capacity, and deterioration of maximum compressive loads after each inelastic cycle.

1.1 OBJECTIVE AND SCOPE OF RESEARCH

To review the available analytical brace models and identify their advantages and disadvantages.

To generate experimental data of axial force - axial displacement hysteresis loops and other related data, i.e. axial force - lateral displacement hysteresis loops and strain readings at some points along the specimen, of a representative universal column section with varied slenderness ratios.

To compare the experimental data with the analytical data obtained from the available model and suggest refinements to the model.

The analytical brace models reviewed are a purely theoretical model, a phenomenological model, and a refined physical theory model. The purely theoretical model is based on simplified theoretical formulations of material properties, member geometries, and components of force equilibrium equations. The phenomenological model is based on simplified hysteretic rules that only mimic observed axial force - axial deformation relationships. The refined physical theory model combines both aforementioned models, in the sense that it is based on adjusted theoretical relationships for material properties and member geometries to better represent experimental data but also uses the same theoretical formulations as the purely theoretical model.

The test program included three specimens of 150 UC 30.0 grade 250 with slenderness ratios of 40, 60 and 80 and one stub column specimen. The specimens were subjected to quasi- statically applied axial loads.

1.2 REVIEW OF PREVIOUS RESEARCH

1.2.1 Experimental studies

(i) **Black, Wenger, Popov (1980)⁽¹⁾** tested 24 struts. The sections were nine wide-flanges, four double-angles, one double-channel, two structural tees, five circular tubes and three square tubes. Eighteen of these struts were designed to be pinned at both ends, while six of them were pinned at one end and fixed at the other. A common effective slenderness ratio of 80 was used for specimens within each structural shape category allowing for a direct comparison of results due to variations in structural shapes. Also, an effective slenderness ratio of 40, close to the range of plastic action, and one of 120, close to the range of elastic buckling, were assigned to both wide-flange and double-angle sections.

The authors examined the effects of loading patterns, end conditions, cross-sectional shapes, and slenderness ratios on the hysteretic response of members. In addition a method of calculating the inelastic cyclic buckling capacity was proposed.

The results of this experimental work showed that:

- The point of inflection of the buckled shapes in the inelastic range coincides with the point of inflection of the buckled shape according to elastic prediction. The buckled shape does not appear to be a function of slenderness ratio.
- The hysteretic performance of a member is somewhat influenced by its cross-sectional shape. The major determining factors appear to be related to a member's susceptibility toward lateral-torsional buckling, local buckling of outstanding legs, and web buckling between stitches in built-up members.
- The most important parameter in determining the hysteretic behaviour is the effective slenderness ratio. The stockier members generate fuller loops than the more slender ones.

- Two sources of the deterioration of cyclic buckling loads were identified: they are the Bauschinger effect, exhibited by the steel subjected to inelastic load reversals; and the effect due to the residual camber or bowing of a specimen.

(ii) **Jain, Goel, and Hanson (1980)⁽²⁾** tested seventeen tube sections with effective slenderness ratios of 30 to 140 and eight angle sections with effective slenderness ratios of 85 and 120. The tube specimens were made from 25-mm x 25-mm steel tubes cold rolled from 12 gauge (approximately 2.5-mm) American Society for Testing and Materials designation A-570 grade C steel. The angle specimen were made from M1020 hot rolled single angle sections with sizes varied from 25 x 25 x 6 mm to 40 x 40 x 3 mm.

The test objectives were to investigate the reduction in maximum compressive strength and the increase in member length with the number of cycles. The effects of mode of buckling, local buckling and cross-sectional shape on the hysteresis loops were also investigated.

Comparisons between the hysteresis loops of tube specimens with different modes of buckling and connection details showed that the mode of buckling and connection details for tube sections did not have much influence on the hysteresis loops for members of a given effective slenderness ratio.

It was considered that local buckling did not influence the hysteretic behaviour of tube specimens, but for angle specimens, local buckling reduced the post-buckling strength. Based on the different behaviour of the specimens after buckling it was concluded that the hysteresis loops for tube, angle, and bar specimens of equal effective slenderness ratio were different in their post buckling range.

1.2.2 Theoretical Brace Models

(i) **Nilforoushan (1973)⁽³⁾** based his formulation of the hysteresis model on several simplifying assumptions. The assumptions were as follows:

- The material had a stress-strain relationship which was represented by an elasto plastic approximation.
- The moment-curvature relationship was ideally elasto-plastic.
- Shear deformation was neglected.

- The relative axial displacement, δ , between the ends of the steel bar bracing, was made up of three components.

$$\delta = \delta_e + \delta_p + \delta_g$$

Where:

δ_e was the displacement due to direct axial force;

δ_p was the displacement due to the plastic hinge rotation;

δ_g was the displacement due to geometric deformation.

The analytical solution of the differential equation of the deflection curve was formulated in the form of elliptic integral of the first and second kind.

He also offered an approximate solution for the hysteretic behaviour of axially loaded members, which led to nearly the same results. The additional assumptions in this procedure were as follows :

- The bar deflects laterally under the buckling load and sustains the buckling load, until the hinge moment is reached at mid-length.
- The shape of the deflected curve of the bar is represented by a half sine wave before hinge formation and the two halves of the bar are considered to rotate as rigid bodies beyond the hinge formation.
- The relative displacement, δ , between the end of the bar is made up of two components :

$$\delta = \delta_e + \delta_p$$

Where : δ_p was the displacement due to the lateral deflection.

(ii) **Nonaka (1977)⁽⁴⁾** proposed an analytical model which included the plastic axial deformation of the brace but limited it to small geometric effects. He solved the beam-column equation directly, obtaining sine curves for beam segments under compression and hyperbolic sine curves for beam segments under tension. The resulting basic equations contained trigonometric functions for compressive axial forces and hyperbolic functions for tensile forces.

1.2.3 Phenomenological Modelling

Based on their test results **Jain, Goel, and Hanson (1980)⁽²⁾** proposed a hysteretic model that incorporated a reduction in maximum compressive strength and an increase in the member length with the number of cycles.

The authors recommended the AISC formula for maximum compressive load to calculate the initial buckling load and $30/(Kl/r)$ times P_y for second cycle buckling load and $25/(Kl/r)$ times P_y for the third and subsequent cycles.

It was also found that the residual elongation was directly proportional to the maximum compressive displacement and inversely proportional to the effective slenderness ratio of the member.

The authors noted that the compressive loads at displacements of $5\Delta y$ and $12\Delta y$ showed a slight reduction with the number of cycles and may be treated as a constant.

The model proposed by Ikeda, Mahin and Dermitzakis (1984)⁽⁶⁾ was based on the data from an experimental program by Black, Wenger and Popov. The model was based on a simplified hysteretic rule that only mimics the observed axial force - axial displacement relationship. Several important phenomena that were incorporated in the model were the deterioration of buckling loads, the post buckling deterioration of brace capacity, and the plastic growth.

1.2.4 Refined Physical Theory Brace Models (Ikeda, Mahin (1984)⁽⁷⁾)

The refined physical theory model was developed to overcome some of the limitations of the previous physical theory brace models.

The features of the refined physical theory model were as follows:

- The axial force-plastic hinge moment interaction curve was based on the experimental interaction curve.
- The tangent modulus was used in place of the modulus of elasticity and defined as a function of the axial force P and the load history.
- The plastic hinge rotation was defined as a function of the axial force P and the load history to represent the gradual transition from the elastic shortening zone to the plastic zone in compression and the degradation of the plastic hinge rotation in the elastic elongation zone in tension.

CHAPTER 2

MODELLING OF HYSTERESIS LOOP

2.1 GENERAL CHARACTERISTICS OF HYSTERESIS LOOP

For theoretical study, the relationship between the axial load and the axial deformation of a brace was divided into several zones. This zone definition applies to the axial load - axial deformation, the axial load - plastic hinge moment and the axial load - plastic hinge rotation relationships, as shown in Figures 2.1(a), (b), and (c).

The first zone, O - A, is the elastic shortening zone in compression (ES1). For a perfectly straight, slender member, the axial force - axial deformation relationship is linear. Due to imperfections, real columns show a small amount of non-linearity right from the start.

The second zone, A - B, is the buckling zone (BU). Buckling can be categorised into two behavioural modes : elastic buckling; and plastic buckling. In the case where the member is not initially straight, elastic buckling takes place and the axial compressive strength cannot reach the Euler buckling load. In the case where the member is straight, elastic buckling takes place if the Euler buckling load is smaller than the compressive yield load, and plastic buckling takes place if the opposite is true. The zone is ended by the formation of plastic hinge.

The third zone, B - C, is the plastic zone in compression (P1). This zone is dominated by the inelastic bending of the brace due to the $P - \Delta$ moments induced by the compressive load P . The magnitude of the load P must decrease with the increasing magnitude of deformation because the $P - \Delta$ moment cannot exceed the member's plastic moment capacity. This zone is characterized by the large plastic rotation and plastic axial deformation at the hinge.

The fourth zone, C - D, is the elastic lengthening zone in compression (EL1). The member enters this zone immediately after decreasing the compressive load and the inelastically strained portion of the brace will again behave elastically. The slope of this zone is smaller than that of the first zone due to the large permanent deflection of the centre of the brace, which results in a curved member rather than a straight member.

The fifth zone, D - E, is the elastic lengthening zone in tension (EL2). This zone represents a zone of continued elastic bending with the brace lengthening while an increasing tensile load is applied. In the fourth and fifth zone, the elastic decrease in the lateral deflection Δ is caused by a decrease in the P - Δ moments induced by the decrease in the compressive load and by the change in sign of the P - Δ moments with the application of tensile load.

The sixth zone, E - F, is the plastic zone in tension (P2). Point E is the start of yielding due to the P - Δ bending moments induced by tensile load. In this zone, the plastic rotation at the hinge starts to decrease and the brace straightens since the P - Δ moment is of opposite sign to the P - Δ moment induced by compressive load. The tensile P - Δ moments reduce as the brace straightens and, therefore, the tensile load required to sustain yielding must increase as the brace straightens.

The seventh zone, F - G, is the yielding zone (PY). Point F is the point at which the brace is fully straightened. This zone is characterized by a nearly constant tensile load P with an increasing elongation δ for an elastic perfectly plastic material or by an increasing tensile load P with an increasing elongation δ for a strain hardening material.

The eighth zone is the elastic shortening zone in tension (ES2). This zone is characterized by a linear relationship between the decreasing tensile load P with decreasing elongation δ .

2.2 PHENOMENOLOGICAL MODEL

(i) Ikeda, Mahin, Dermitzakis (1984)⁽⁶⁾. This model incorporated the following characteristics of inelastic buckling behaviour:

- Deterioration of buckling loads with cycling. This behaviour was associated with the residual camber of the strut and hysteretic degradation of the tangent moduli.
- Post buckling deterioration of the brace capacity.
- Plastic growth which was defined as a net elongation of braces which have yielded by tensile loads during cyclic inelastic load reversals.

The features of the model proposed by the above authors were as follows:

- Division of axial force - axial displacement relationship into ten different zones as shown in Figure 2.2.
- Shifting of control points by the amount of permanent deformation (equals to the permanent deformation after the yield point).
- Translation of the tensile yield point by a factor times the inelastic shortening during the current cycle.

The proposed model was defined with the following parameters (Fig. 2.3):

- Material properties. These parameters included the yield stress and modulus of elasticity.
- Initial buckling loads. The initial buckling loads were evaluated by equation 1.5-1 of the AISC specifications as follows:

$$P_{cr} = \left[1 - \frac{(kL/r)^2}{2C_c^2} \right] \sigma_y A \quad \text{for } (kL/r) < C_c \quad (2.1)$$

$$P_{cr} = \frac{\pi^2 AE}{(kL/r)^2} \quad \text{for } C_c < kL/r \leq 200 \quad (2.2)$$

$$C_c = \sqrt{(2\pi^2 E / \sigma_y)} \quad (2.3)$$

In evaluating buckling loads other factors to be accounted for were excessive initial camber and material non-linearities.

- Growth factor, growth limit, and hardening ratio. A growth limit was used to define the maximum value of the axial elongation of a strut. It represented tensile rupture of the brace. Hardening ratio was used to define the slope of the tensile yielding portion of a brace's hysteresis loops.
- Post buckling parameters. The parameters PCRF, U34, U45, P45, and C5 were used for two different purposes: (1) to define a linear approximation of the strut's post buckling behaviour and (2) to define the deterioration of buckling loads for subsequent cycles.
- Reversed post buckling parameters. The parameters U6, P6, U7, P7, U8, P8, and C8 were used to define linear approximations of the reversed (reloading) post-buckling stage of the cyclic inelastic behaviour (Zones 6, 7, 8, and 9).

Figure 2.4 shows the application of some of the parameters in modelling the hysteresis loops. After the element deforms in tension beyond the yield point, a permanent deformation occurs and all displacement control points shift by this amount. Every time the element exits Zone 4, the peak compressive load capacity of the brace (PCR) is reduced to the lowest reached in Zone 4, but it is not less than the final buckling load (PCRF).

Limitations of the model. (1) In this model one of the two criteria for the selection of parameters defining post buckling stage is as follows. The values of experimental buckling load are plotted as a function of the minimum axial displacement at each cycle minus the axial displacement at the start of the cycle. Then the parameters are selected to best fit the experimental curve. But during the test it was observed that the residual displacement depends on maximum tensile load reached. The larger the residual lateral displacement of each cycle remaining at the beginning of the compression phase, the smaller the subsequent buckling load. As mentioned in their report this tendency was not included in the two criteria.

(2) Another feature of this model is the dependency of input parameters on displacement history. The report mentions that the model relies on having applicable experimental or analytical data for the type of strut analyzed and the history of loading employed.

(ii) Jain, Goel, and Hanson (1980)⁽²⁾. The hysteretic model proposed by Jain, Goel, and Hanson is shown in terms of normalized axial load - axial displacement ordinates ($P/P_y - \delta/\delta_y$) in Figure 2.5.

The coordinates of control points:

A = buckling point with the maximum compressive load given by the

Equations (2.1) to (2.3);

B = $[-18/(kL/r) , -5]$

C = $[-12/(kL/r) , -12]$

E = $[1 , (1+\epsilon L/\delta_y)]$

$$\epsilon = 1.75 \left\{ \frac{0.55 \delta}{(kL/r)} + 0.0002 \delta^2 \right\} \quad (2.4)$$

To locate point D, a line OD' is drawn from the origin at a slope of one-third times the initial elastic slope E_s that intersects the line CE at point D'. Intercept OD is taken as $60/(kL/r)$ times the distance OD'.

If the direction of axial displacement is reversed anywhere along CC', the member retraces the same segment, if reversal occurs from the branch C'D, the member unloads elastically along KL or L'K, and if reversal occurs from the branch DE, the member unloads elastically along IJ. If reversal occurs before H, the member follows segment JI or J'I otherwise it returns along J"D.

2.3 REFINED PHYSICAL THEORY BRACE MODEL (Ikeda, Mahin (1984)⁽⁷⁾)

The refined physical theory model was developed to overcome some of the limitations of the previous physical theory brace models. Previous physical theory brace models assumed elasto-perfectly plastic material properties for both the plastic hinge and the beam segments. This assumption causes a kink in the transition between elastic elongation zone and plastic zone under tensile loading while such kink has not been observed in experimental data.

Previous models also assumed that the values of the modulus of elasticity did not vary during cyclic buckling processes. Since test results showed the tangent modulus or the secant modulus of elasticity provided better results than the initial modulus of elasticity in evaluating buckling loads, the tangent modulus that varies with axial load was used in this model.

The features of the refined physical theory model were as follows:

- The axial force-plastic hinge moment interaction curve was based on the experimental interaction curve.
- The tangent modulus was used in place of the modulus of elasticity and defined as a function of the axial force P and the load history.
- The plastic hinge rotation was defined as a function of the axial force P and the load history to represent the gradual transition from the elastic shortening zone to the plastic zone in compression and the degradation of plastic hinge rotation in the elastic elongation zone in tension.

The axial displacement, δ , was made up of seven components,

$$\delta = \delta_e + \delta_g + \delta_p + \delta_{po} + \delta_{ty} + \delta_m + \delta_{mo} \quad (2.5)$$

where:

δ_e = elastic axial displacement;

δ_g = geometric shortening;

δ_p = plastic hinge displacement;

δ_{po} = accumulated plastic hinge displacement;

δ_{ty} = tensile yield displacement;

δ_m = residual displacement due to material nonlinearities;

δ_{mo} = accumulated residual displacement.

$$\delta_e = \frac{L}{A} \int_0^P \frac{dP^*}{E_t(P^*)} \quad (2.6)$$

$$\delta_g = -h_1(\kappa)\theta^2 L \quad (2.7)$$

where:

$$h_1(\kappa) = \begin{cases} \frac{\frac{\sin \kappa}{\kappa} + 1}{16 \cos^2 \frac{\kappa}{2}} & \text{if } P < 0 \\ \frac{\frac{\sinh \kappa}{\kappa} + 1}{16 \cosh^2 \frac{\kappa}{2}} & \text{if } P > 0 \end{cases} \quad (2.8)$$

$$\delta_p = - \int_{P_o}^P \frac{dM(P^*)}{dP^*} \frac{d\theta}{dP^*} dP^* \quad (2.9)$$

$$= - \left(\frac{dM(P^*)}{dP^*} \theta \right) \Big|_{P_o}^P + \int_{P_o}^P \frac{d^2 M(P^*)}{dP^{*2}} \theta(P^*) dP^* \quad (2.10)$$

$$\delta_{ty} = \underline{\delta} - (\delta_e + \delta_g + \delta_p + \delta_{po} + \delta_m + \delta_{mo}) \Big|_{P=P_y} \quad (2.11)$$

$$\delta_m = (\delta_e + \delta_g) \Big|_{E_t=E_t^+} - (\delta_e + \delta_g) \Big|_{E_t=E_t^-} \quad (2.12)$$

where:

E_{t+} = value of tangent modulus of elasticity just after the load history reversal;

E_t = value of tangent modulus of elasticity just before the load history reversal.

The plastic hinge moment M was related to the plastic hinge rotation angle θ by,

$$M = g(\kappa) \frac{EI}{L} \theta \quad (2.13)$$

where:

$$g(\kappa) = \begin{cases} \frac{\kappa}{2} \tan \frac{\kappa}{2} & \text{if } P < 0 \\ -\frac{\kappa}{2} \tanh \frac{\kappa}{2} & \text{if } P > 0 \end{cases} \quad (2.14)$$

$$\kappa^2 = \frac{|P|L^2}{EI} \quad (2.15)$$

2.3.1 Empirical formulas employed in the model

Axial force - plastic hinge moment interaction relationship:

$$M = \underline{M}^*(P) \quad (2.16)$$

$$\underline{M}^*(P) = \underline{M}(P) \alpha_i \quad i = t \text{ or } c \quad (2.17)$$

$$m = 1 + b_1 p + c_1 p^2, \quad 0 \leq p \leq p_{12} \quad (2.18)$$

$$m = a_2 + b_2 p + c_2 p^2, \quad p_{12} \leq p \leq 1 \quad (2.19)$$

$$a_2 + b_2 + c_2 \leq m \leq 1, \quad p = 1 \quad (2.20)$$

where:

\underline{M}^* = function for empirical P-M interaction curve as a function of P ;

α_t = magnification factor for the P-M interaction curve on the tension side;

α_c = magnification factor for the P-M interaction curve on the compression side;

m = normalized plastic hinge moment, M/M_p ;

p = normalized axial force, P/P_y .

Tangent modulus of elasticity. Figure 2.6 illustrates the tangent modulus model.

Two pairs of linear idealization curves were used to describe the tangent modulus model. Four parameters e_1 , e_2 , e_3 , and e_4 were needed for the curves. The tangent modulus functions were as follows:

when the axial force decreases;

$$e = \begin{cases} -\frac{(e_2 - e_1)}{(1 - e_4)} p + \left\{ \frac{(e_2 - e_1)}{(1 - e_4)} e_4 + e_2 \right\} & \text{if } p \geq e_4 \\ -\frac{(e_3 - e_2)}{(1 + e_4)} p + \left\{ \frac{(e_3 - e_2)}{(1 + e_4)} e_4 + e_2 \right\} & \text{if } p \leq e_4 \end{cases} \quad (2.21)$$

when the axial force increases;

$$e = \begin{cases} +\frac{(e_3 - e_2)}{(1 + e_4)} p + \left\{ -\frac{(e_3 - e_2)}{(1 + e_4)} + e_3 \right\} & \text{if } p \geq e_4 \\ +\frac{(e_2 - e_1)}{(1 - e_4)} p + \left\{ \frac{(e_2 - e_1)}{(1 - e_4)} + e_3 \right\} & \text{if } p \leq e_4 \end{cases} \quad (2.22)$$

Axial force plastic hinge rotation curve. To better represent the actual axial force - plastic rotation curve, two observed empirical features were included in this model, they were firstly a degradation of plastic hinge rotation in zone EL2 and secondly a gradual transition from zone ES1 to P1 as shown in Figure 2.7.

In zone EL1, θ was constant and equalled the value from the previous zone. The gradual transition from zone ES1 to P1 was implemented with the addition of transition zone EL2, where

$$\theta_2 = \left(1 - \frac{(P/P_y)}{\beta} \right) \theta \quad (2.23)$$

β is the ordinate of the point on the P/P_y axis that defines zone EL2 with the zero crossing point of zone EL1.

2.3.2 Method for calculation from zone to zone

(1) Zone ES1

$$\delta = \delta_e \Big|_0^P + \delta_g \Big|_P + \delta_{po} + \delta_{ty} + \delta_{mo} \quad (2.24)$$

δ_e was determined by Equation 2.6 and δ_g by Equation 2.7.

(2) Buckling load

If $\theta \neq 0$, P_{cr} is the solution of the simultaneous Equations 2.13 and 2.16.

If $\theta = 0$, P_{cr} is the smaller value between yield load and Euler's buckling load.

(3) Zone BU ($\theta = 0$ and $|P_{cr}| \leq |P_y|$)

$$\delta = (\delta_e + \delta_g) \Big|_{P=P_{cr}} + \delta_{po} + \delta_{ty} + \delta_{mo} \quad (2.25)$$

(4) Zone P1

$$\delta = \delta_e + \delta_g + \delta_p + \delta_{po} + \delta_{ty} + \delta_m + \delta_{mo} \quad (2.26)$$

If $-P_y < P^* < -P_y P_{12}$

$$\underline{M}^*(P) = \underline{M}(P) \alpha_i = \underline{M}(P^*) \alpha_i$$

$$\underline{M}(P^*) = + M_p \left\{ a_2 + b_2 \left(\frac{-P^*}{P_y} \right) + c_2 \left(\frac{-P^*}{P_y} \right)^2 \right\}$$

$$\frac{d\underline{M}(P^*)}{dP^*} = + M_p \left\{ b_2 \left(-\frac{1}{P_y} \right) + 2 c_2 \left(\frac{-P^*}{P_y} \right) \left(-\frac{1}{P_y} \right) \right\}$$

$$= - \frac{M_p}{P_y} \left\{ b_2 + 2 c_2 \left(\frac{-P^*}{P_y} \right) \right\} \quad (2.27)$$

$$\frac{d^2 \underline{M}(P^*)}{dP^{*2}} = + 2c_2 \frac{M_p}{P_y^2} \quad (2.28)$$

If $-P_y p_{12} < P^* < 0$

$$M(P^*) = + M_p \left\{ 1 + b_1 \left(\frac{-P^*}{P_y} \right) + c_1 \left(\frac{-P^*}{P_y} \right)^2 \right\}$$

$$\frac{dM(P^*)}{dP^*} = - \frac{M_p}{P_y} \{ b_1 + 2 c_1 \left(\frac{-P^*}{P_y} \right) \} \quad (2.29)$$

$$\frac{d^2M(P^*)}{dP^{*2}} = + 2c_1 \frac{M_p}{P_y^2} \quad (2.30)$$

(5) Zone P2

$$\delta = \delta_e + \delta_g + \delta_p + \delta_{po} + \delta_{ty} + \delta_m + \delta_{mo}$$

If $+P_y p_{12} < P^* < +P_y$

$$\underline{M}^*(P) = \underline{M}(P) \alpha_i = \underline{M}(P^*) \alpha_i$$

$$\underline{M}(P^*) = - M_p \left\{ a_2 + b_2 \left(\frac{P^*}{P_y} \right) + c_2 \left(\frac{P^*}{P_y} \right)^2 \right\}$$

$$\frac{d\underline{M}(P^*)}{dP^*} = - M_p \left\{ b_2 \left(\frac{1}{P_y} \right) + 2 c_2 \left(\frac{P^*}{P_y} \right) \left(\frac{1}{P_y} \right) \right\}$$

$$= - \frac{M_p}{P_y} \{ b_2 + 2 c_2 \left(\frac{P^*}{P_y} \right) \} \quad (2.31)$$

$$\frac{d^2\underline{M}(P^*)}{dP^{*2}} = - 2c_2 \frac{M_p}{P_y^2} \quad (2.32)$$

If $0 < P^* < +P_y$ p_{12}

$$\underline{M}(P^*) = - M_p \left\{ 1 + b_1 \left(\frac{P^*}{P_y} \right) + c_1 \left(\frac{P^*}{P_y} \right)^2 \right\} \quad (2.33)$$

$$\frac{d\underline{M}(P^*)}{dP^*} = - \frac{M_p}{P_y} \left\{ b_1 + 2 c_1 \left(\frac{P^*}{P_y} \right) \right\} \quad (2.34)$$

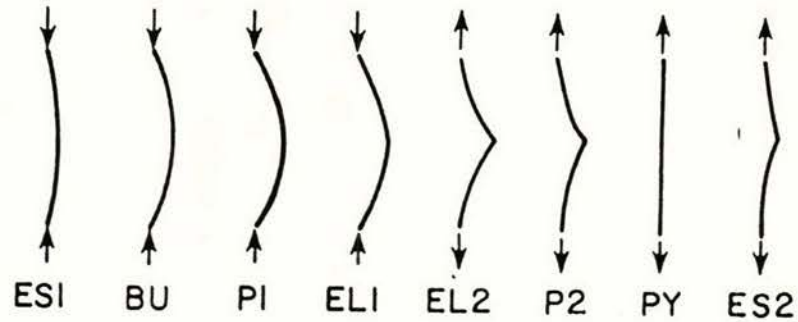
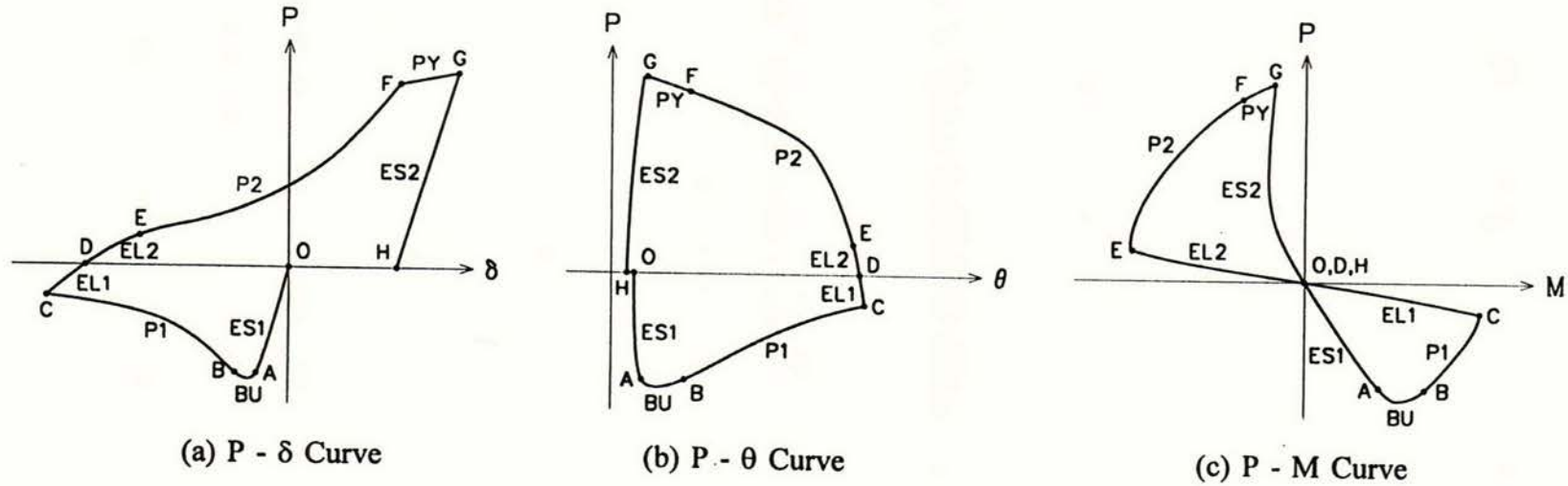
$$\frac{d^2\underline{M}(P^*)}{dP^{*2}} = - 2c_1 \frac{M_p}{P_y^2} \quad (2.35)$$

2.3.3 Integration procedure for plastic hinge axial displacement

In this research Simpson's composite rule was used to calculate the integral in Equation 2.10. Simpson's composite rule over $n=2m$ sub-intervals of $[a,b]$ can be expressed without the error term as:

$$\int_a^b f(x) dx = \frac{h}{3} [f(a) + 2 \sum_{j=1}^{m-1} f(x_{2j}) + 4 \sum_{j=1}^m f(x_{2j-1}) + f(b)] \quad (2.36)$$

where $a = x_0 < x_1 < \dots < x_{2m} = b$, $h = (b-a)/2m$, and $x_j = x_0 + jh$ for each $j = 0, 1, \dots, 2m$.



(d) Basic behaviour of a brace associated with each zone

Notes: ES1 = Elastic shortening zone in compression;
 BU = Buckling zone;
 P1 = Plastic zone in compression;
 EL1 = Elastic elongation zone in compression;
 EL2 = Elastic elongation zone in tension;
 P2 = Plastic zone in tension;
 PY = Yielding zone;
 ES2 = Elastic shortening zone in tension.

Figure 2.1 Definition of different zones⁽⁷⁾

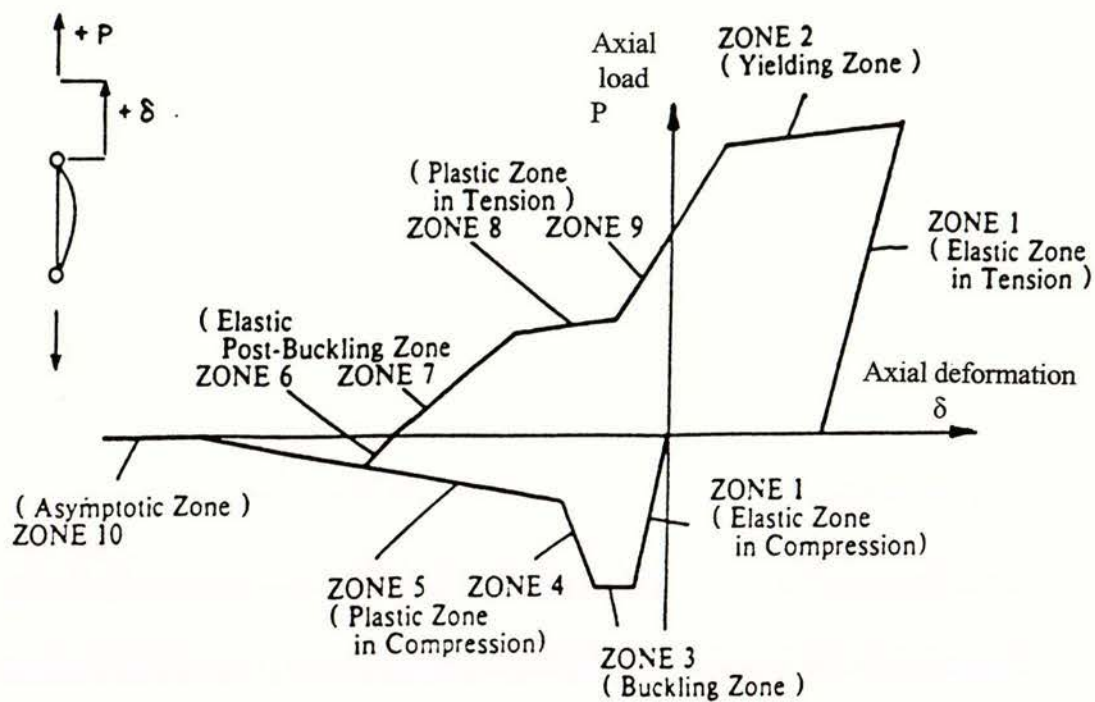


Figure 2.2 Physical explanation of zones used in the refined phenomenological model⁽⁶⁾

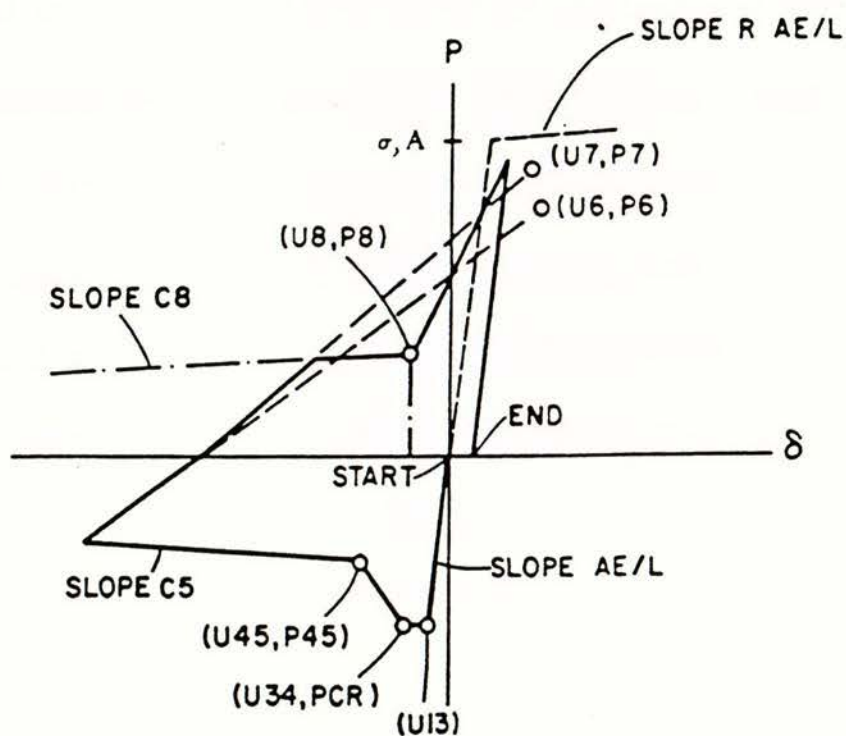


Figure 2.3 Input parameters⁽⁶⁾

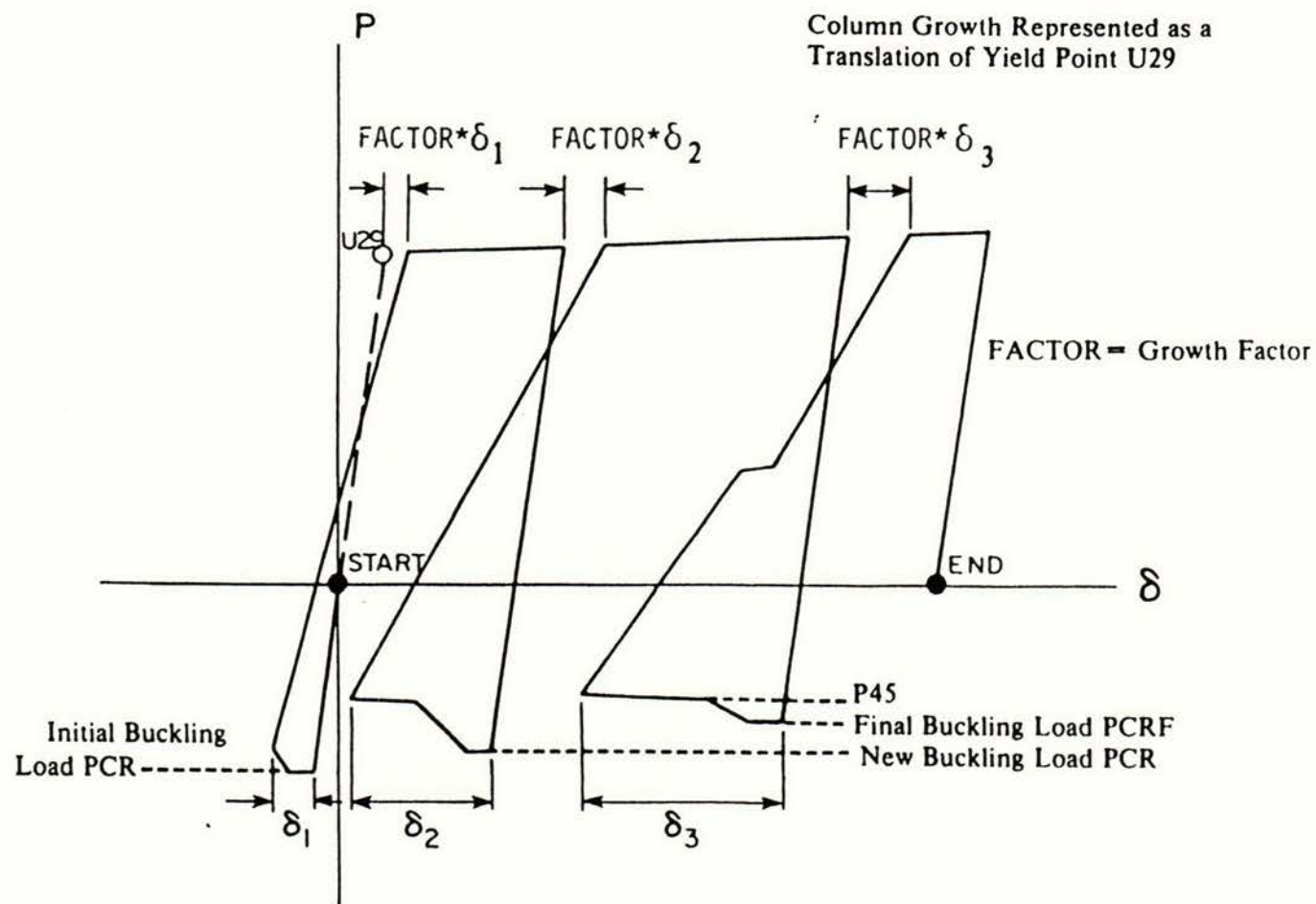


Figure 2.4 Hysteresis phenomenological model proposed by Ikeda, Mahin and Dermitzakis⁽⁶⁾

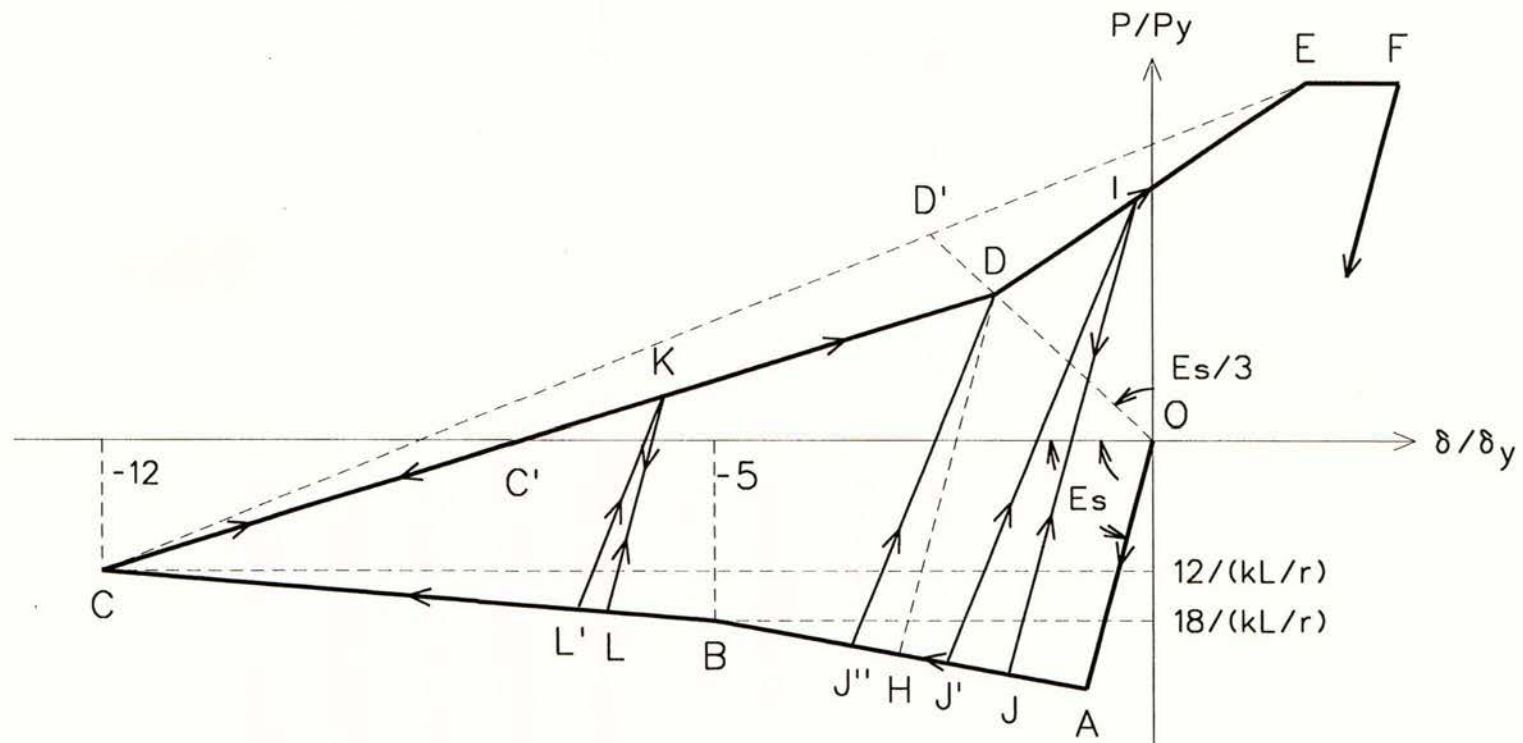


Figure 2.5 Phenomenological model proposed by Jain, Goel and Hanson ⁽²⁾

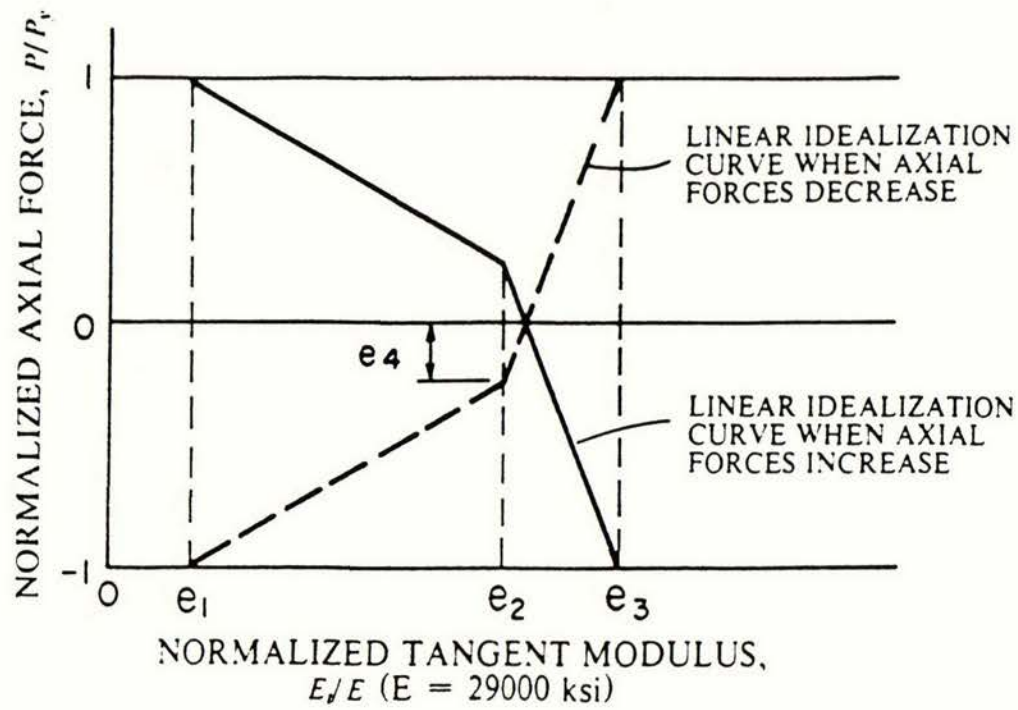


Figure 2.6 Linear idealization curves for tangent modulus history⁽⁷⁾

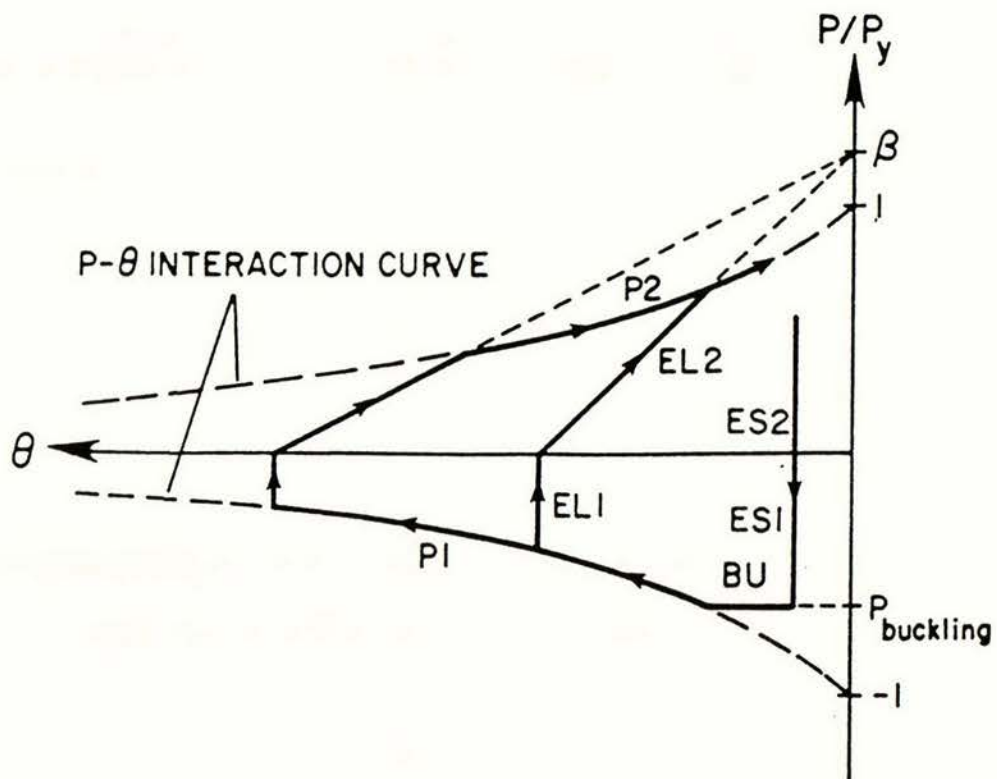


Figure 2.7 Analytical axial force - plastic hinge rotation curve model⁽⁷⁾

CHAPTER 3

EXPERIMENTAL PROGRAMME

The objectives of the test were firstly to obtain the relationship between axial force and axial displacement for the UC section and secondly to obtain the additional supporting data from lateral deflection measurements and strain gauges readings to better grasp the fundamental behaviour of the brace members.

3.1 TEST SET-UP

3.1.1 Testing equipment

The tests were done in the DARTEC 10 MN universal testing machine at University of Canterbury. The pinned-pinned end conditions were provided by pins between cleats and end clevises bolted to the specimen and DARTEC machine. The specimen with fixed-fixed end conditions was directly bolted to the cross head and actuator of the DARTEC machine.

3.1.2 Instrumentation

A potentiometer was used to monitor horizontal lateral displacement on a macro level at the centre line of the specimen with pinned-pinned end conditions and three potentiometers were used at the centre line, and top and bottom inflection points of specimen with fixed-fixed end conditions. A potentiometer was mounted between the end clevises for axial displacement measurement for the specimen with pinned-pinned end conditions and between the end plates for the specimen with fixed-fixed end conditions. The output signal from the axial displacement potentiometer was directly transformed by a computer program in the data logger into an axial displacement reading on the computer screen. This reading was used to control the test manually by changing the direction of axial displacement after the designed maximum axial displacement was reached.

The specimens were gauged to provide data on a micro level of strain distribution along their length. The strain gauges were concentrated at the locations of the theoretical plastic hinges. Figures 3.1 to 3.3 show the distribution of strain gauges and potentiometers along each specimen.

3.2 SPECIMEN

In this test only one type of UC section, i.e. 150 UC 30, was tested with effective slenderness ratio of 40, 60 and 80. The criterion for the selection of this section type was the selected type should represent the variety of commercially available UC section types.

3.2.1 Specimen selection

Based on the above criterion, a statistical study of geometric parameters of UC section was done. The geometric parameters for a UC section are depth, flange width, flange thickness, and web thickness. The procedure was as follows:

1. Select one section type to represent the whole list.
2. Divide the geometric parameters of each section type with the corresponding geometric parameters of the selected section type.
3. Find the standard deviation of geometric parameter ratios for each section type and normalized the standard deviation with the average value of parameter ratios of that section type.
4. Calculate the average of the normalized standard deviations of the list.
5. Repeat step 1 to 4 for each section type in the list.
6. The selected section which gives minimum average normalized standard deviation is the most representative section type, geometrically, for the list.

Table 3.1 shows the calculation from step 1 to 4 for 150 UC 30.0 as the selected section type and Figure 3.4 shows the distribution of the corrected standard deviations in the list. This procedure resulted in 200 UC 52.2 as shown in Figure 3.5 as the most representative section type for the list. The capacity of the available

clevises restricted the choice to a smaller section and a 150 UC 30.0 was chosen as a second best representative section type.

3.2.2. Initial crookedness

The initial crookedness was measured to determine direction of buckling and to check whether the initial deflection complies with the tolerance of $L/1000$. The results are shown in Figure 3.6 to Figure 3.8. The dimensions of cross section for each specimen were also measured at the quarter points of the specimen.

All measured deflection values fell below the tolerance of $L/1000$.

3.2.3 Loading history and test procedure

The designed loading history can be based on several criteria. It can be based on random loading from an available earthquake record which is normally used in dynamic testing. Another criterion is to develop a certain relationship between parameters in a model. This type of loading history was used by Jain, Goel, and Hanson as shown in Figure 3.9. It was designed to derive the coordinates of control points in the proposed model (discussed in previous chapter) and a relationship between residual strain as a function of maximum compressive displacement and slenderness ratio.

Gugerli devised a loading history (Fig. 3.10) to provide information regarding (a) hysteresis loops for cycling between the same deformation limits during different sequences of the test, (b) maximum compressive forces throughout the test, and (c) fracture of the specimen.

For this test the loading history is shown in Figure 3.11. In the first cycle the specimens were tensioned to $0.5 \Delta^*y$, where Δ^*y denotes nominal axial yield displacement corresponding to a nominal yield stress of 250 MPa. In the second to the sixth cycle the amplitude of maximum and minimum displacement were increased from Δ^*y to $5 \Delta^*y$ by Δ^*y . From the seventh cycle the amplitude was increased by $5 \Delta^*y$ in each new cycle up to $30 \Delta^*y$ or failure.

The test was controlled by displacement. After a maximum displacement was reached the direction of displacement was reversed and this was followed by a

decrease in axial force. Whereas after a minimum displacement, the reversal of displacement direction did not change the axial force direction.

3.2.4. Connection details

All the specimens were connected with fillet welds to end plates of 50 mm thickness. The specimen end plates were bolted to plates and cleats for specimens with pinned-pinned end conditions and directly to the actuator and head of Dartec machine for fixed-fixed end conditions. Ten M24 and eight 1" high strength bolts were used at each end for specimen with pinned-pinned end conditions and fixed-fixed end conditions respectively as shown in Figure 3.12. All the M24 bolts were pretensioned to minimize the effects of bolt deformation in the specimen response.

Table 3.1 Geometric comparison of available UC column sections with respect to 150 UC 30.0

SECTION	d/d'	bf/bf'	tf/tf'	tw/tw'	avg	s	s/avg
310 UC 158	2.083	2.033	2.660	2.379	2.288	0.2518	0.1100
137	2.045	2.020	2.309	2.091	2.116	0.1141	0.0539
118	2.000	2.007	1.989	1.803	1.950	0.0849	0.0436
96.8	1.962	1.993	1.638	1.500	1.773	0.2103	0.1186
250 UC 89.5	1.656	1.673	1.840	1.591	1.690	0.0920	0.0545
72.9	1.618	1.660	1.511	1.303	1.523	0.1381	0.0907
200 UC 59.5	1.338	1.340	1.511	1.409	1.399	0.0704	0.0503
52.2	1.312	1.333	1.330	1.212	1.297	0.0496	0.0382
46.2	1.293	1.327	1.170	1.106	1.224	0.0896	0.0732
150 UC 37.2	1.032	1.007	1.223	1.227	1.122	0.1035	0.0922
30.0	1.000	1.000	1.000	1.000	1.000	0.0000	0.0000
23.4	0.968	0.993	0.723	0.924	0.902	0.1062	0.1177
110 UC 14.8	0.618	0.647	0.745	0.758	0.692	0.0604	0.0873

Notes : d = overall depth;
 bf = flange width;
 tf = flange thickness;
 ' = corresponding parameter of 150 UC 30.0;
 avg = average value of parameter ratios;
 s = standard deviation.

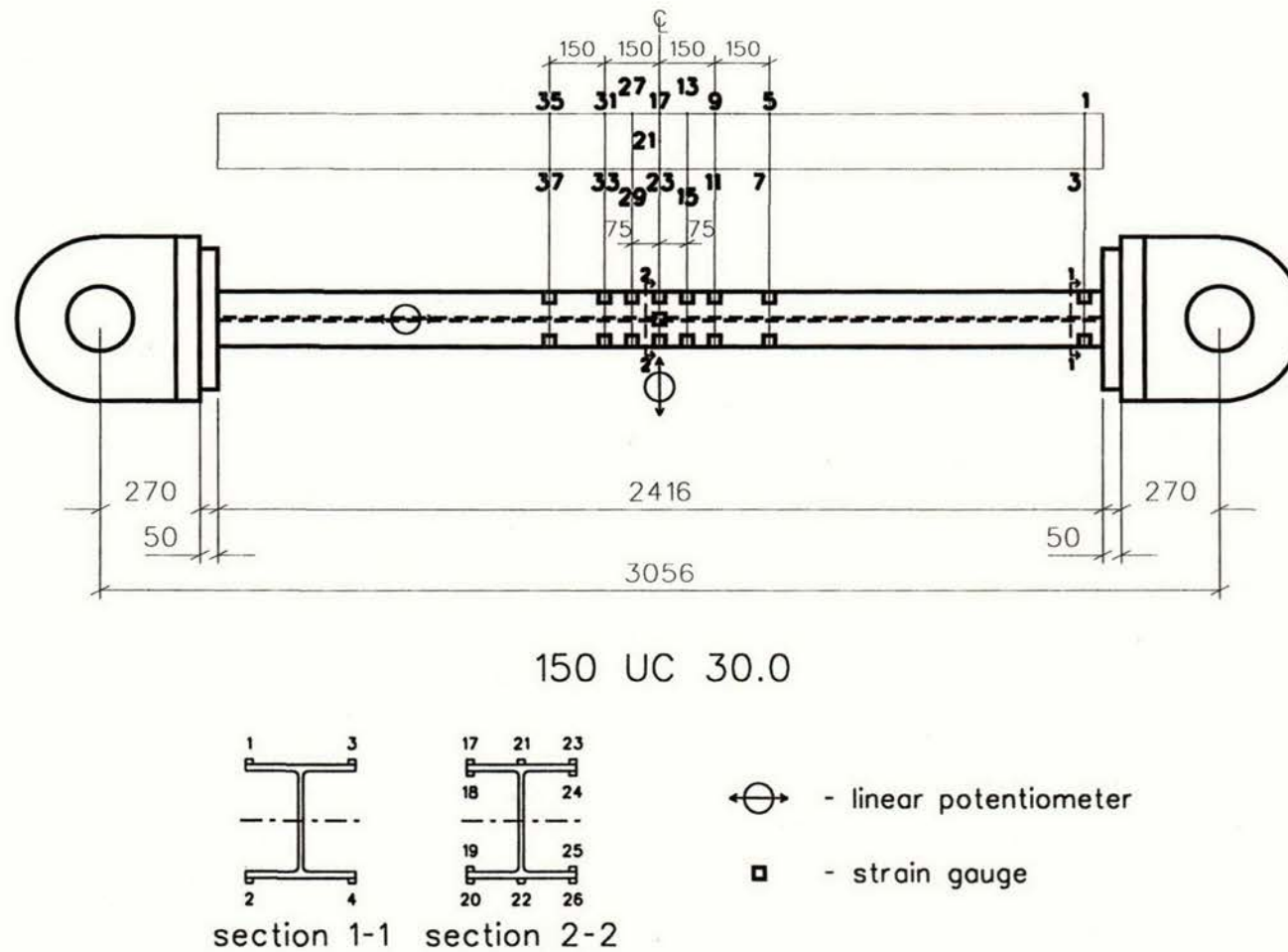


Figure 3.1 Position of strain gauges and linear potentiometers on specimen 1

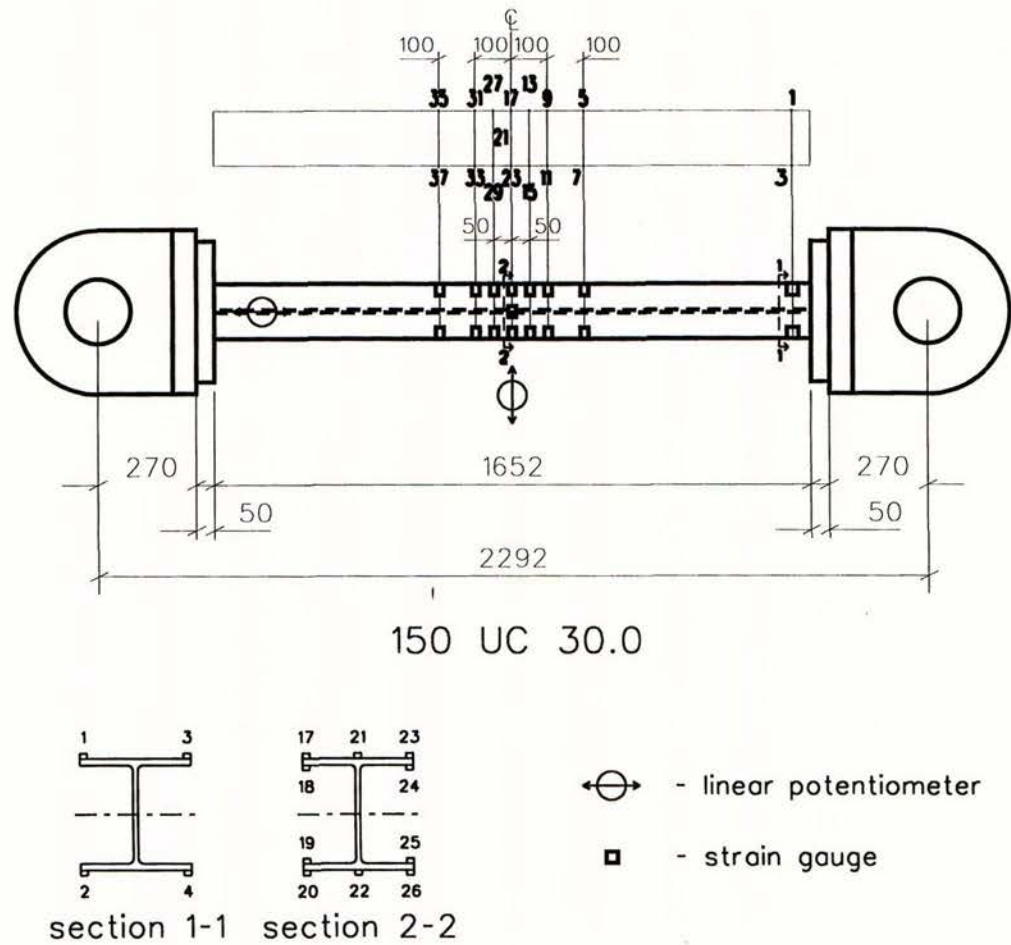


Figure 3.2 Position of strain gauges and linear potentiometers on specimen 2

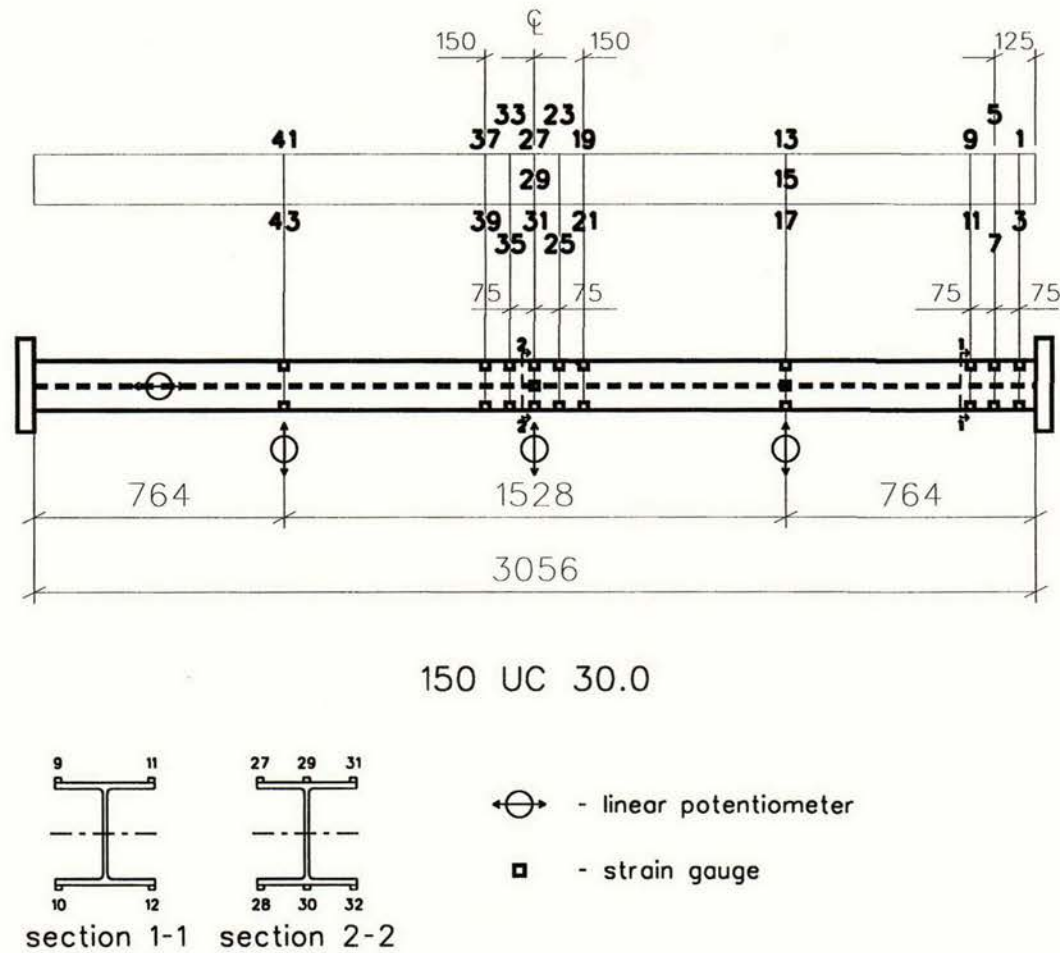
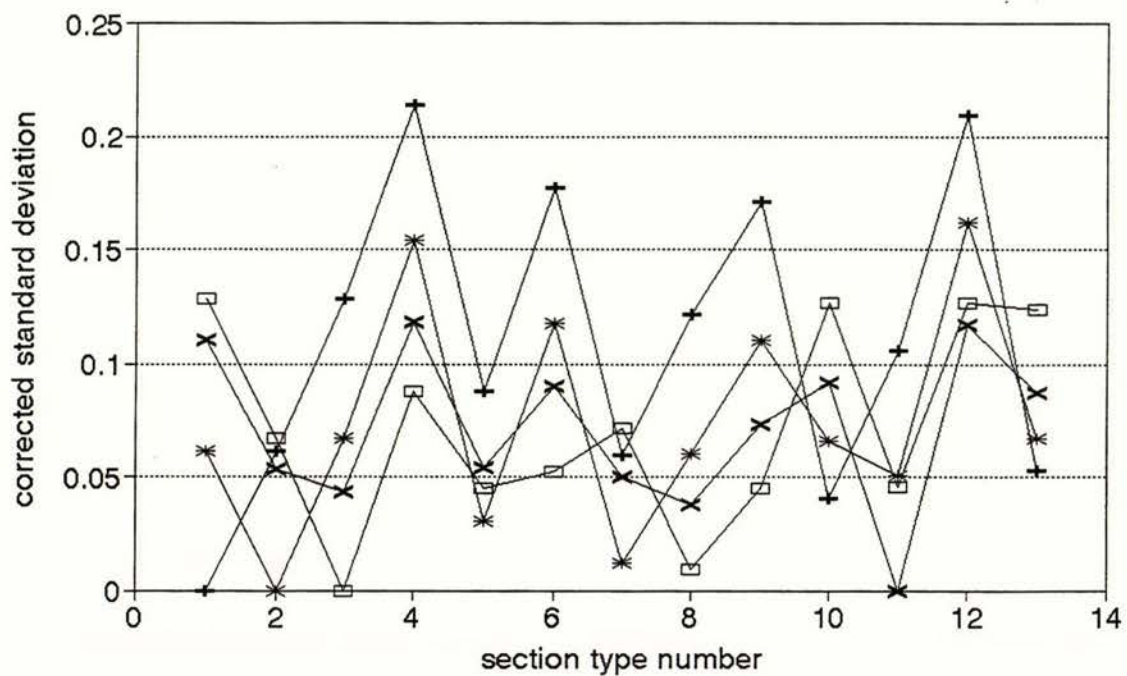
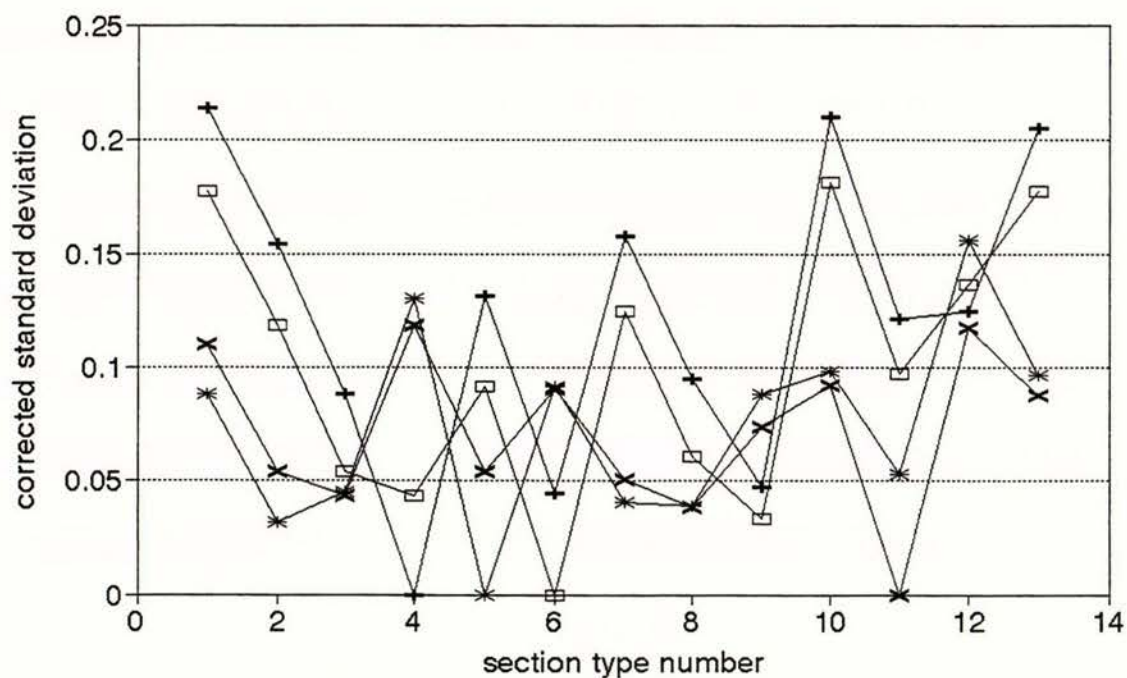


Figure 3.3 Position of strain gauges and linear potentiometers on specimen 3



(a) —x— 150 UC 30.0 —+— 310 UC 158 —*— 310 UC 137 —□— 310 UC 118



(b) —x— 150 UC 30.0 —+— 310 UC 96.8 —*— 250 UC 89.5 —□— 250 UC 72.9

Figure 3.4 Corrected standard deviation versus section type with 150 UC 30.0 as a standard of comparison

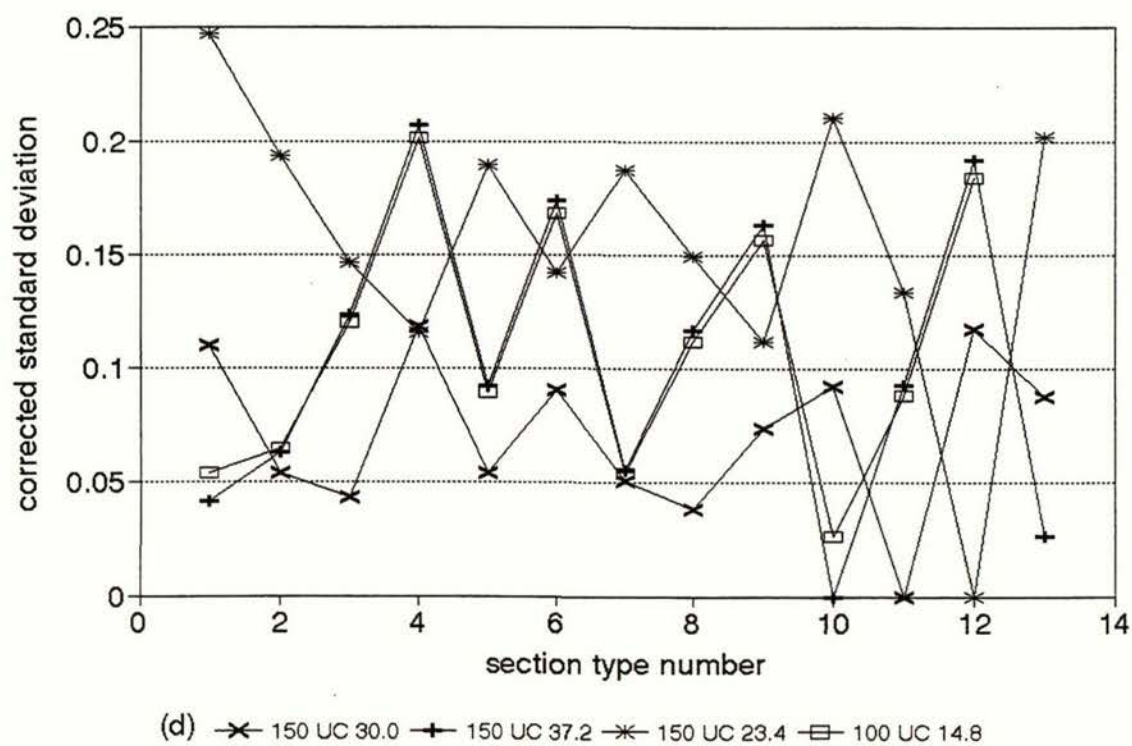
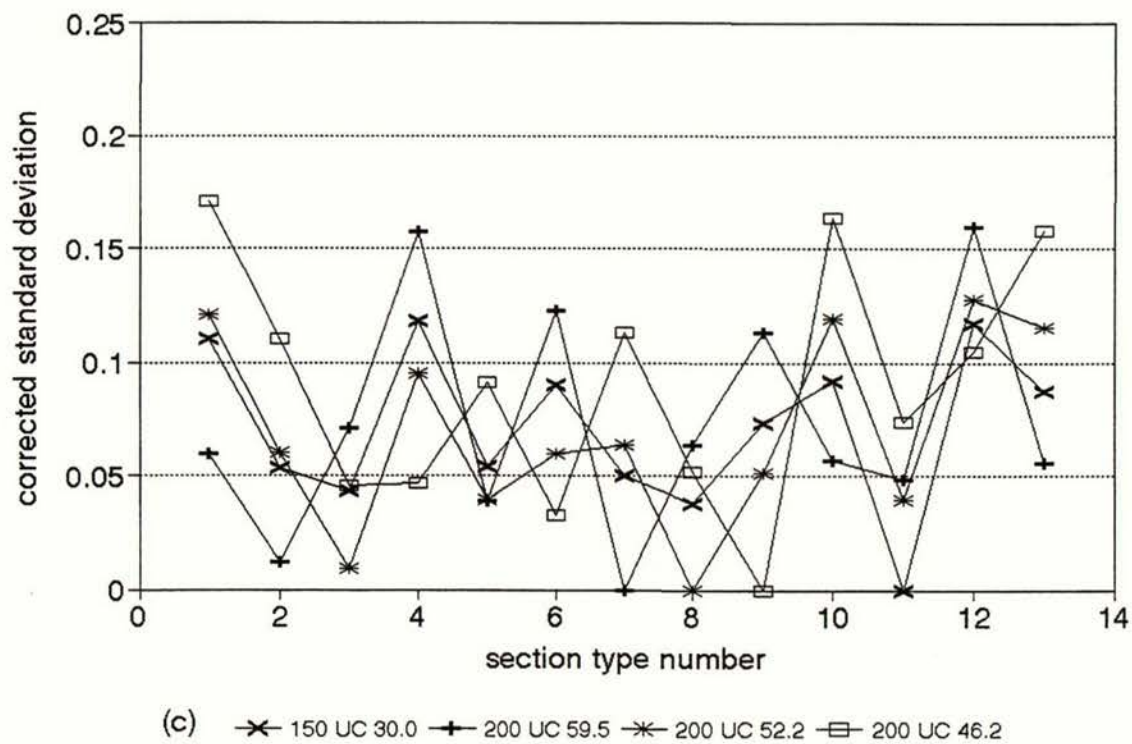


Figure 3.4 Corrected standard deviation versus section type with 150 UC 30.0 as a standard of comparison

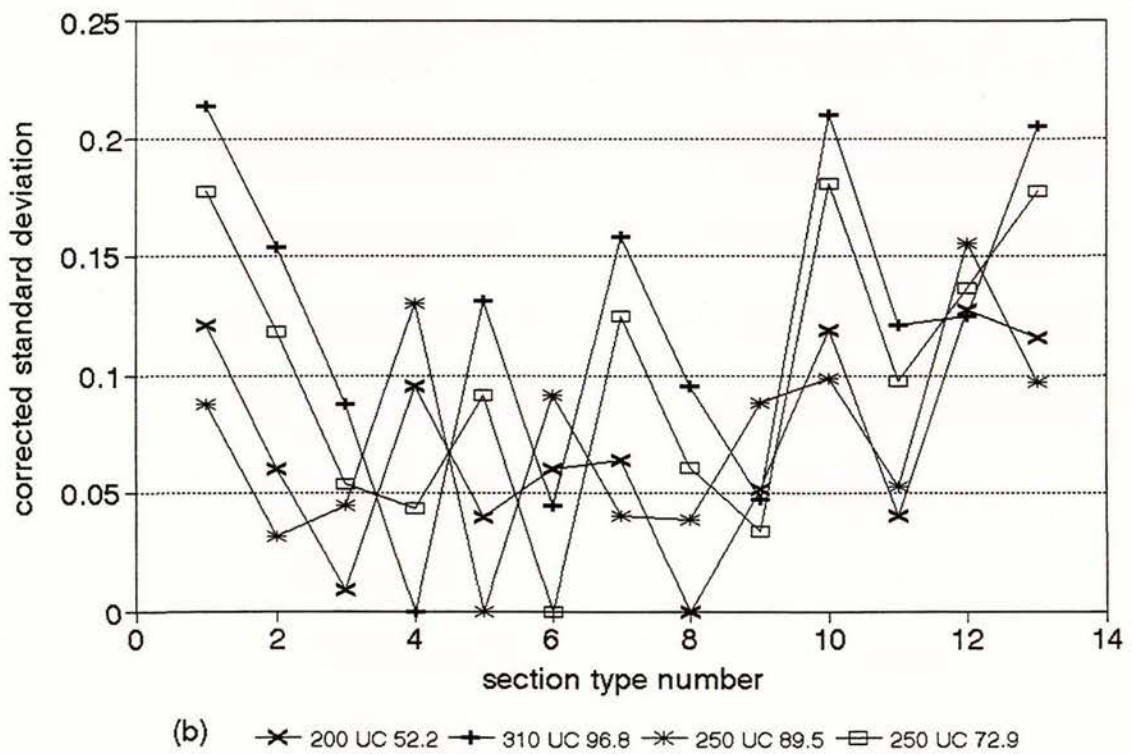
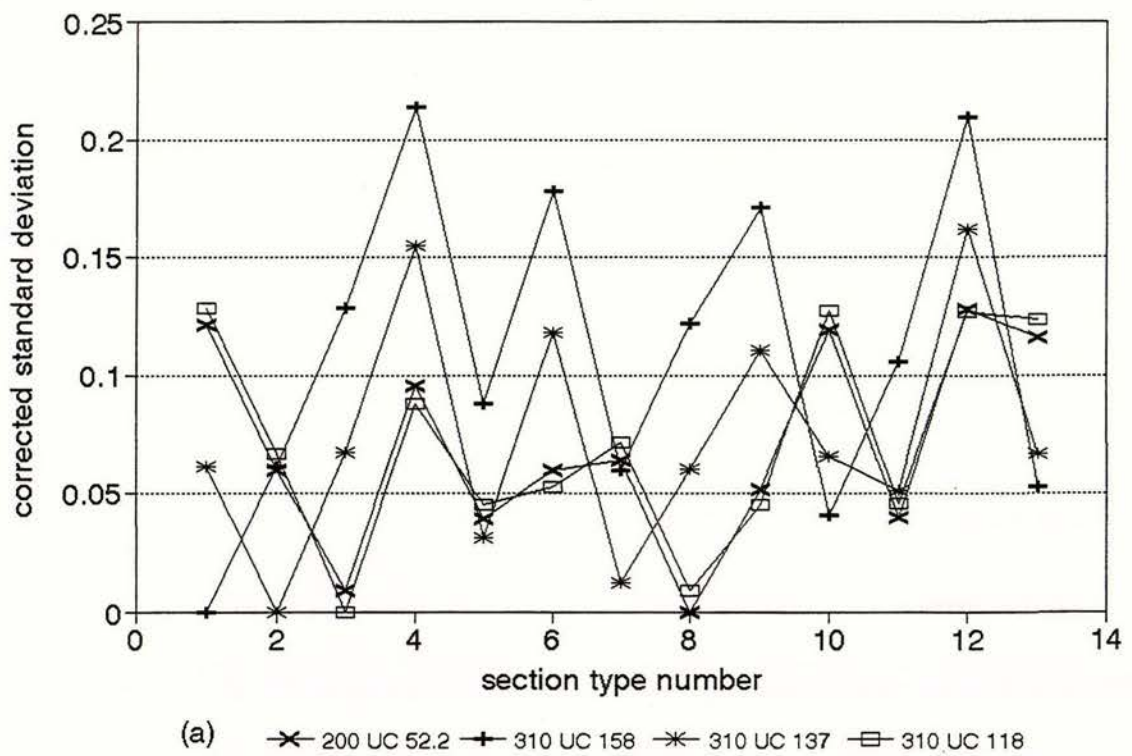
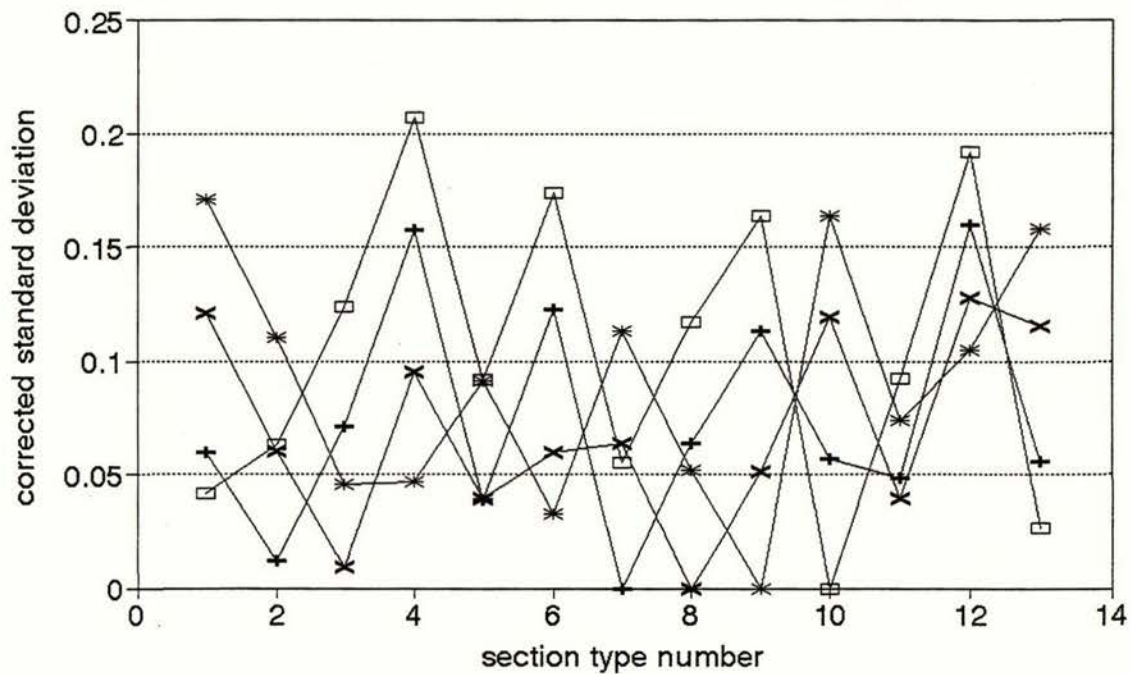
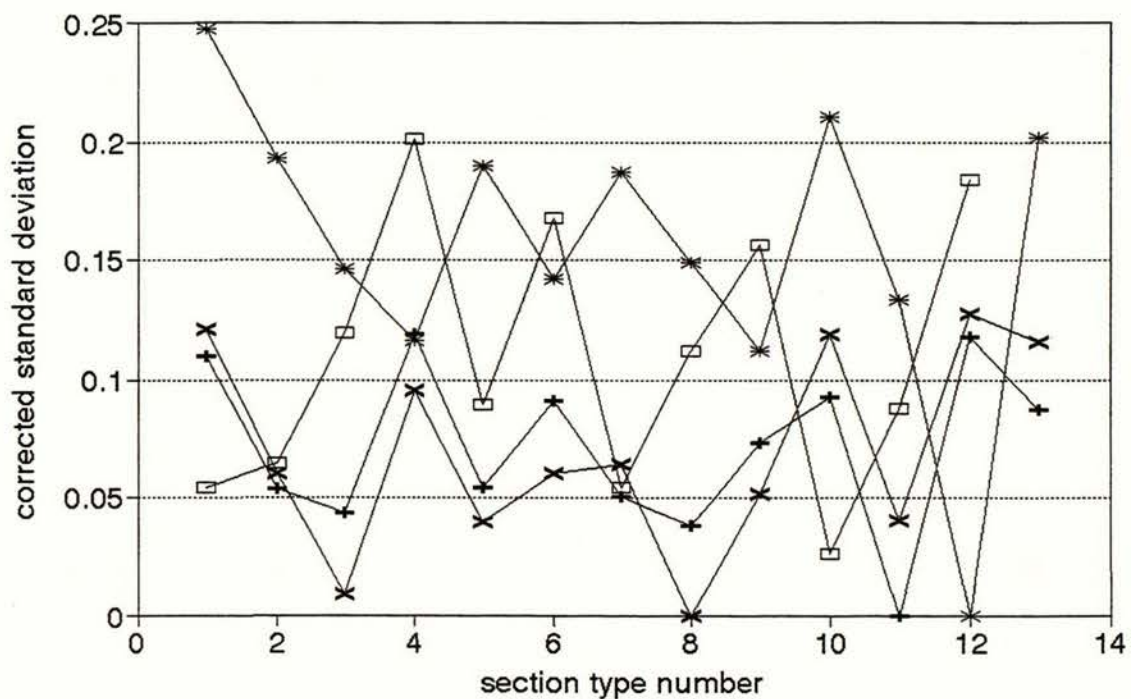


Figure 3.5 Corrected standard deviation versus section type with 200 UC 52.2 as a standard of comparison.

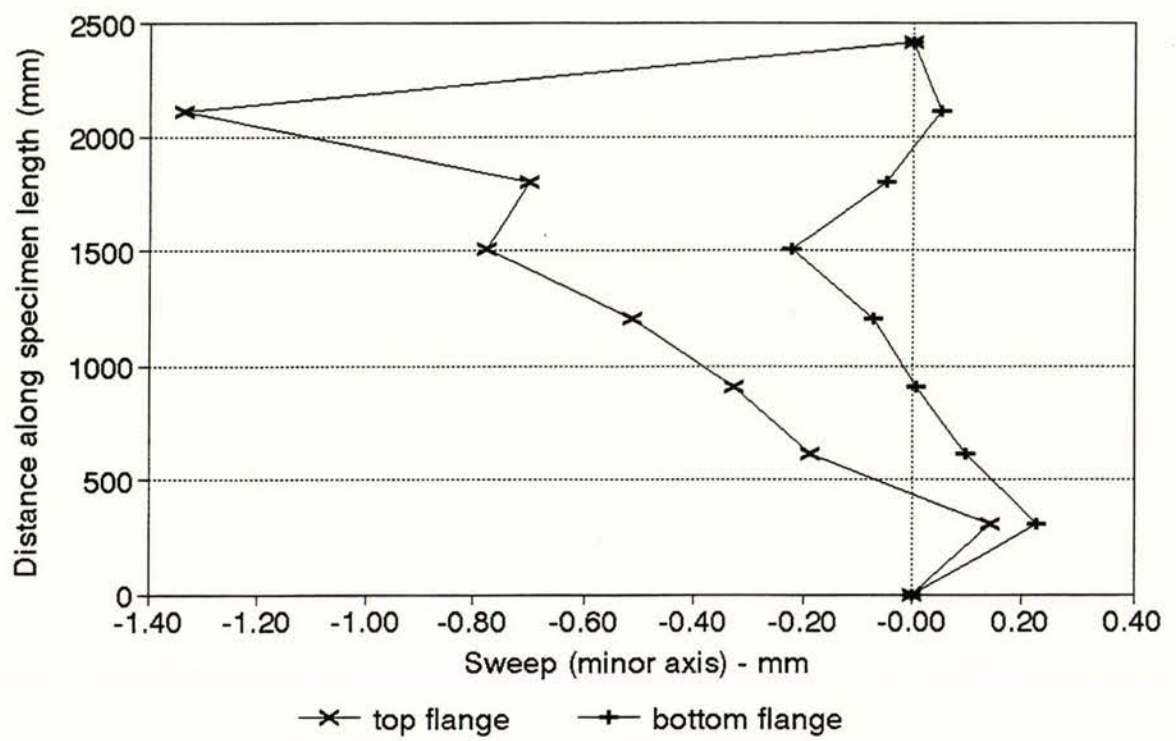


(c) —x— 200 UC 52.2 —+— 200 UC 59.5 —*— 200 UC 46.2 —□— 150 UC 37.2

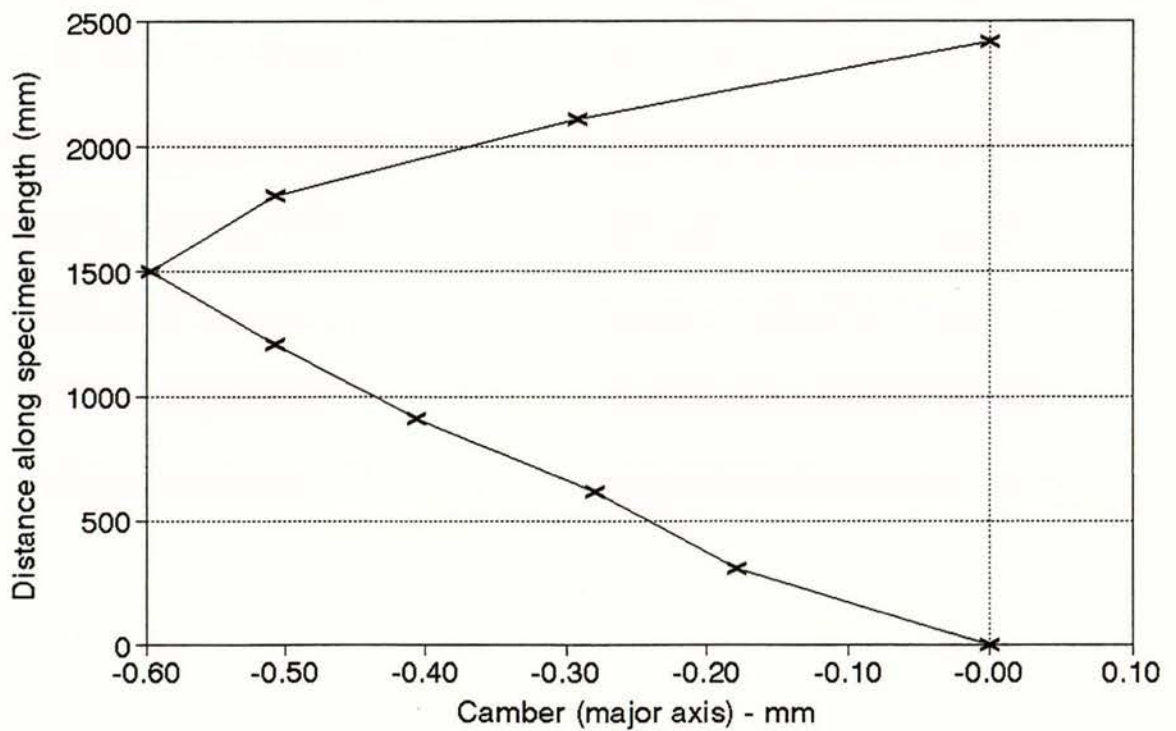


(d) —x— 200 UC 52.2 —+— 150 UC 30.0 —*— 150 UC 23.4 —□— 100 UC 14.8

Figure 3.5 Corrected standard deviation versus section type with 200 UC 52.2 as a standard of comparison.

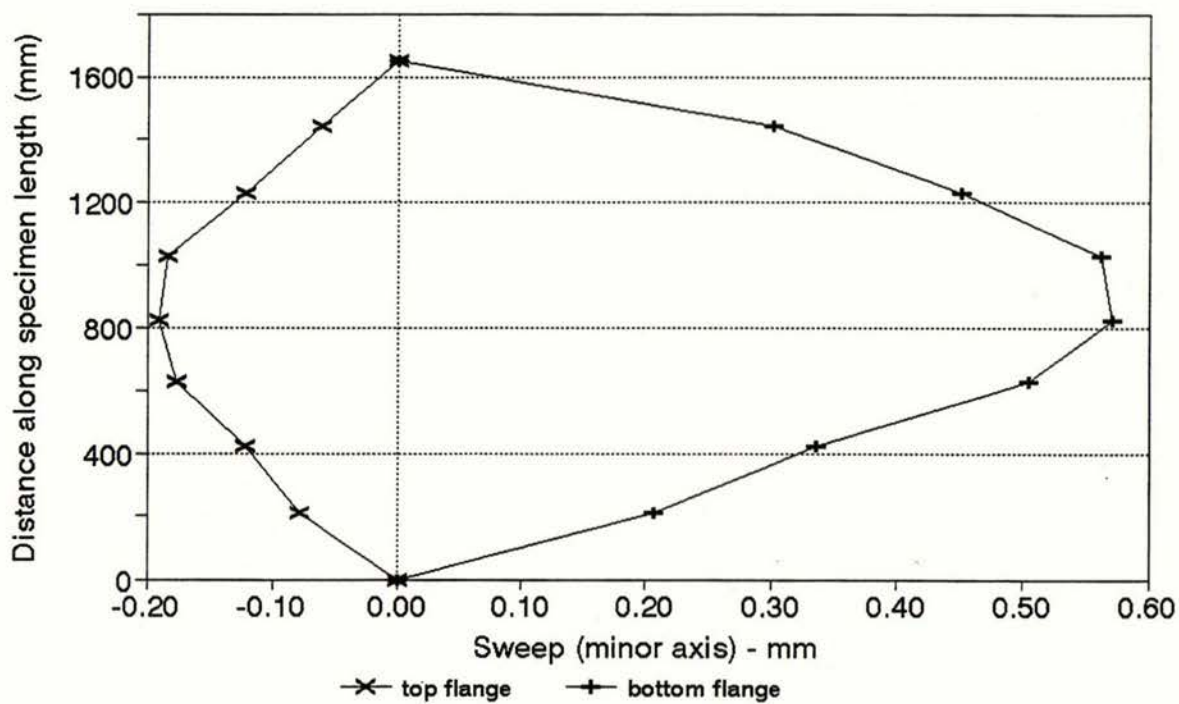


(a) Initial sweep of column specimen 1

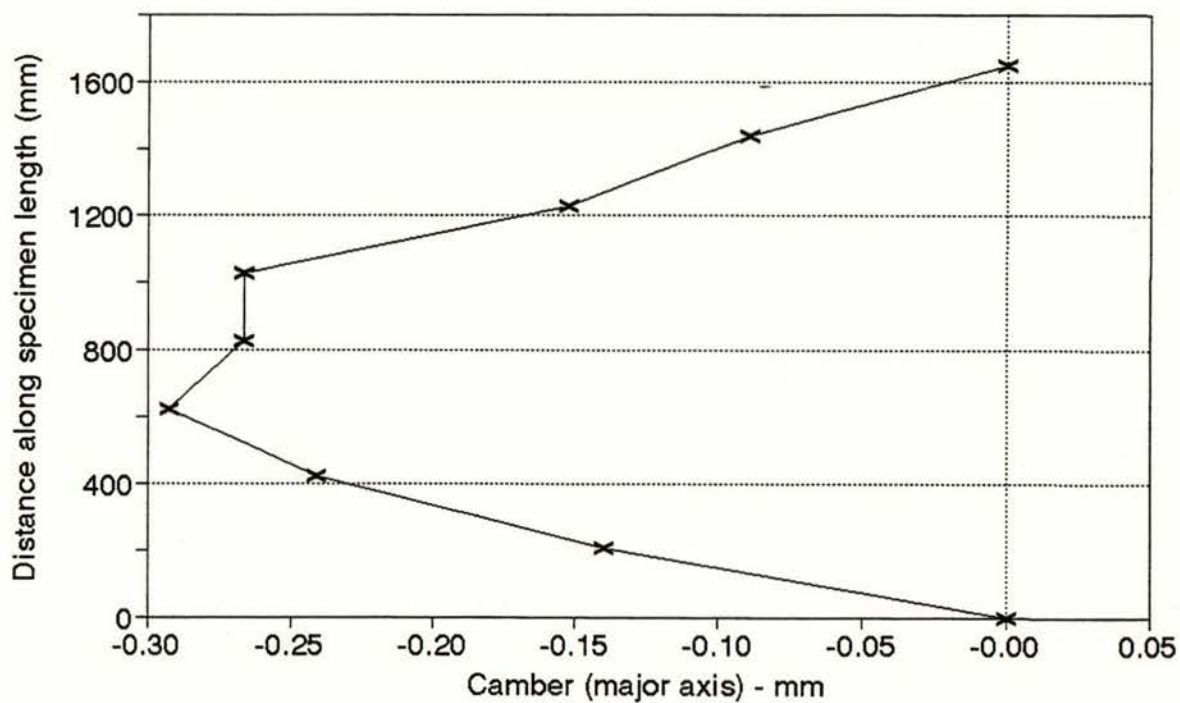


(b) Initial camber of column specimen 1

Figure 3.6 Initial crookedness of specimen 1

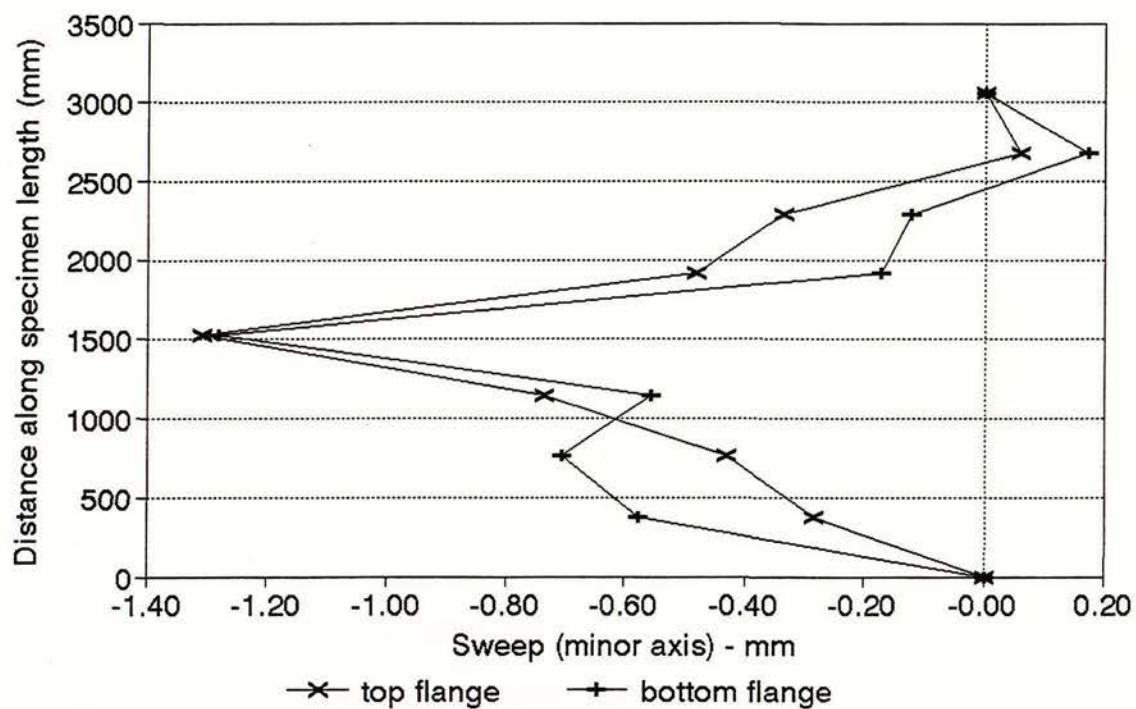


(a) Initial sweep of column specimen 2

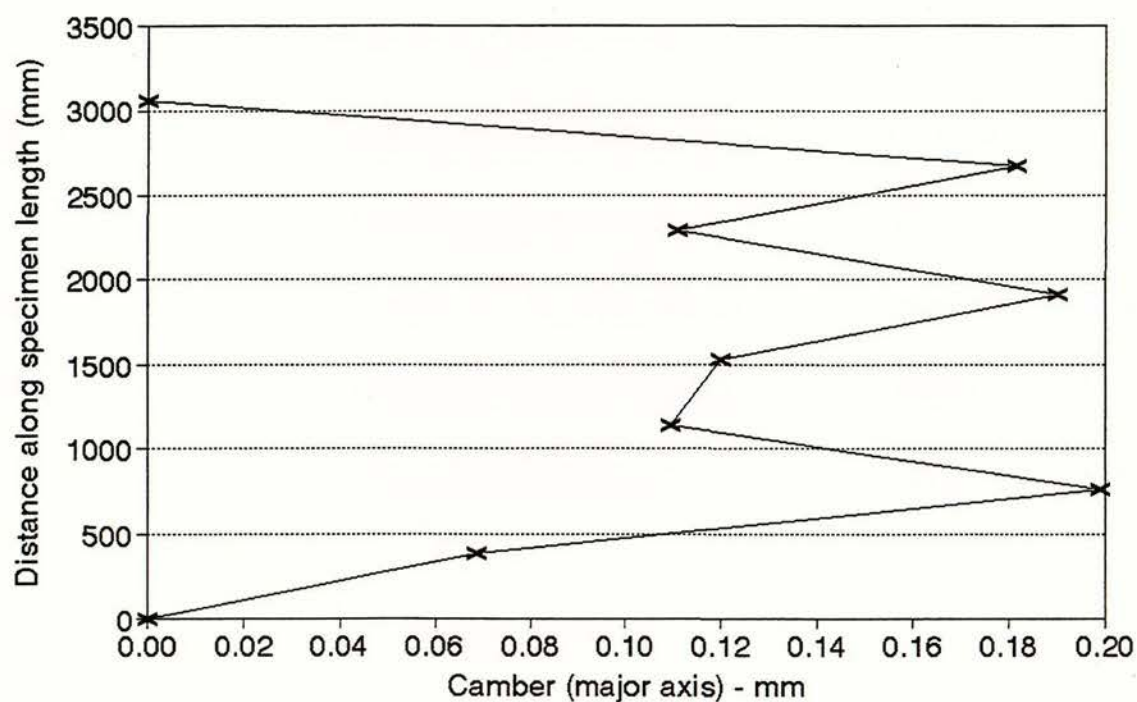


(b) Initial camber of column specimen 2

Figure 3.7 Initial crookedness of specimen 2

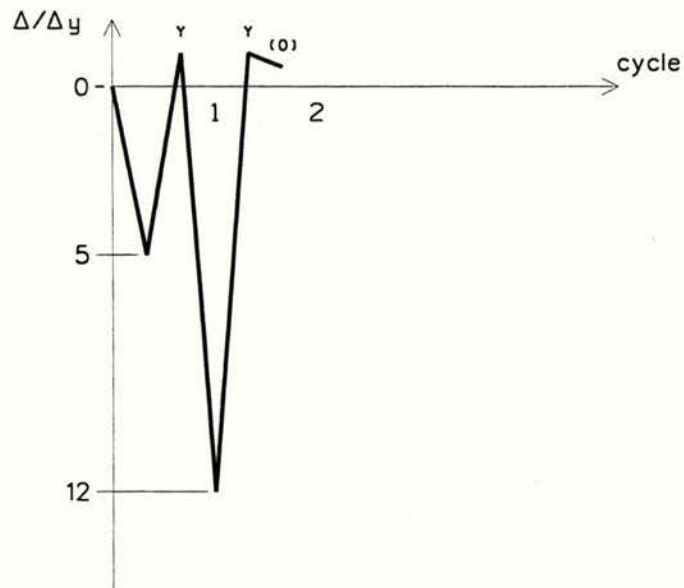


(a) Initial sweep of column specimen 3

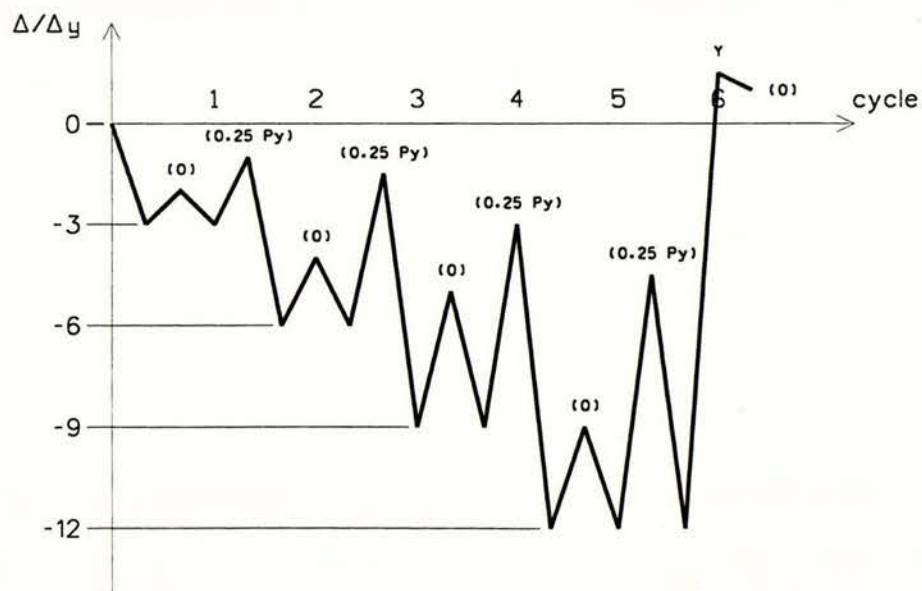


(b) Initial camber of column specimen 3

Figure 3.8 Initial crookedness of specimen 3

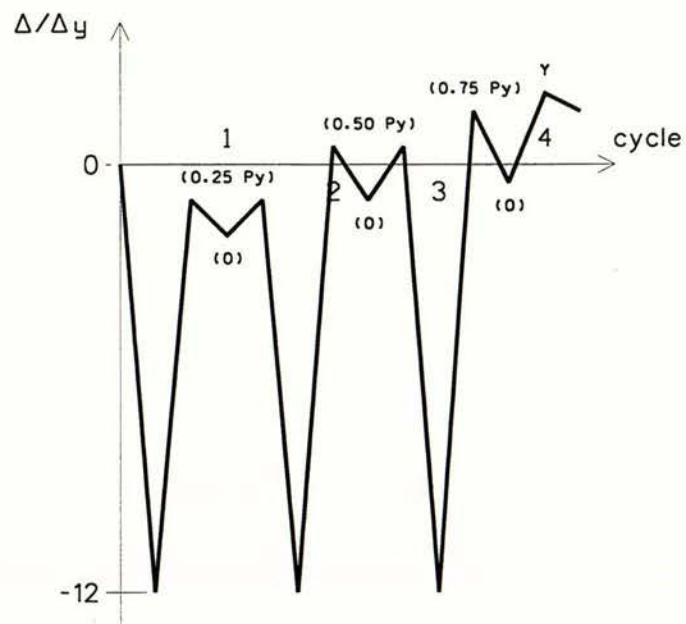


(a) Sequence 1

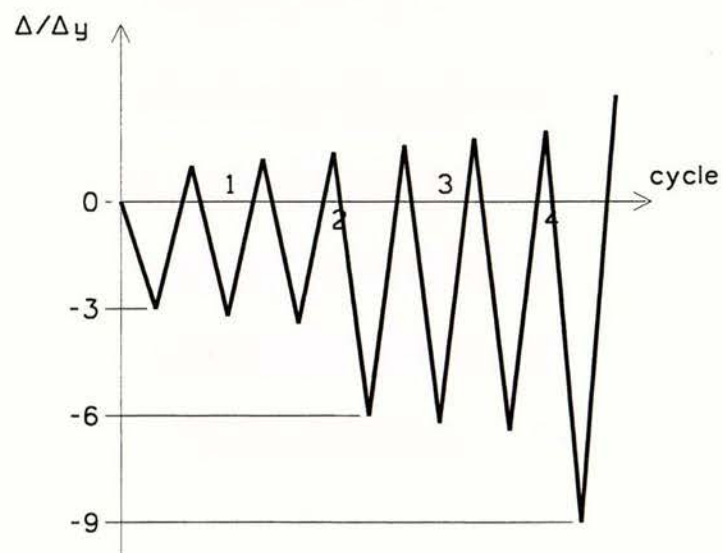


(b) Sequence 2

Figure 3.9 Loading history used by Jain, Goel, and Hanson⁽²⁾



(c) Sequence 3



(d) Sequence 4

Figure 3.9 Loading history used by Jain, Goel, and Hanson⁽²⁾

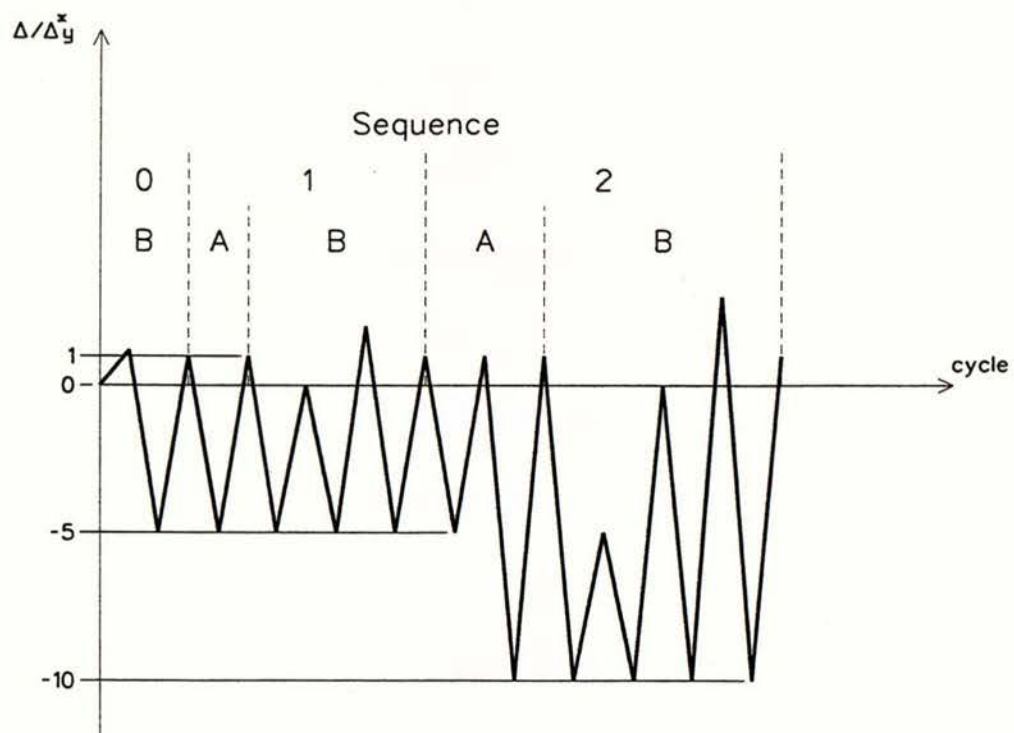


Figure 3.10 Imposed displacements used by Gugerli⁽¹¹⁾

(a) Specimen #1 - 150 UC 30

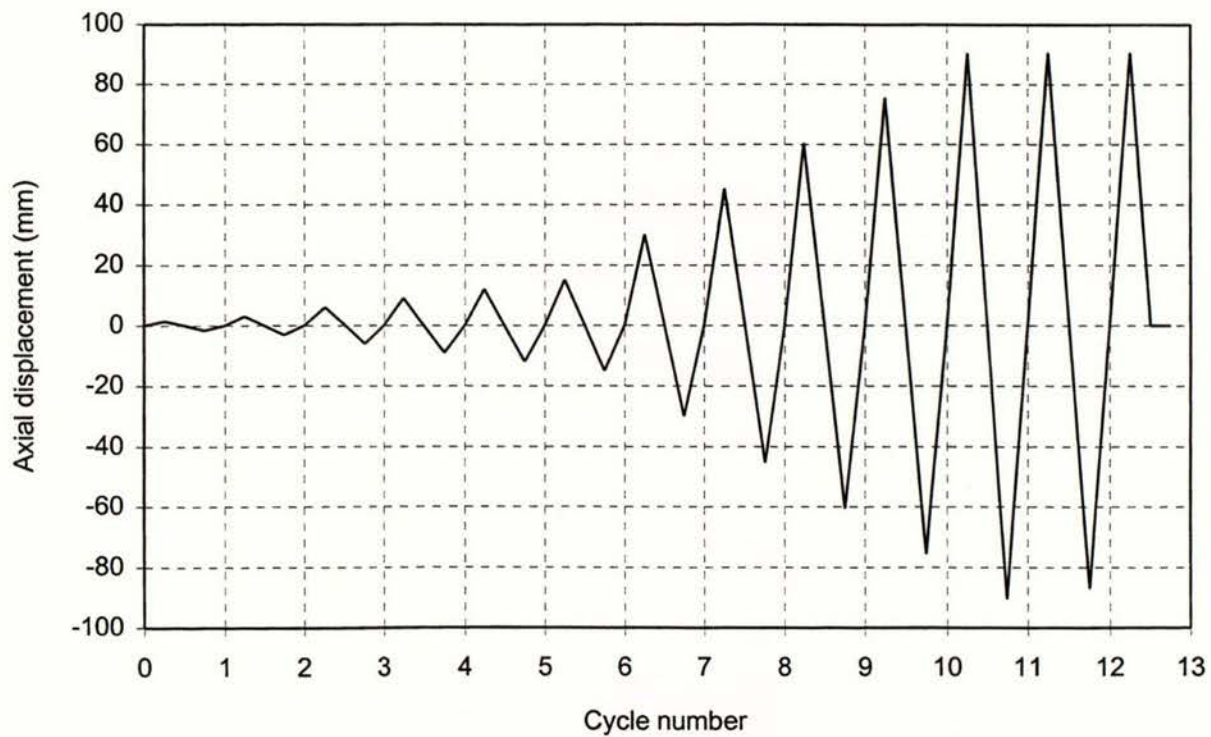
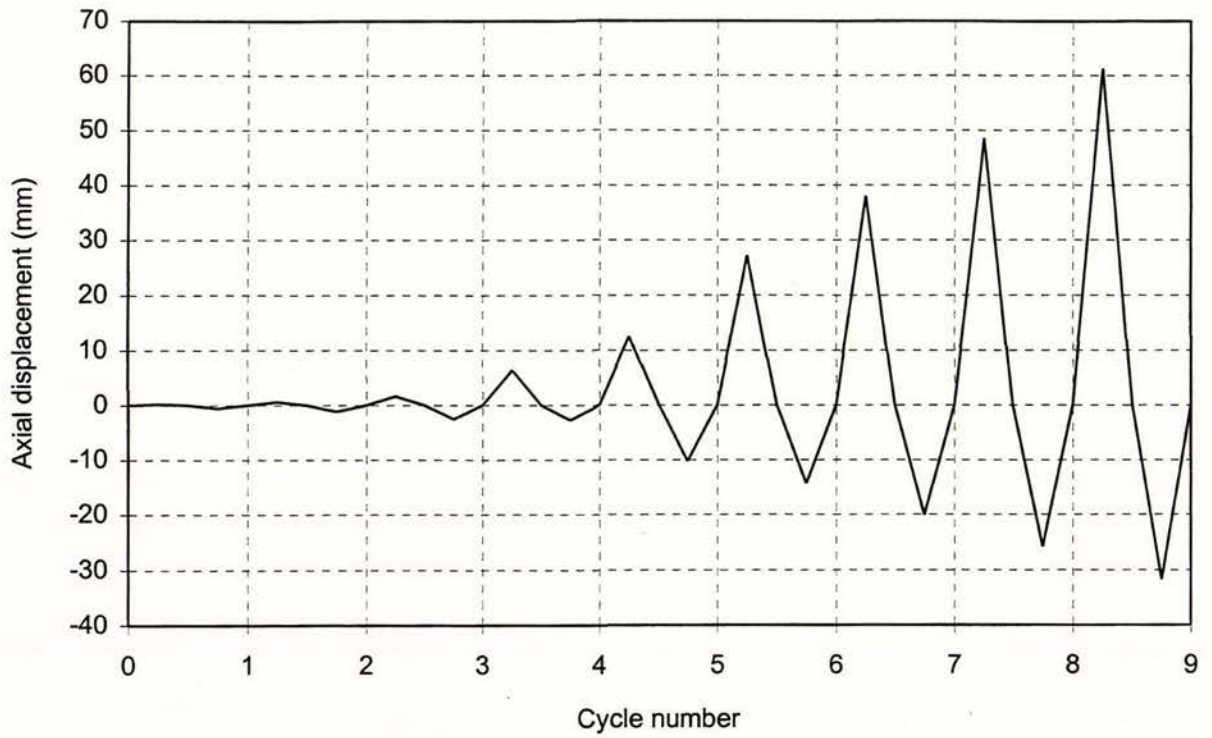


Figure 3.11 Imposed displacements for the specimens in this report

(b) Specimen #2 - 150 UC 30



(c) Specimen #3 - 150 UC 30

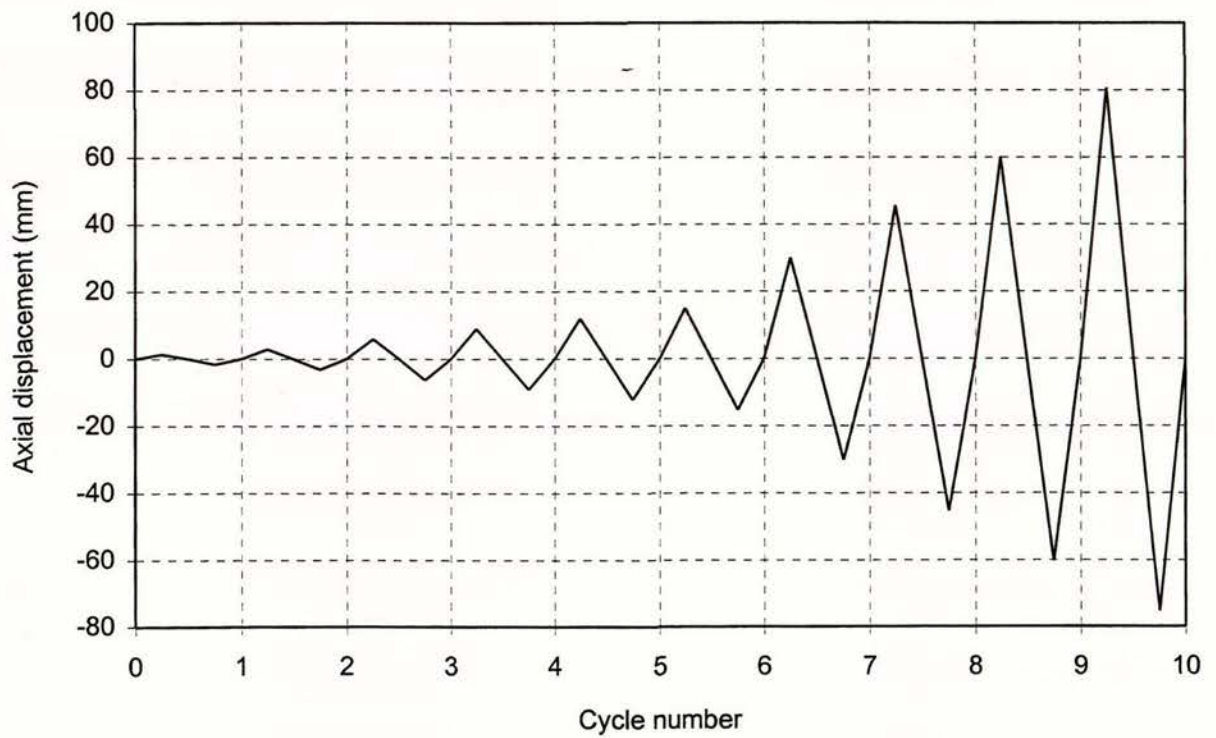
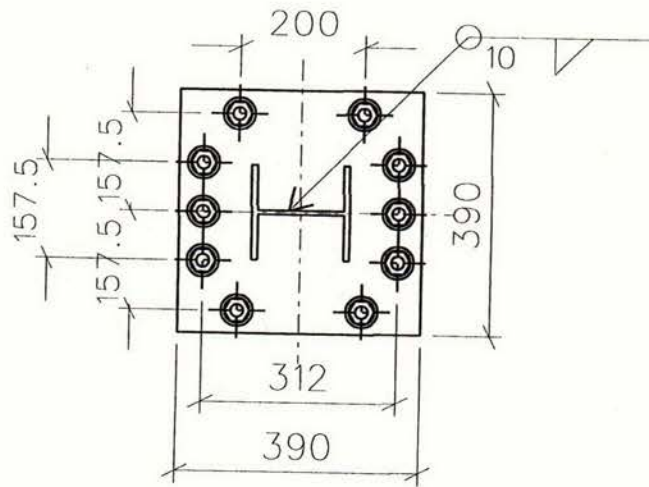
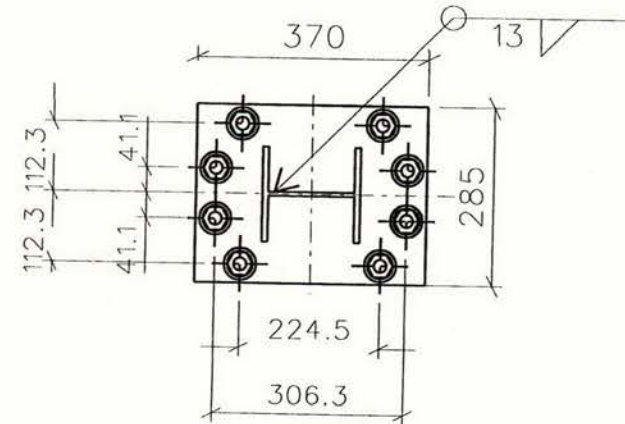


Figure 3.11 Imposed displacements for the specimens in this report



M24 bolts
specimen no.1 and no. 2



1" bolts
specimen no.3

Figure 3.12 End connection details.

CHAPTER 4

EXPERIMENTAL RESULTS

4.1 GENERAL

The first specimen tested was specimen 2. In this first test an electronic digital counter was used to measure the lateral displacement at the centre line. The lateral displacement measurement by the digital counter proved to be not stable, because it can only read the absolute change in distance. This means that if somehow the specimen vibrates, the digital counter will keep accumulating the distance travelled in the vibration. Every time the lateral displacement reverses its direction, the digital counter has to be restarted. For this reason the lateral displacement data for specimen 2 was not used to produce the axial force versus plastic hinge moment interaction curve in the following section. For the other two specimens a 500 mm-travel linear potentiometer was used and the axial force versus plastic hinge moment curves were produced.

The feed-back from the stroke displacement reading of the Dartec machine was used for controlling the test for the first three cycles. The rest of the test was controlled by the reading of a 300 mm-travel linear potentiometer for axial displacement measurement, because stroke displacement reading was not sensitive for small displacements.

4.2 MATERIAL PROPERTIES

4.2.1 Monotonic test

The objective of this test was to determine the values of tangent modulus, yield stress, hardening ratio, and value of strain at fracture. Four coupons were extracted from the wide flange specimen, two from the web on each side of the section strong axis and two from the diametrically opposed flange as shown in Figure 4.1. An extensometer

having a gauge length of 51 mm was attached to the necked portion of the coupon. The coupon was then inserted into a 1000 kN capacity Avery testing machine and pulled to failure. The force and displacement data were recorded on a data logger. The values of tangent modulus and hardening ratio could not be measured, because the extensometer did not perform as expected. The summary of test results is shown in Table 4.1.

4.2.2 Stub Column Cyclic Test

The object of this test was to generate cyclic stress versus strain data for the full section. The length of the stub column was 500 mm which was within the range specified in Technical Memorandum No.3 of Structural Stability Research Council. Two frames were placed about the mid-height of the stub column to give a 250 mm gauge length. Two potentiometers were mounted in opposite positions on these frames as shown in Figure 4.2. The average of the readings taken was used to determine the strains during testing.

The generated stress - strain data were used to produce the tangent modulus histories. The stress - strain relationship was also reproduced analytically by a computer program "STEEL TEST" developed by L.L.Dodd and J.Restrepo, because the scans taken during the test were not enough to produce smooth tangent modulus histories. There was a good agreement between the measured and calculated stress versus strain relationships as shown in Figure 4.3. Figure 4.4 compares the tangent modulus history produced from the experimental stress versus strain data to the one from the analytical data.

The yield stress observed in this stub-column test was 325 MPa, while the average of the monotonic coupon tests was 315 MPa.

4.3 OVERALL BEHAVIOUR OF BRACE SPECIMEN UNDER CYCLIC LOADING

4.3.1 Deflected shape and lateral displacement

The overall curvature of the specimens followed the initial crookedness and this direction of curvature remained unchanged in later cycles.

Figure 4.5a shows the deflected shape of specimen 3 under maximum compressive axial displacement of 15.3 mm in cycle 6. This figure shows the segments between either end and the central plastic hinge were almost straight. Figure 4.5b shows that even after reaching tensile yield load at axial displacement of 30.0 mm in the next cycle there was still some residual lateral displacement and curvature in the specimen. The deflected shape for specimen 1 and 2 under the maximum compressive axial displacement was a sinusoidal curve from cycle to cycle until the occurrence of local buckling.

4.3.2 Yield lines

The thin white plaster paint on the specimen gave visual information on the spread of the yield lines and also whether they are compressive or tensile yield lines. The former were associated with cracks perpendicular to member axis while a diagonal yield lines was typical for tensile yield lines as shown in Figure 4.6. Generally the first yield lines started to appear from the bottom end and then spread to the top of the specimen. During later cycles into the plastic deformation phase, the yield lines were concentrated in the plastic hinge regions. Yield lines near the central hinge did not appear dramatically, because most of the scale, around the centre of each specimen, was removed for strain gauge installation.

4.3.3 Hysteresis loops

Figure 4.7 shows the hysteresis loops for specimens 1 to 3 with slenderness value of 40, 60 and 80. The smaller slenderness produced fuller loops and the more slender member generated slim or pinched loops as expected. This can be explained by the fact that, for a given cross section, smaller slenderness produces smaller lateral displacement, for the same axial load level. This means that the axial force should be higher to reach the plastic moment capacity in the member with smaller slenderness for a given level of lateral displacement. This higher axial load explains the fuller loops of member with smaller slenderness value. The sizes of the hysteresis loops in compression are not directly proportional to their slenderness ratios because the axial displacement

values for a given level of lateral displacement are not the same for different slenderness ratios.

4.3.4 Maximum and minimum axial loads

Table 4.2 and figure 4.1(b) shows the maximum and minimum axial load in each cycle. For the specimens with slenderness ratios of 60 and 80, the buckling loads in later cycles were significantly smaller than in the first cycle, with the largest decrease occurring from the first to the second cycle. For the specimen with a slenderness ratio of 40, the buckling loads decreased more uniformly from cycle to cycle until failure.

4.3.5 Maximum and minimum axial displacements

Table 4.3 shows the imposed maximum and minimum axial displacement values in each cycle. These were plotted previously in figure 3.11. The maximum and minimum ductilities have also been calculated from these displacements and the displacement at ductility one, using the experimental yield stress. The maximum and minimum axial ductilities during each cycle are plotted in figure 4.1(c).

4.3.6 Hinge moment versus axial force

Axial force versus hinge moment curves for the plastic hinge position give important information about the extent of plastic deformation at the hinge. They also give an indication of the extent of strain hardening or softening.

The axial force versus axial displacement hysteresis loops showed strain hardening in specimen 1 and this was also evident in the axial force versus plastic hinge moment curves as the outward translation of yield surfaces as shown in Figure 4.8. The axial force versus plastic hinge moment curves for specimen 3 are given in Figure 4.9. Specimen 3 did not experience as much strain hardening as specimen 1 because local buckling occurred relatively earlier. After local buckling, for reloading in tension, part of work done by the axial force has to be allocated to straighten the local buckle first, before it straightens the whole brace length.

Strain softening can be identified in specimen 3 as the decrease of plastic hinge moment capacity in compression after the occurrence of local buckling. Whereas specimen 1 showed an increase in plastic hinge moment capacity in compression at low axial load level.

4.4 INELASTIC BEHAVIOUR OF BRACE SPECIMEN UNDER CYCLIC LOADING

4.4.1 General shape of cyclic strain curves

The shape of the strain history curve can be differentiated according to the position of the section with respect to the plastic hinge i.e. inside or outside the plastic hinge region. In the plastic hinge region the strain history for the compression side shows an approximately sinusoidal curve in tensile and compressive strain where maximum and minimum values were reached at the same time as maximum and minimum axial displacement respectively. After a few cycles the strain history in the tension side showed residual tensile strain that increased from cycle to cycle with the increase in axial displacement excursion. On the tension side the maximum strain was reached at minimum axial displacement, while the minimum strain was reached after the elastic compressive deformation diminished in the tension range. Figure 4.10 shows the strain history of specimen 1 and 3 at the centre.

Outside the plastic hinge region the strain history showed the same pattern on the compression and tension side. The strain history showed residual strain that increases from cycle to cycle with a larger residual strain in tension side.

4.4.2 Curvature in plastic hinge regions

Figures 4.11 to 4.14 show curvature distribution at maximum compressive displacement (load condition C) and zero load after tension (load condition H) for specimen 1 and 3. Points C and H are shown in Figure 2.1a. Curvature at a cross section was calculated from the strain readings by dividing the difference of two strain gauge readings by the distance between the gauges.

The following points can be summarized from the curvature plots for specimen 1 and 3:

1. The positions of inflection point at quarter points from each end of the fixed-fixed end condition specimen were confirmed.
2. Beyond the first buckling load the maximum curvature of each cycle increases with increasing axial deformation amplitude. The difference in the values of the slenderness ratio did not cause any significant changes in the maximum curvature for the same level of axial deformation amplitude.
3. The residual curvature at zero load after tension was larger for the specimen with the smaller slenderness ratio.

The maximum curvatures in specimens 1 and 3 are not significantly different, so specimen 3 with the smaller slenderness ratio will have a smaller contribution from geometric axial displacement. The total axial displacements for both specimen 1 and 3 are similar. This means that more plastic deformation must occur in specimen 3 to compensate for the smaller geometric axial displacements. The larger plastic deformation in specimen 3 means that the plastic hinge region spreads further across and along the specimen.

4.4.3 Local buckling

Local buckling started to appear in cycle 12 with maximum compressive load of 230.4 kN for specimen 1, in cycle 8 with maximum compressive load of 504.9 kN for specimen 2, and in cycle 7 with maximum compressive load of 764.6 kN for specimen 3 as shown in Figures 4.15 to 4.17. This test result suggests that an increase in slenderness ratio delays local buckling because specimens with larger slenderness ratio have smaller axial loads. The local buckle, which formed first on the concave side of the plastic hinge region, grew during member contraction. Buckles on the convex side formed later in the loading history. The buckle on the concave flange had almost disappeared during tensile loading near yielding.

Table 4.1. Tensile coupon test results

	1A	1B	2A	2B
F_y (kN)	61.5	61.3	46.2	45.6
F_m (kN)	90.0	91.0	65.6	66.0
L_e (mm)	51	51	51	51
L_u (mm)	76	77	73.5	72
b (mm)	20.13	20.21	20.22	20.24
d (mm)	9.86	9.89	7.02	7.09
b_u (mm)	12.90	12.80	13.52	13.68
d_u (mm)	4.60	4.64	2.90	3.04
R_y (MPa)	310	306	325	318
R_m (MPa)	453	455	462	460
A (%)	49	51	44	41

Notes: F_y is the yield force
 F_m is the maximum force
 L_e is the extensometer gauge length
 L_u is the final gauge length
 b is the width of the test piece
 d is the thickness of the test piece
 b_u is the final width of the test piece
 d_u is the final thickness of the test piece
 R_y is the yield stress
 R_m is the tensile strength
 A is the percentage elongation after fracture

Table 4.2 Maximum and minimum axial load values (kN)

Cycle	Specimen #1		Specimen #2		Specimen #3	
0	0	0	0	0	0	0
1	-289.9	454.1	-276.7	111.8	-517.7	482.1
2	-720.2	848.5	-546.7	289.2	-926.5	832.1
3	-1266.9	1249.5	-1090.5	735.6	-1204.2	1258.2
4	-1164.4	1250.5	-841.7	1275.6	-1067.3	1265.9
5	-525.5	1232.2	-646.0	1289.1	-950.7	1278.5
6	-418.4	1167.6	-565.0	1333.4	-827.2	1270.8
7	-442.5	1228.3	-504.9	1392.2	-764.6	1279.4
8	-407.8	1327.6	-528.4	1451.0	-676.8	1299.7
9	-398.2	1389.3		1500.2	-619.0	1329.6
10	-404.0	1277.5			-572.7	1366.2
11	-388.6	1478.0				1151.1
12	-230.4	1054.8				
13	-203.4	886.0				

Table 4.3 Maximum and minimum axial displacements (mm)

Cycle	Specimen #1		Specimen #2		Specimen #3	
0	0	0	0	0	0	0
1	-1.549	1.475	-0.575	0.225	-1.623	1.328
2	-3.097	3.097	-1.188	0.575	-3.173	2.804
3	-6.047	6.047	-2.588	1.613	-6.198	5.902
4	-9.07	9.07	-2.725	6.425	-9.149	8.927
5	-12.02	12.02	-10.285	12.53	-12.17	11.88
6	-15.04	15.04	-14.376	27.20	-15.27	14.98
7	-30.01	30.08	-20.134	38.01	-30.25	30.03
8	-45.42	45.35	-25.885	48.54	-45.38	45.67
9	-60.61	60.39	-31.802	61.35	-60.43	60.20
10	-75.66	75.58			-75.55	75.33
11	-90.55	90.55			fracture	80.72
12	-87.16	90.63				
13	-0.074	90.70				

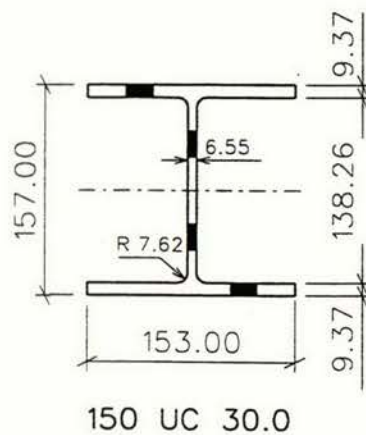
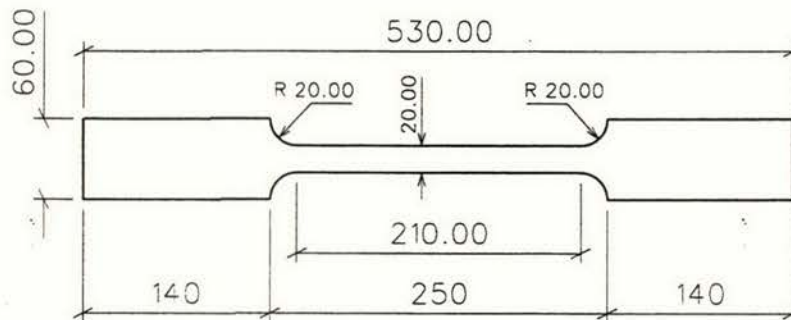
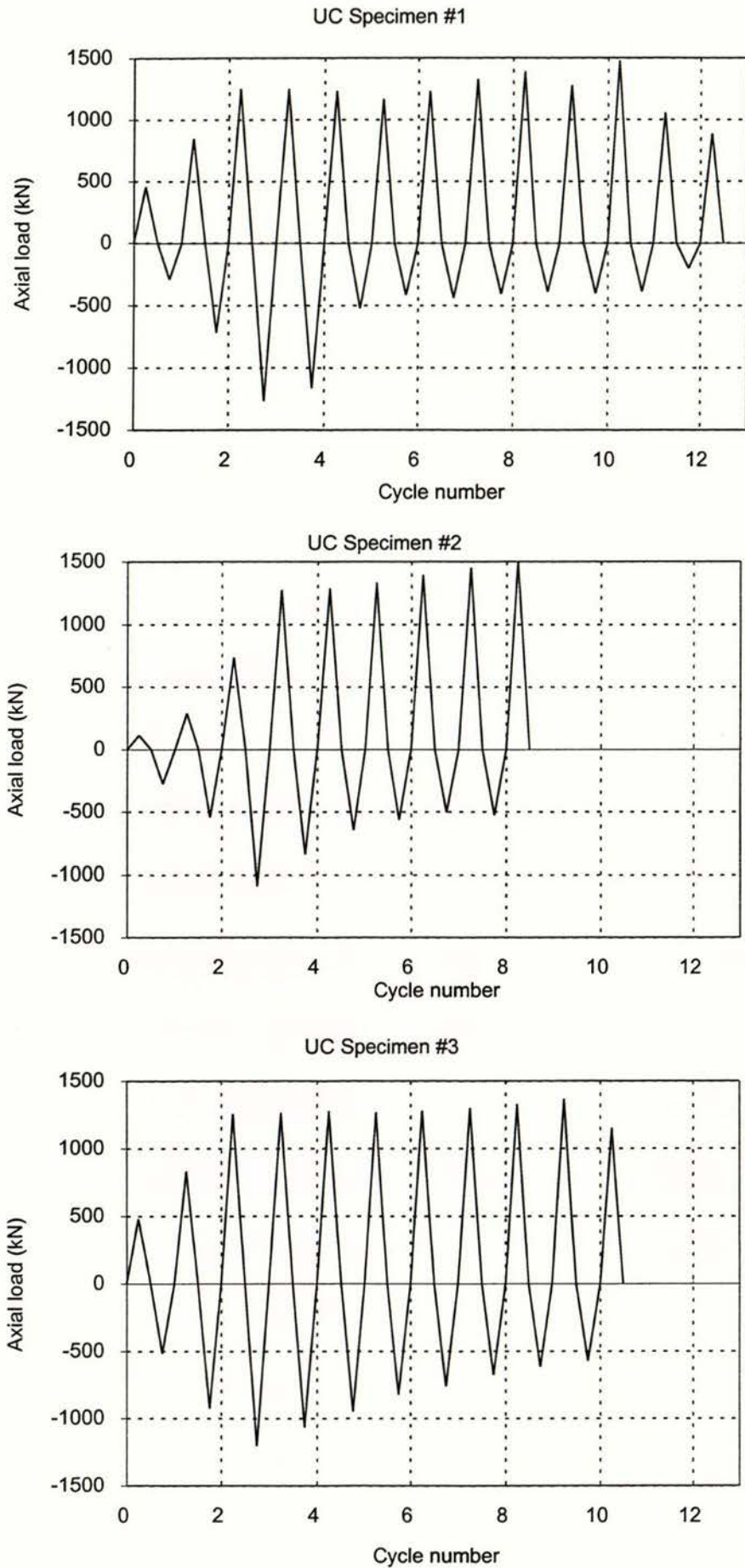


Figure 4.1 (a) Tensile test coupon



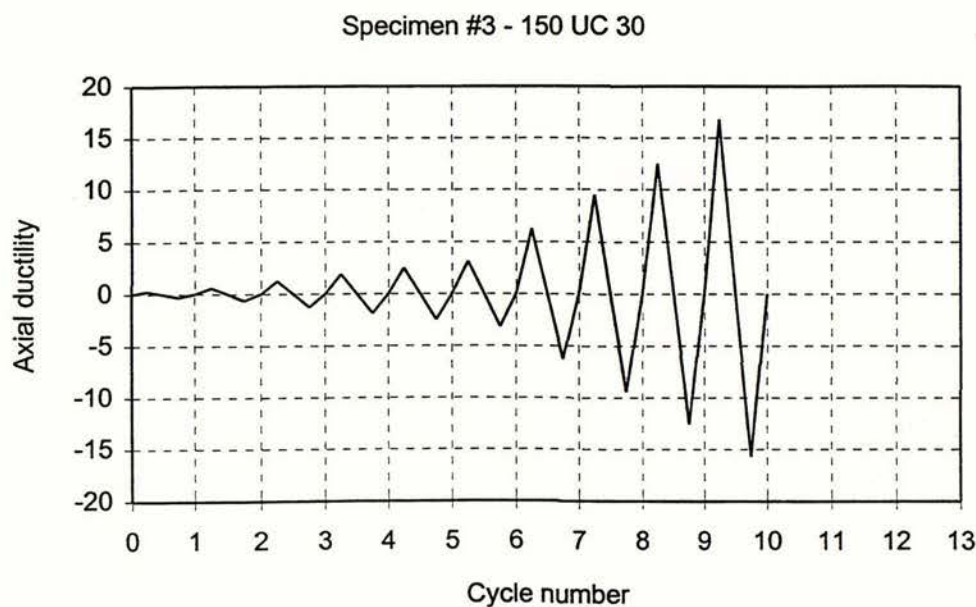
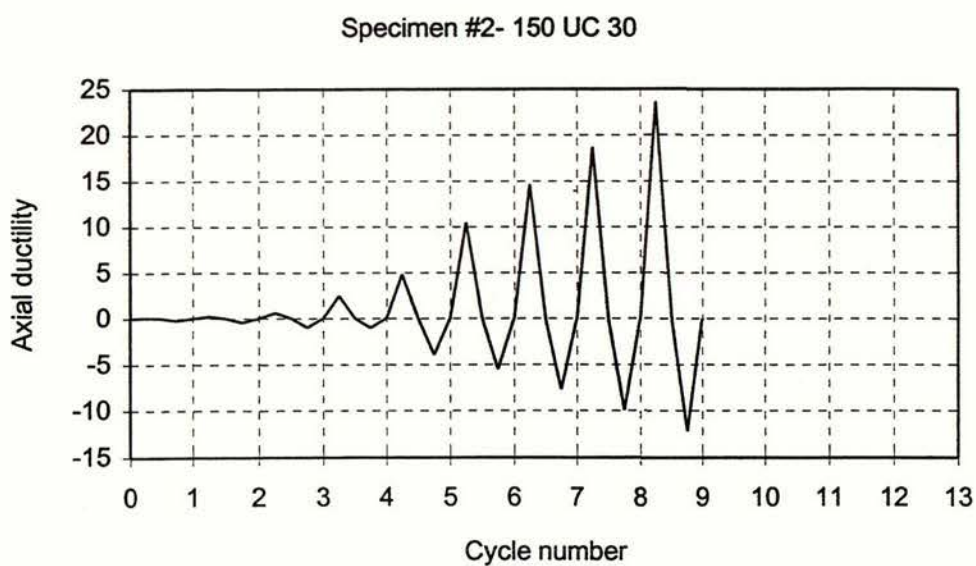
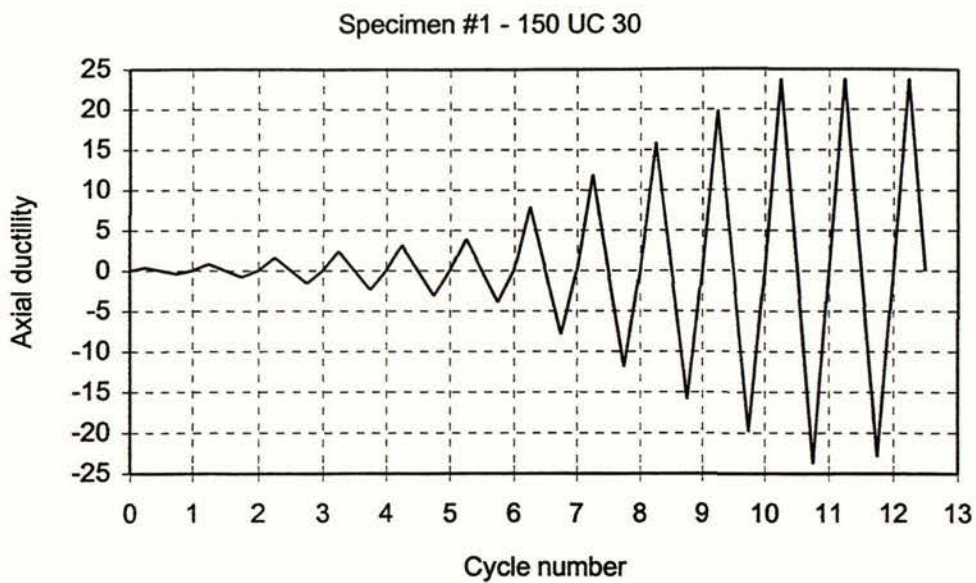


Figure 4.1 (c) Maximum and minimum axial ductilities per cycle

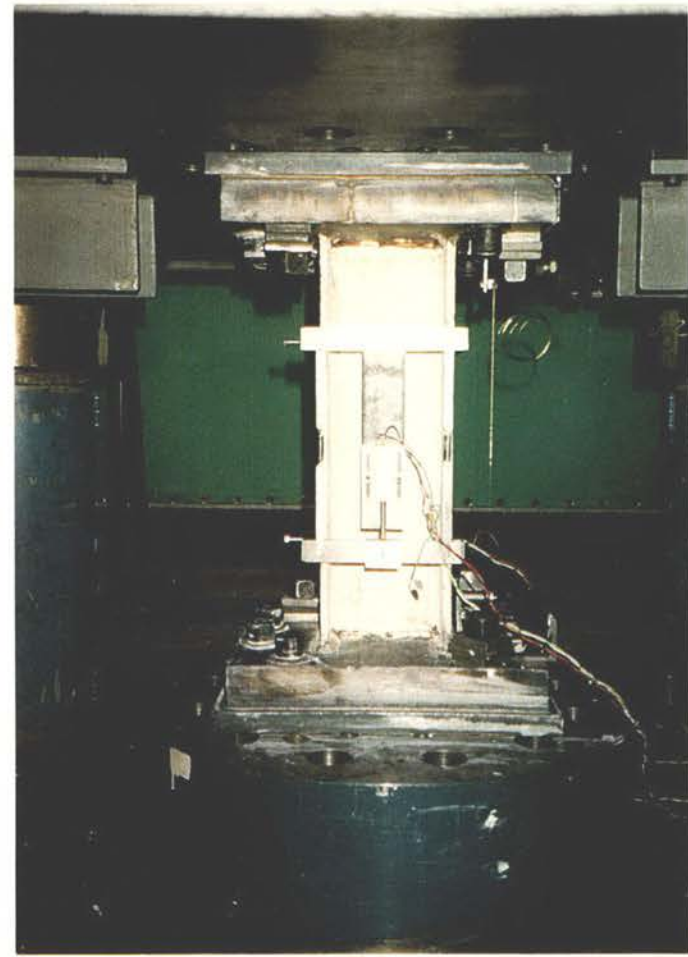
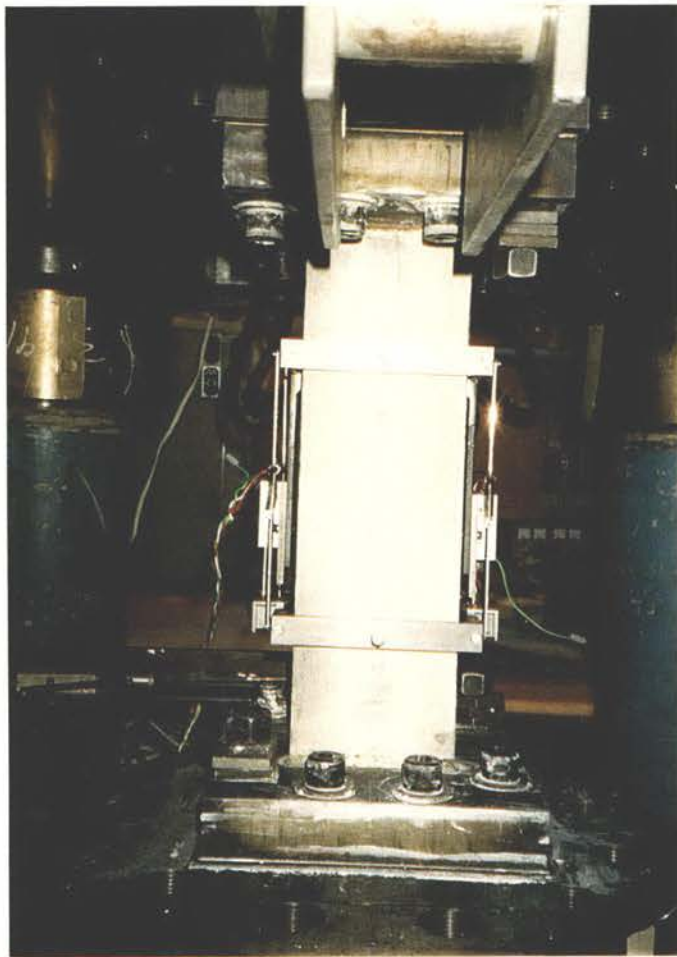
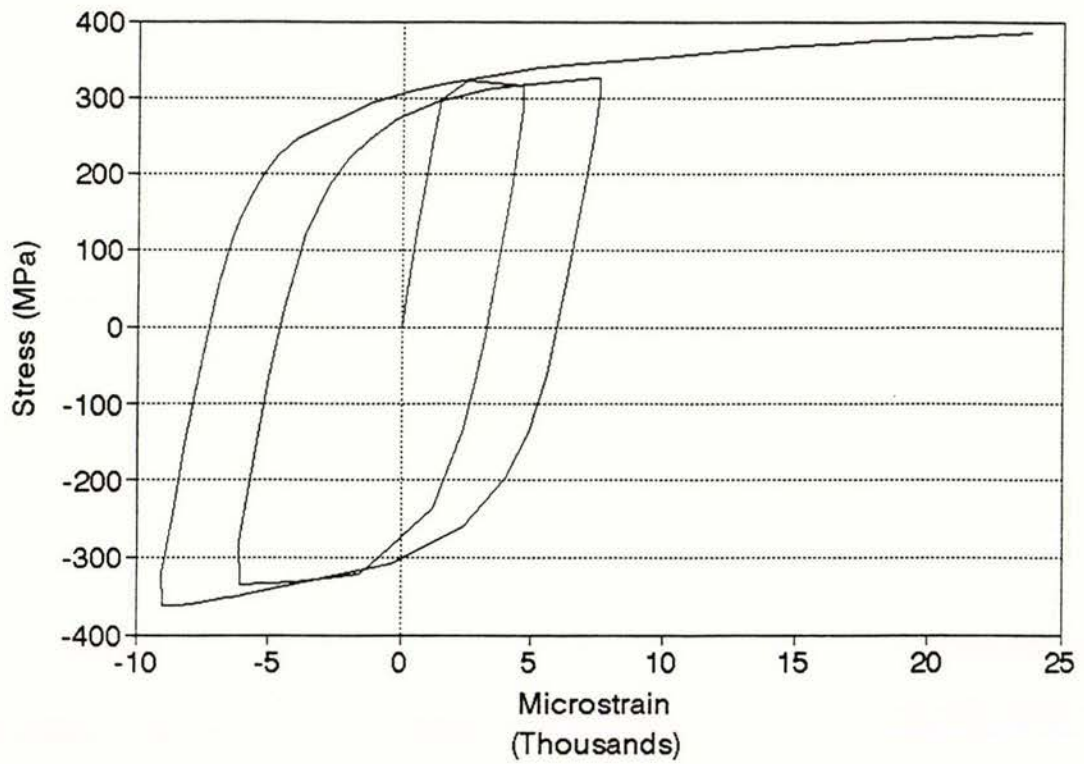
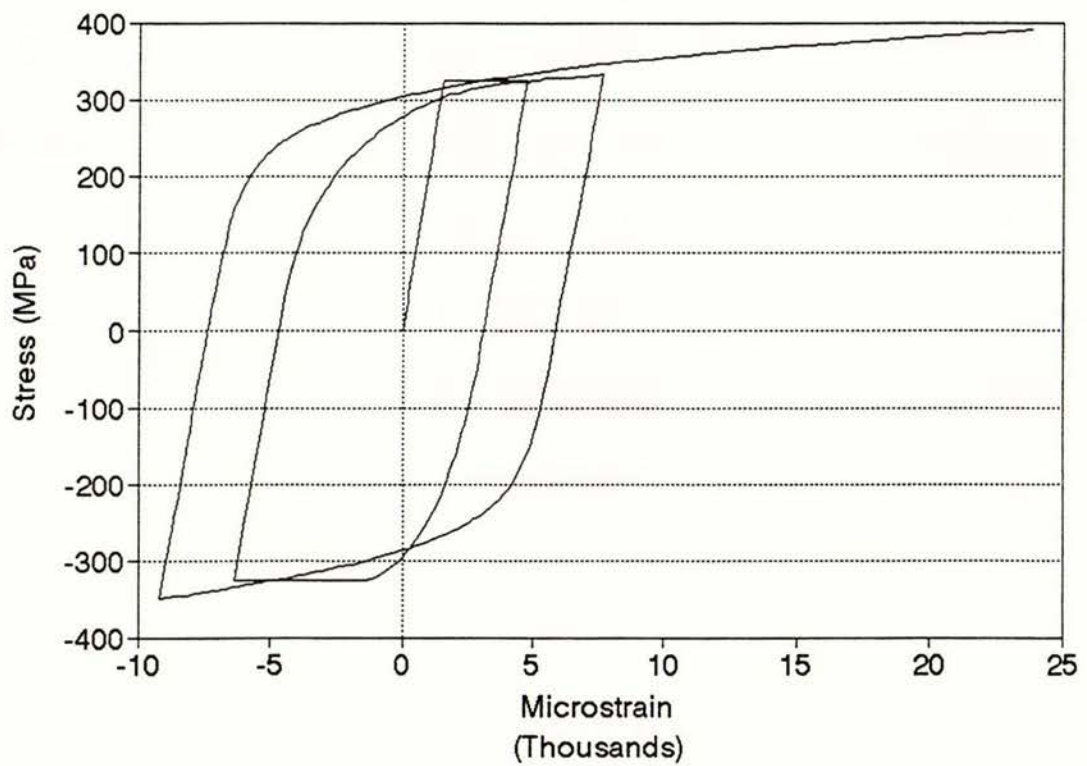


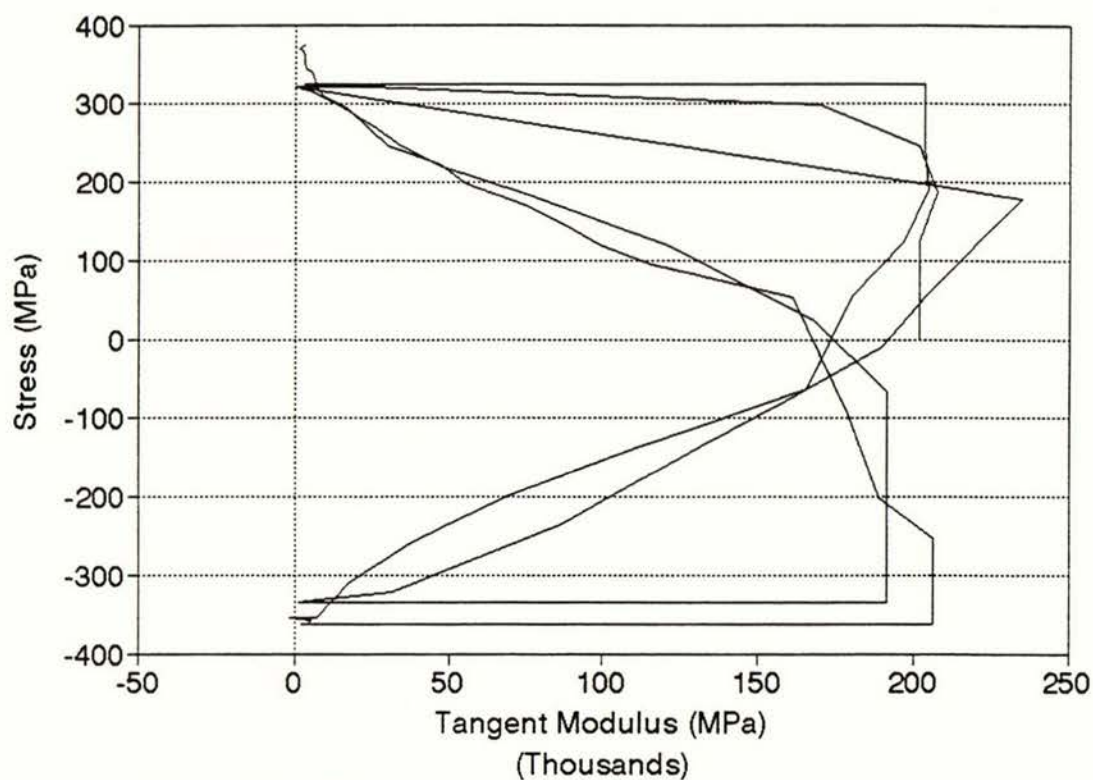
Figure 4.2 Stub column cyclic test set up



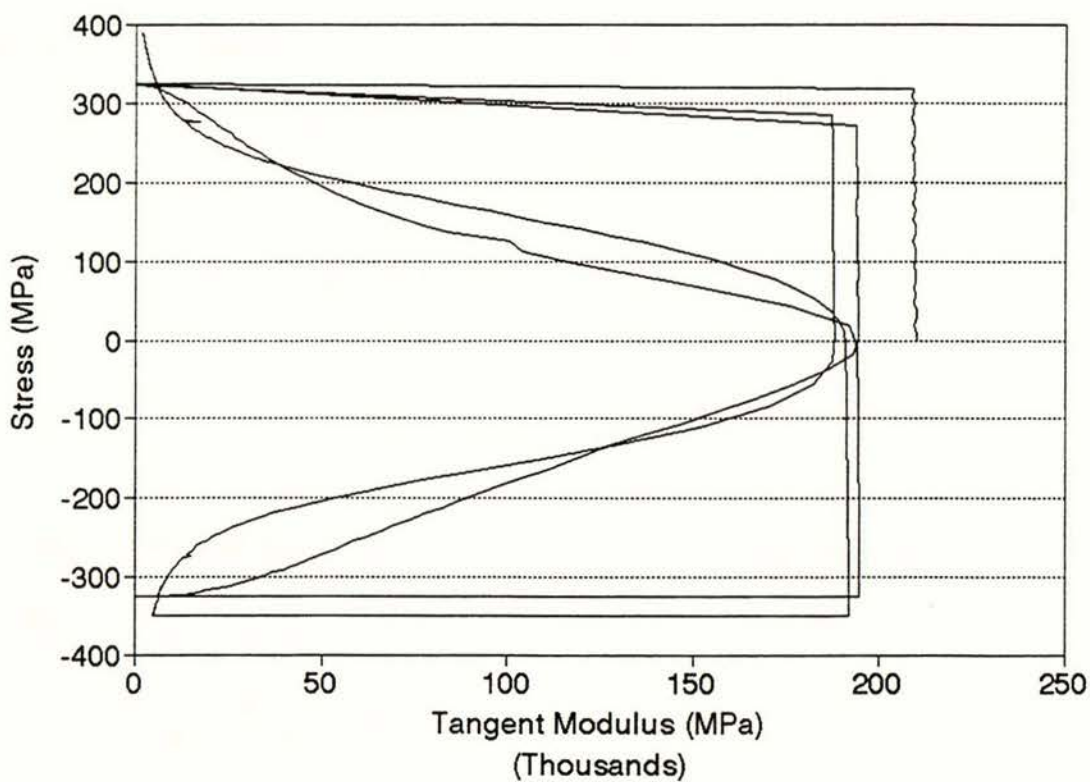
(a) Experimental stress - strain relationship of stub column specimen



(b) Calculated stress - strain relationship of stub column specimen
Figure 4.3 Experimental and calculated stress - strain relationship



(a) Experimental tangent modulus history of stub column specimen



(b) Calculated tangent modulus history of stub column specimen

Figure 4.4 Experimental and calculated tangent modulus history

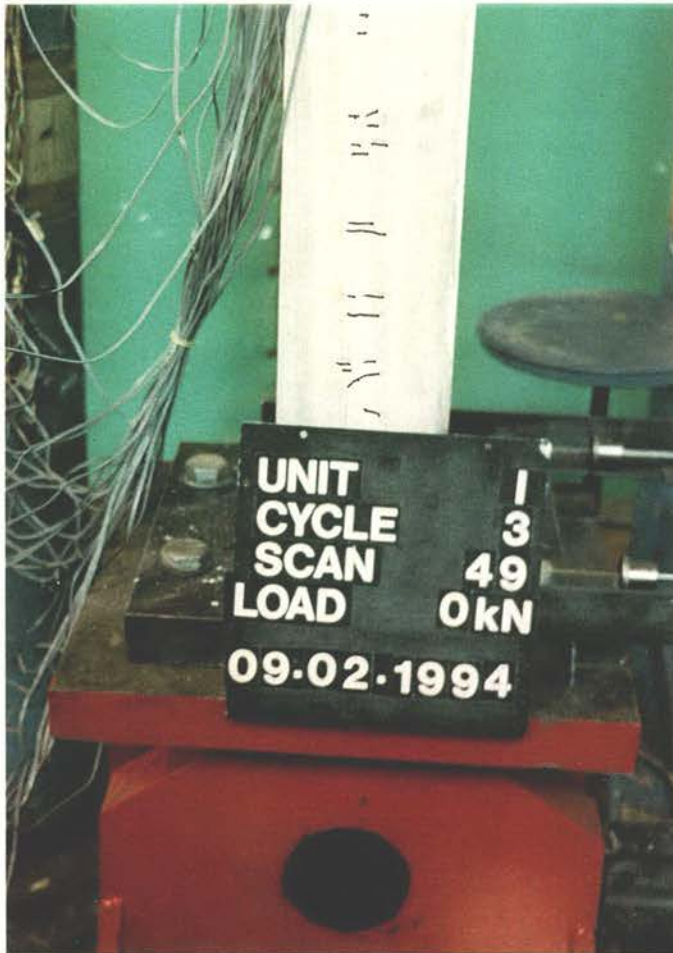


(a) At maximum compressive axial displacement

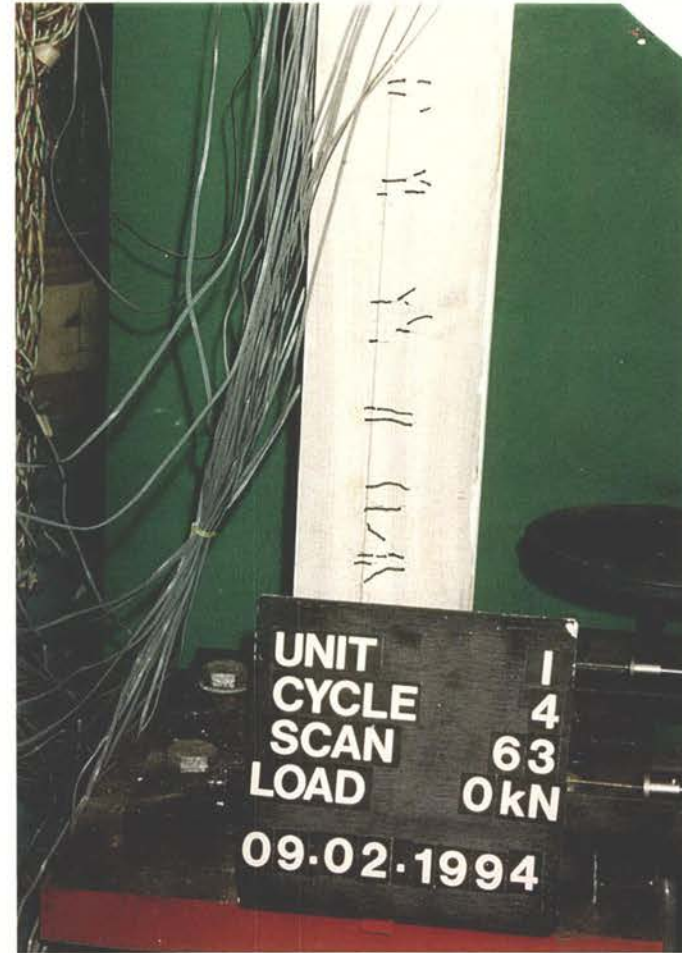


(b) At maximum tensile axial displacement

Figure 4.5 Deflected shape of specimen with fixed-fixed end condition

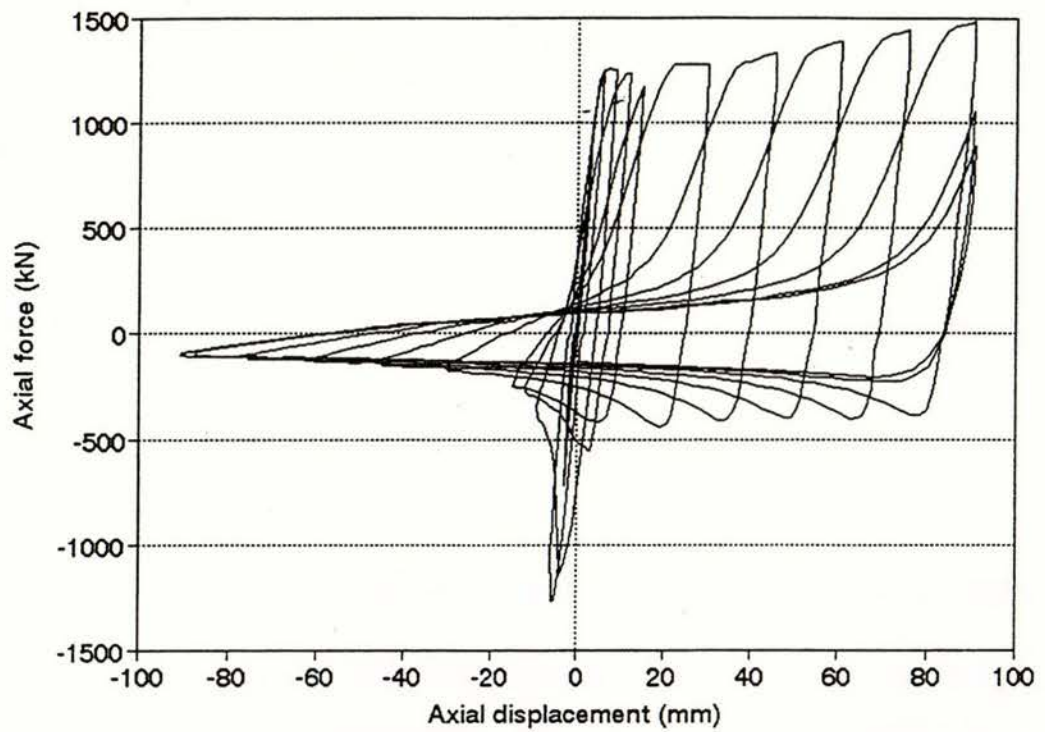


(a) After compression

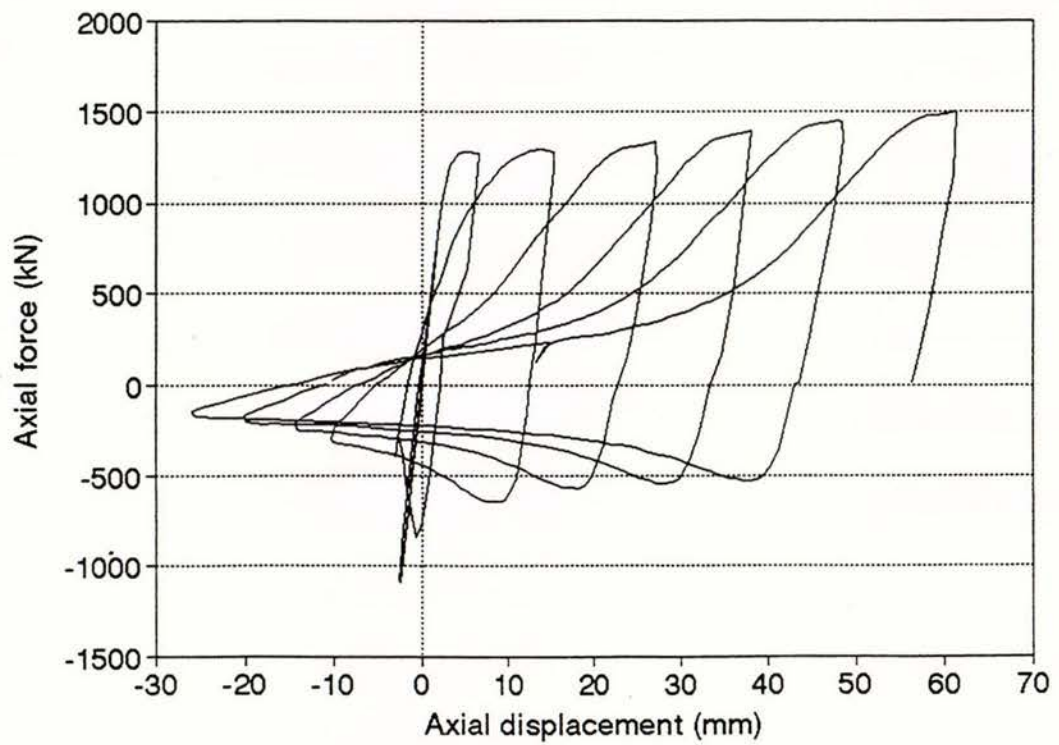


(b) After tension

Figure 4.6 Yield line patterns under compression and tension

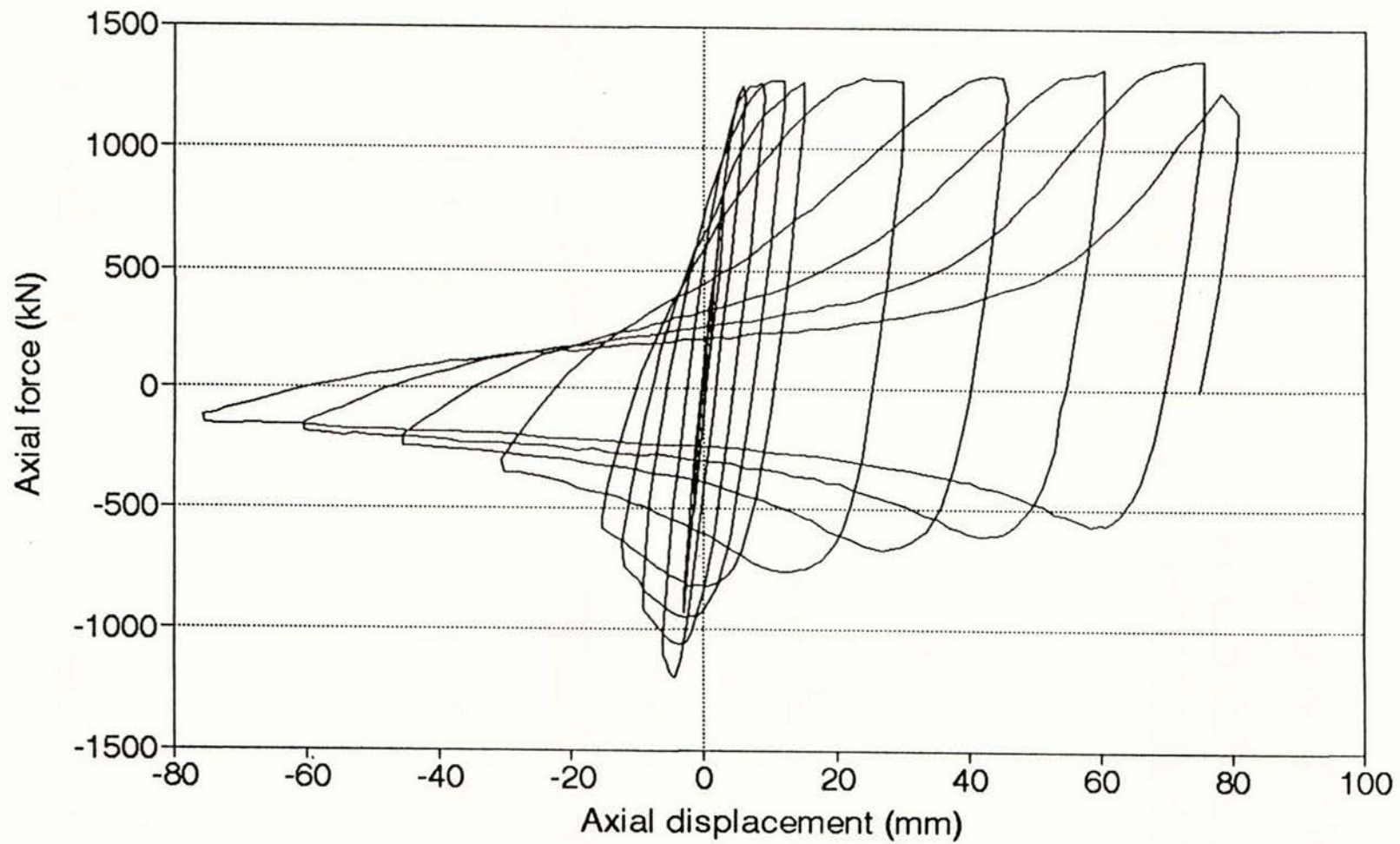


(a) Hysteresis loops from cycle 1 to 13 of specimen 1



(b) Hysteresis loops from cycle 1 to 9 of specimen 2

Figure 4.7 Hysteresis loops of specimen 1, 2, and 3



(c) Hysteresis loops from cycle 1 to 11 of specimen 3

Figure 4.7 Hysteresis loops of specimen 1, 2, and 3

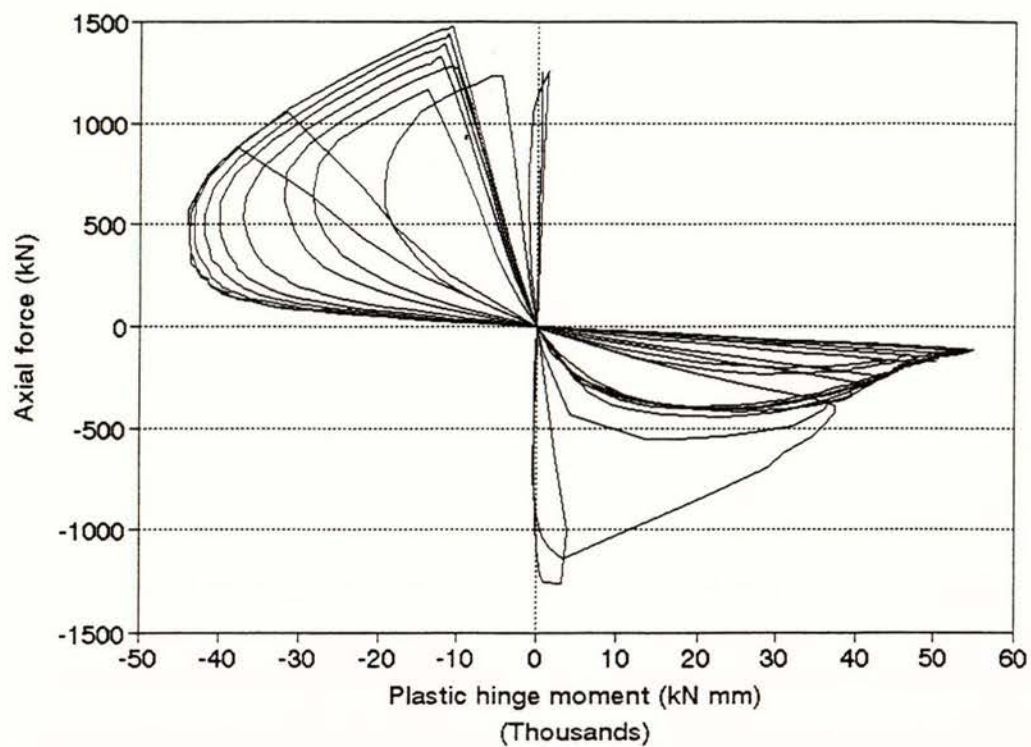


Figure 4.8 Axial force - plastic hinge moment interaction curves of specimen 1.

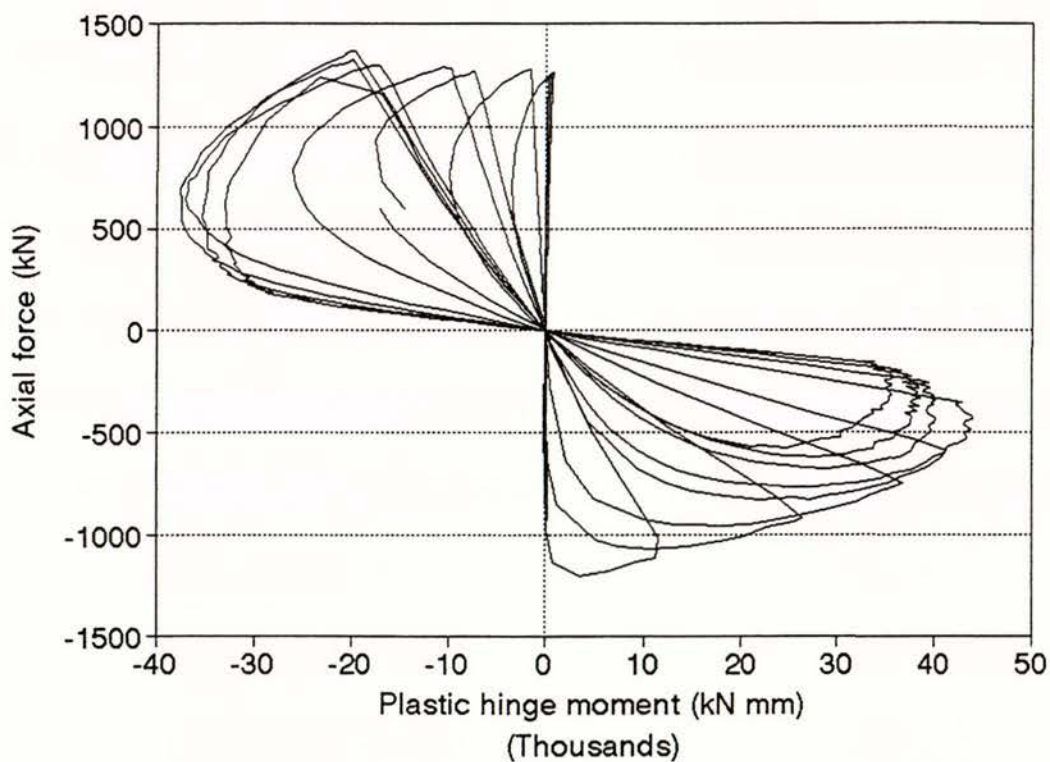
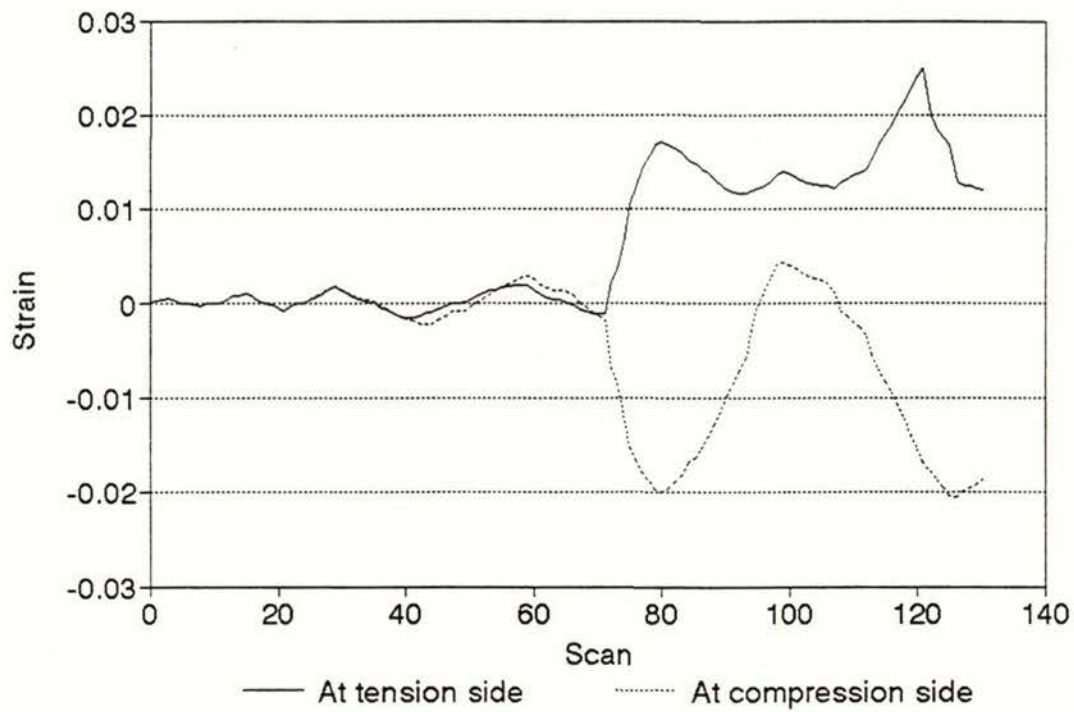
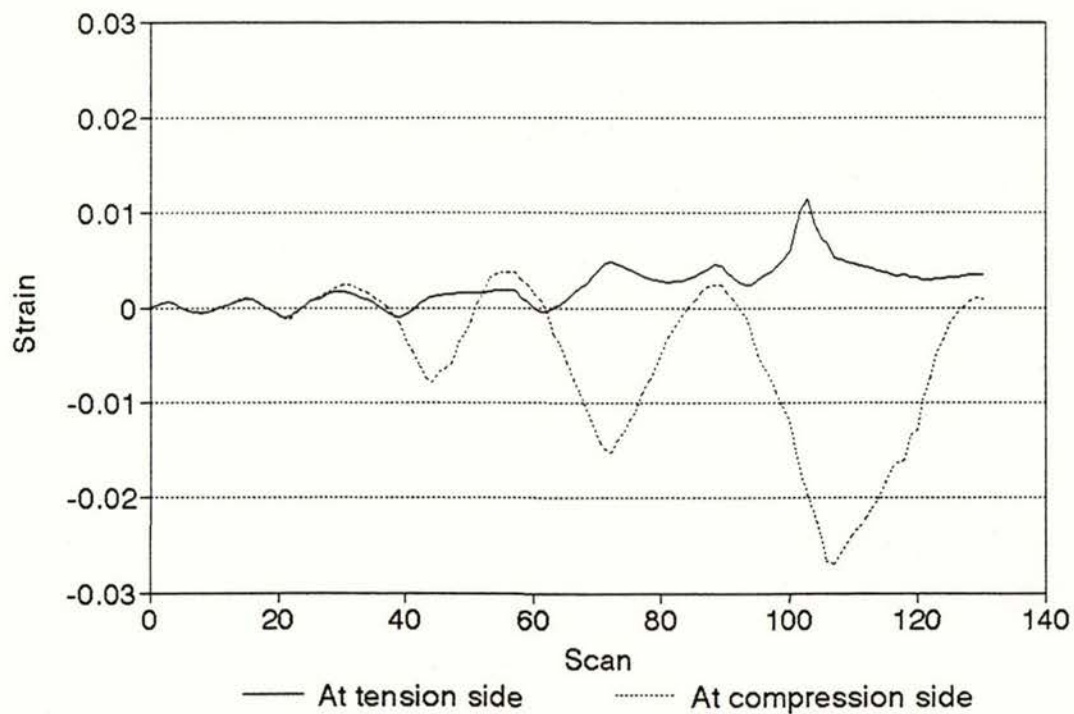


Figure 4.9 Axial force - plastic hinge moment interaction curves of specimen 3.

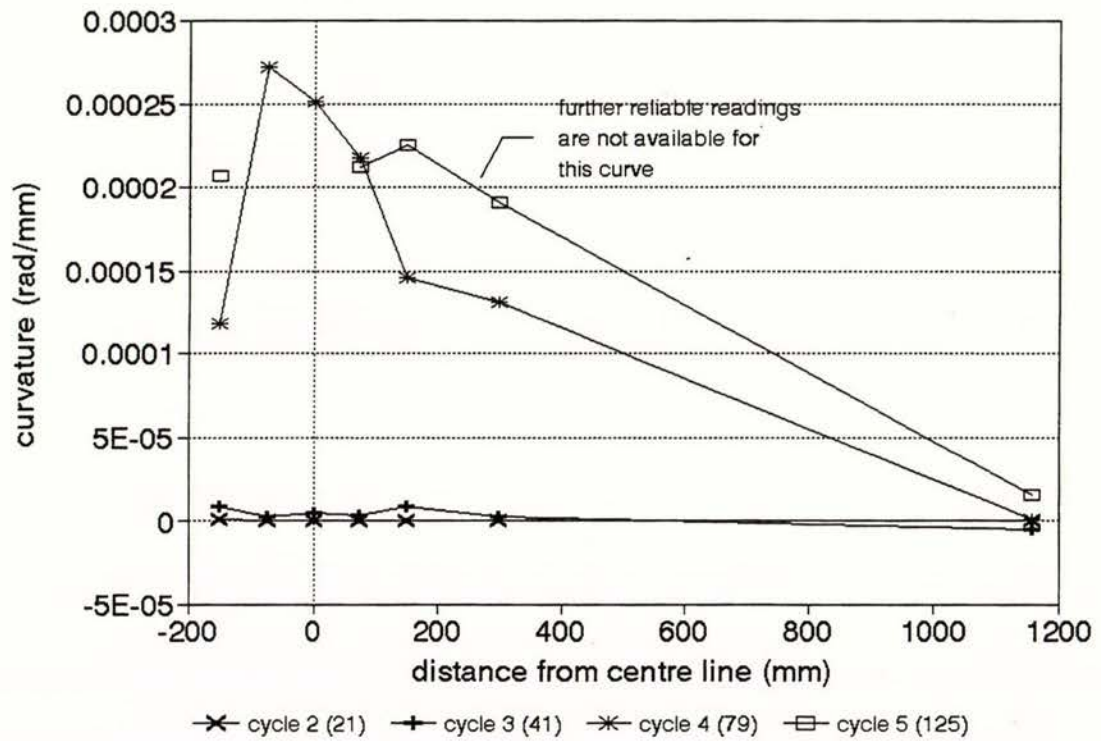


(b) Strain history at top flange of specimen 1

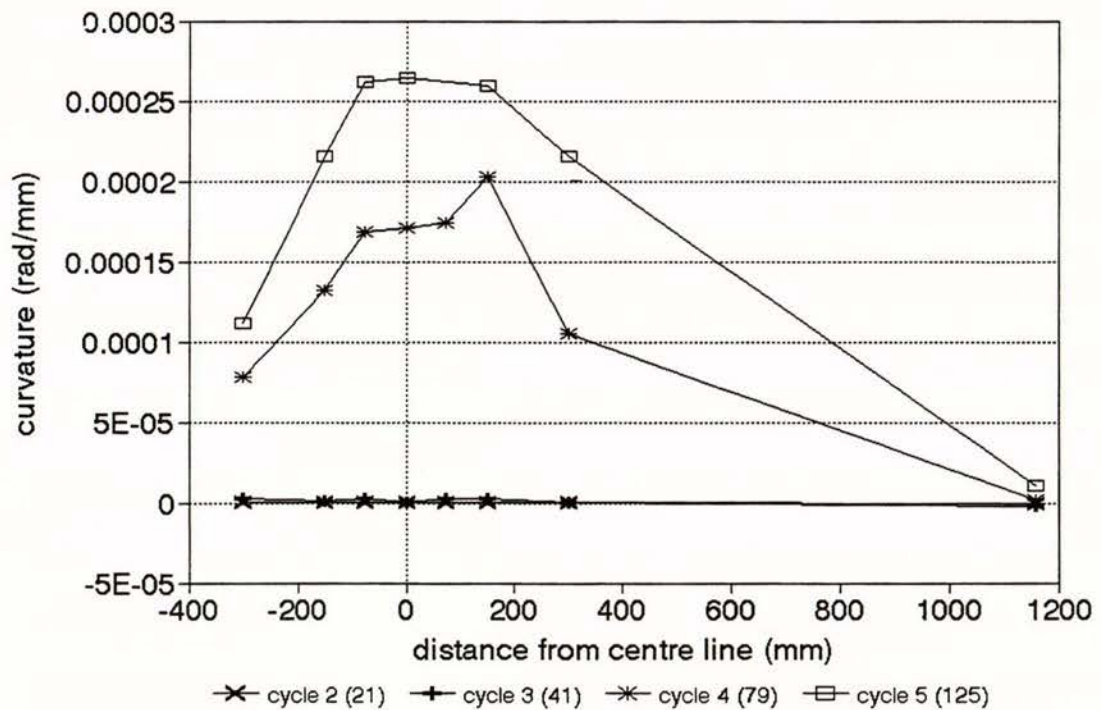


(b) Strain history at top flange of specimen 3

Figure 4.10 Strain history of specimen 1 and 3 at the centre

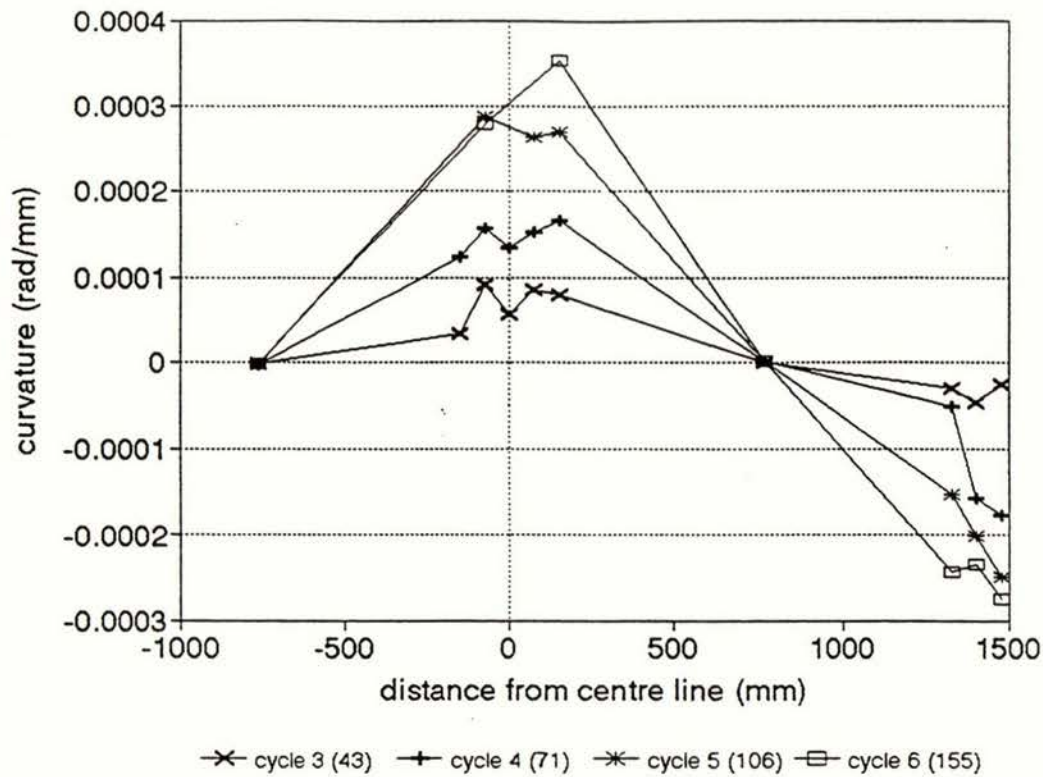


(a) Curvature distribution from cycle 2 to 5 at top flange

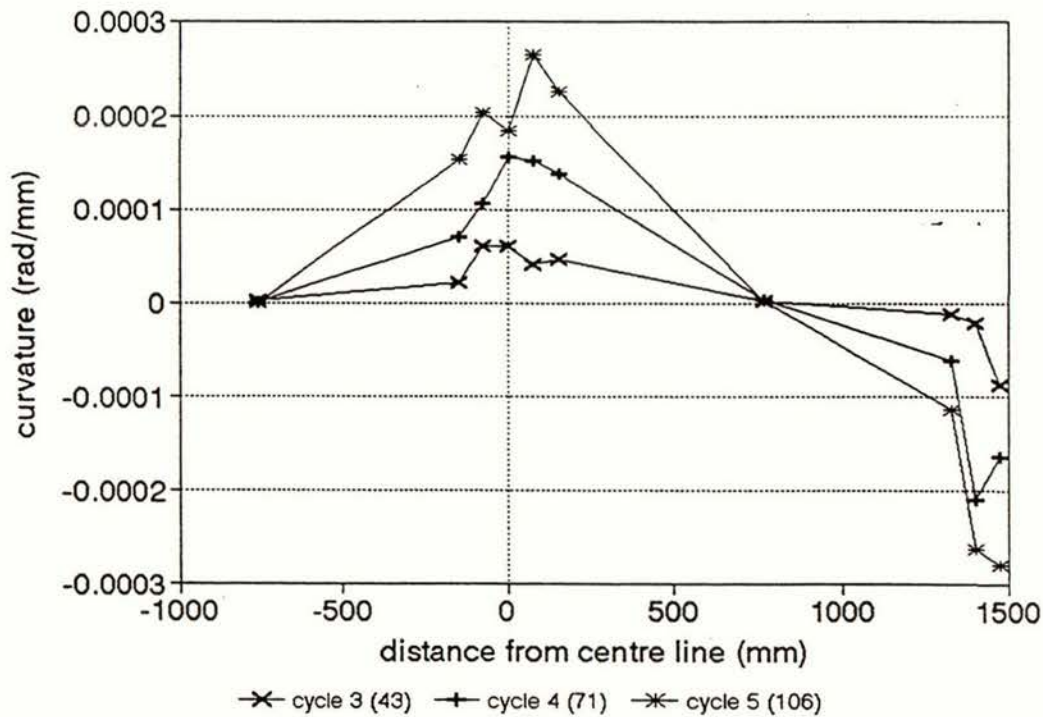


(b) Curvature distribution from cycle 2 to 5 at bottom flange

Figure 4.11 Curvature distribution at load condition C of specimen 1

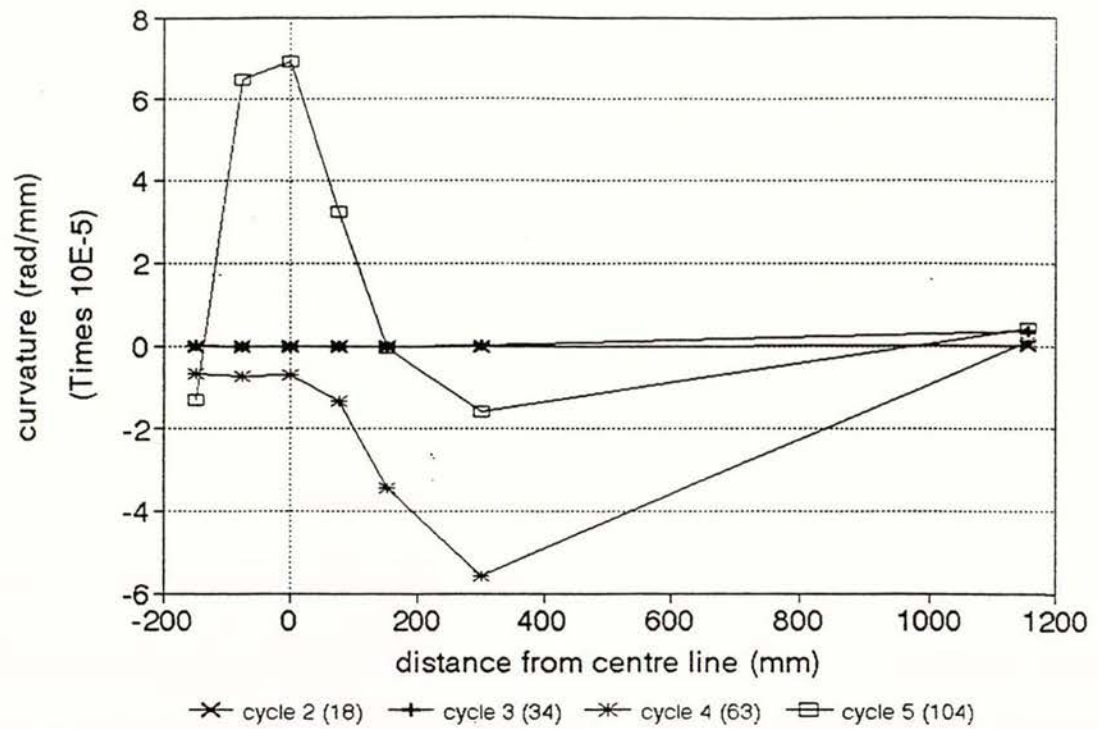


(a) Curvature distribution from cycle 3 to 6 at top flange

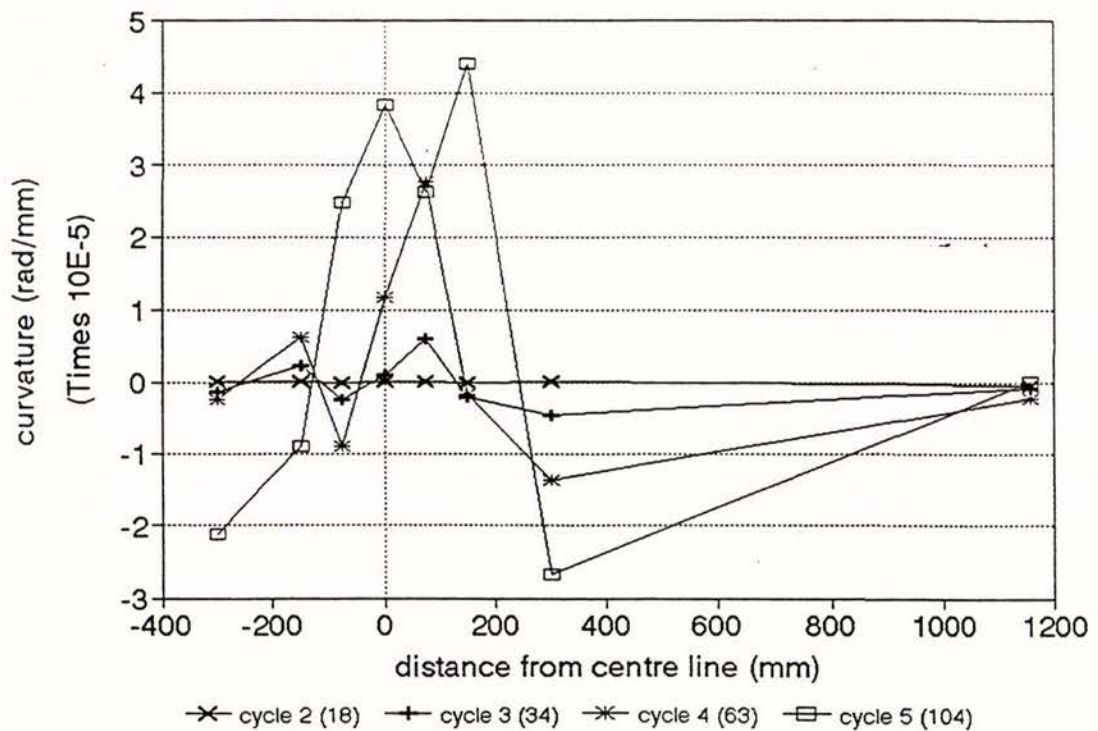


(b) Curvature distribution from cycle 3 to 5 at bottom flange

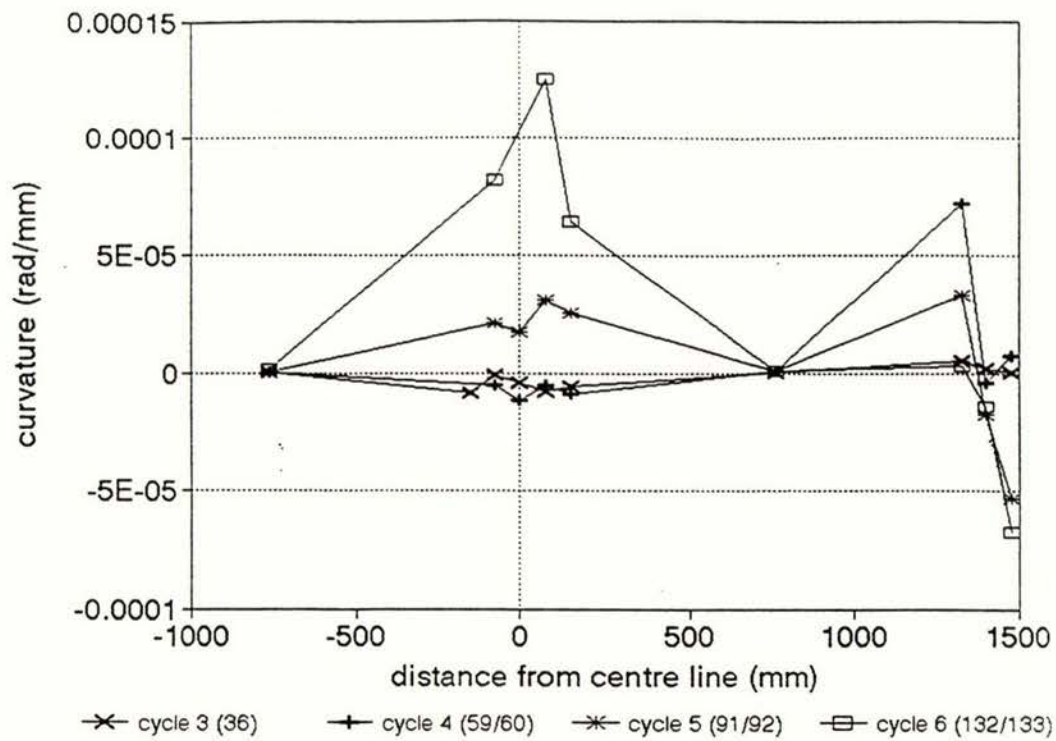
Figure 4.12 Curvature distribution at load condition C of specimen 3



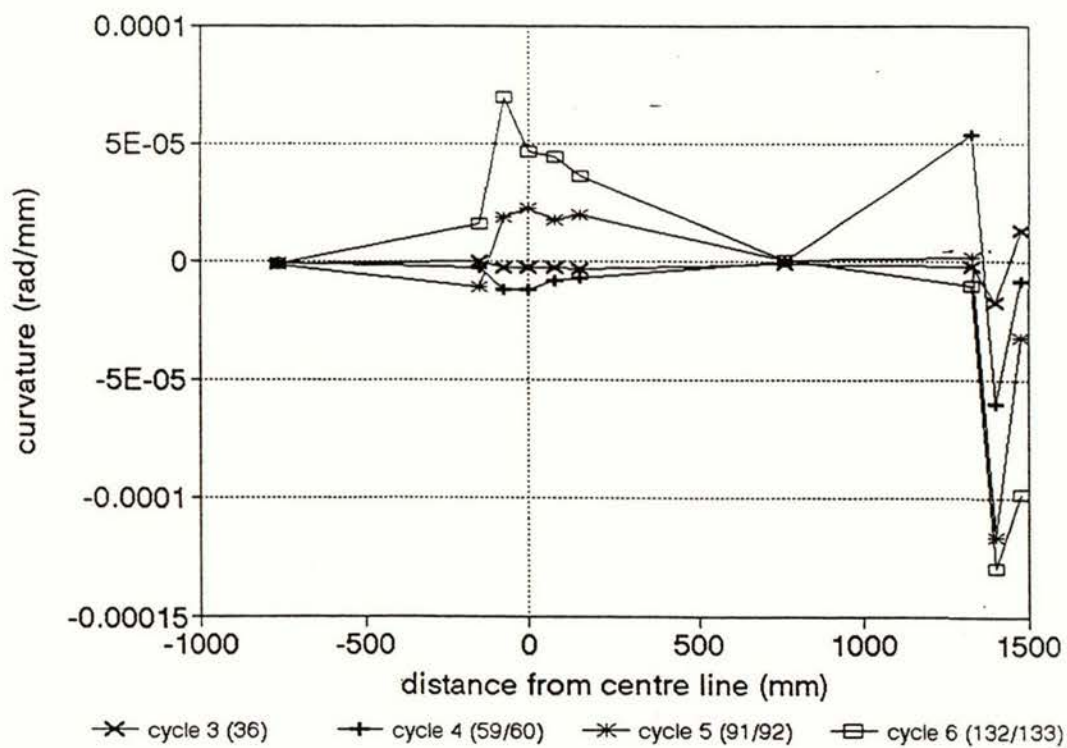
(a) Curvature distribution from cycle 2 to 5 at top flange



(b) Curvature distribution from cycle 2 to 5 at bottom flange
Figure 4.13 Curvature distribution at load condition H of specimen 1



(a) Curvature distribution from cycle 3 to 6 at top flange

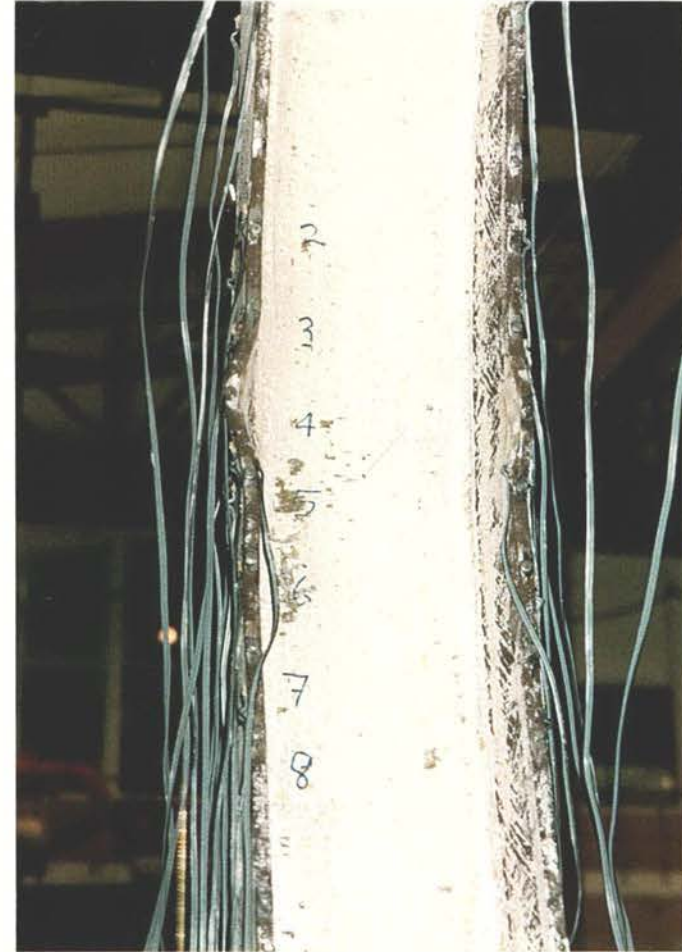


(b) Curvature distribution from cycle 3 to 6 at bottom flange

Figure 4.14 Curvature distribution at load condition H of specimen 3



(a) Overall view at maximum compression of cycle 12



(b) Local buckling at centre hinge

Figure 4.15 Local buckling of specimen 1



(a) Overall view at maximum compression of cycle 8

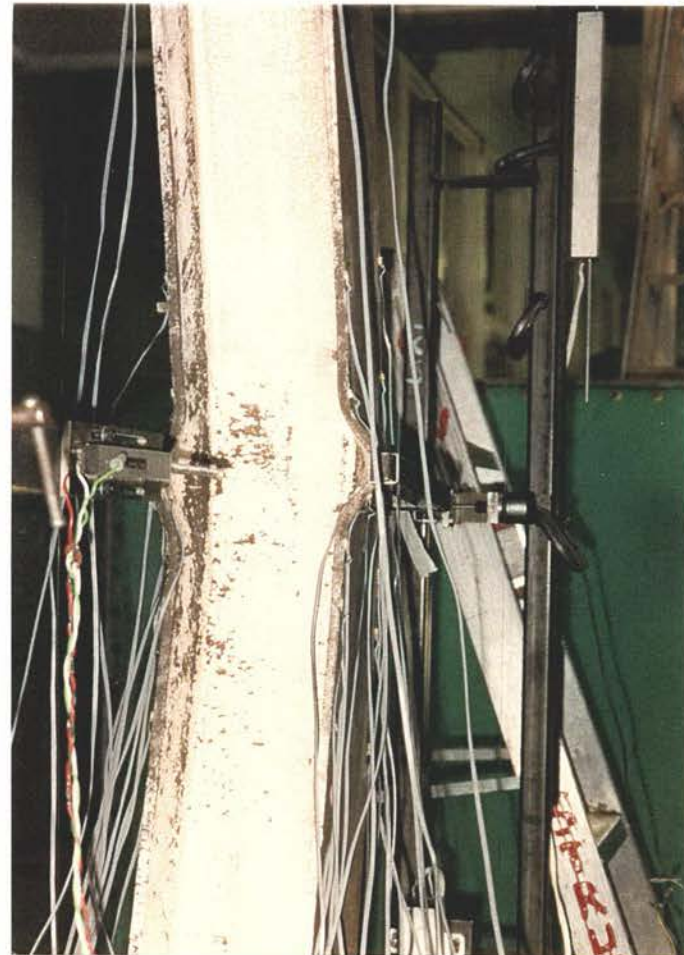


(b) Local buckling at centre hinge in cycle 8

Figure 4.16 Local buckling of specimen 2



(c) Restraightening of local buckling in cycle 9

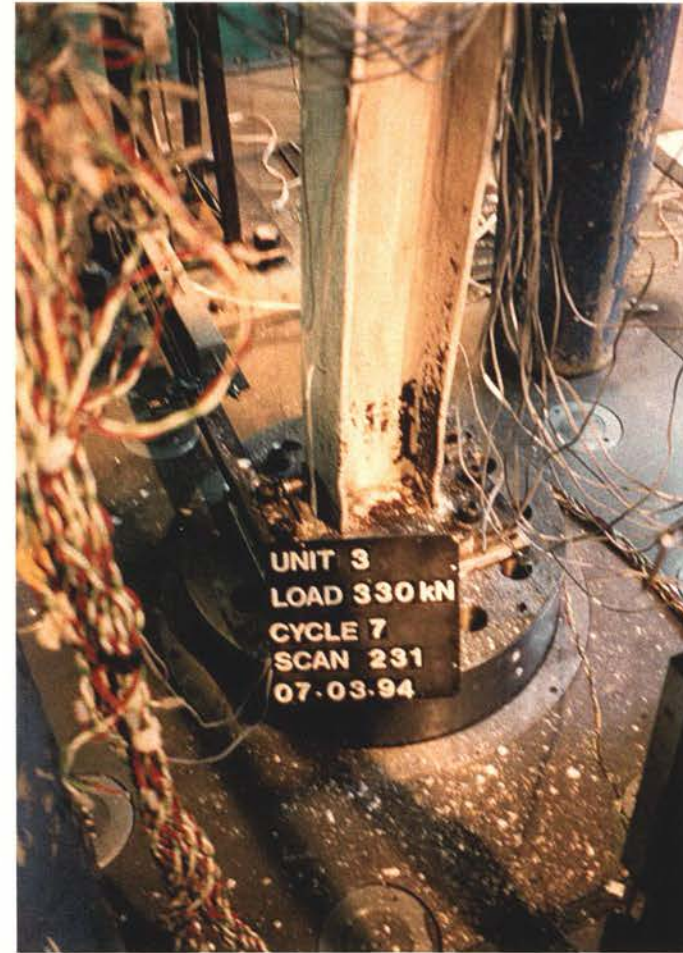


(d) Reappearance of local buckling in cycle 9

Figure 4.16 Local buckling of specimen 2



(a) Overall view at maximum compression of cycle 7

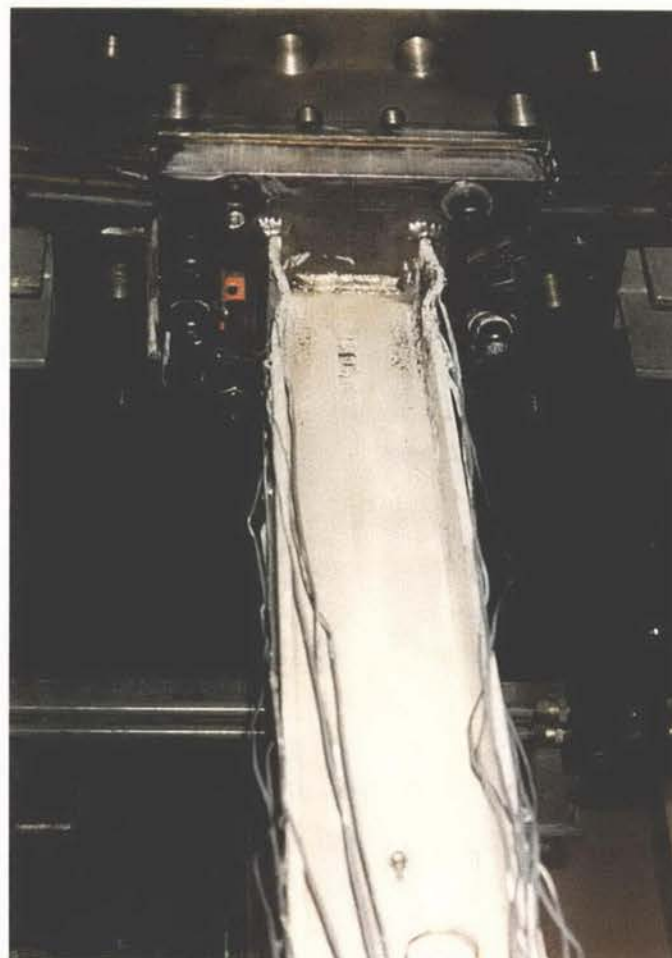


(b) Local buckling at bottom hinge in cycle 7

Figure 4.17 Local buckling of specimen 3



(c) Local buckling at centre hinge in cycle 7



(d) Local buckling at top hinge in cycle 7

Figure 4.17 Local buckling of specimen 3



(e) Overall view at maximum compression of cycle 8



(f) Local buckling at centre hinge in cycle 8

Figure 4.17 Local buckling of specimen 3

CHAPTER 5

DISCUSSION

5.1 INTRODUCTION

This chapter discusses the data preparation for the Ikeda refined physical theory brace model and compares the analytical results with the experimental results. The analytical model was implemented in a spreadsheet program. There are several advantages in developing the analytical model in a spreadsheet program as a preliminary stage, before it is written in a programming language. It allows the execution of the calculation in a step by step fashion without worrying about the automation of the procedure and it helps the analyst to become familiar with the analytical model.

5.2 INPUT DATA FOR ANALYSIS

5.2.1 Axial force - plastic hinge moment relationship

Table 5.1 summarizes the formulas for the fully theoretical plastic interaction curve. The formulas were derived on the assumption of linear distribution of plastic strains and rigid-perfectly plastic material properties. By equating these theoretical formulas in Table 5.1 with the empirical ones in Section 2.3.1, the coefficients of the empirical axial force - plastic hinge moment interaction curve can be obtained as follows:

$$a_2 = 1 - \left(\frac{A_w}{2A_f} \right)^2$$

$$b_2 = \left(\frac{A A_w}{2 A_f^2} \right)$$

$$c_2 = - \left(\frac{A_w}{2A_f} \right)^2 \quad (5.1)$$

$$a_1 = 0, \quad b_1 = 0 \quad (5.2)$$

To better represent the experimental P - M interaction curves, the theoretical interaction curves were adjusted by the coefficients $\alpha_t = \alpha_c = 1.3$ as shown in table 5.2.

5.2.2 Hysteretic behaviour of the tangent modulus of elasticity

The parameters e_1 , e_2 , e_3 , and e_4 determine the slope of the hysteresis loops. Larger values relate to fuller loops, while smaller values relate to pinched ones. For a slender specimen the tension side of the plastic hinge experiences a larger cumulative tensile strain because of the relatively lower level of axial buckling load in compression. This larger cumulative tensile strain is one of the reasons for the more severe deterioration of the tangent modulus of elasticity in a slender member that causes the pinched hysteresis curves in the tension range.

The values of these parameters is shown in Table 5.2.

5.2.3 Axial force plastic hinge rotation curve

In zone EL2, θ decreases following the straight line, where this line is defined by the zero crossing point of zone EL1 and the point having the coordinate $(0, \beta)$. β is used as the empirical parameter, to incorporate the degradation of θ in zone EL2 for axial force - plastic hinge rotation curve.

An additional parameter is introduced in this report following the observation, that the specimen was not perfectly straight, even under yield load. This additional parameter is the minimum plastic hinge rotation after buckling. This parameter is a function of several variables, such as the maximum hinge rotation angle reached in previous cycles and the maximum axial displacement applied. In this report it is taken as a constant, with the consequence that the buckling load is constant, after the corresponding cycle at which this parameter is started to be applied, every time the axial load reaches the yield load.

5.2.4 Effect of boundary condition

Two types of boundary condition, pinned-pinned and fixed-fixed, were used in these test. There are three plastic hinges which are at both ends and at the centre of the specimen for fixed-fixed boundary condition. The plastic hinge at the ends is half as effective as the plastic hinge at the centre in contributing to total axial displacement because of the restraint from the end plates. Half of the actual specimen length was used in the spreadsheet calculations and the resulting axial displacement was multiplied by a factor of two to give the total displacement.

5.3 COMPARISON OF ANALYTICAL RESULTS WITH EXPERIMENTAL RESULTS

The calculation of analytical results was based on Ikeda's refined physical theory brace model. Table 5.3 shows the analytical results of specimen 3. Table 5.4 shows the numerical integration for one of plastic hinge axial displacements in Table 5.3.

5.3.1 Axial force - axial displacement curves

Figures 5.1 to 5.3 compare the analytical axial force versus axial displacement curves with the experimental curves for specimen 1 to 3 with slenderness ratios of 80, 60, and 40 respectively.

The following points can be summarized from the comparison:

1. The analytical $P-\delta$ curves have sharper and larger peaks than the experimental curves in tension during later cycles with large axial displacement values. This was caused by the fact that the model did not take into account the effect of strain hardening.
2. The buckling loads of the analytical curves are larger than the experimental curves. In the model the buckling load is a function of the tangent modulus and the residual plastic hinge rotation angle. The buckling load in the model will be the same after the brace experiences yield load because the tangent

modulus history is unchanged with cycling and the residual plastic hinge rotation angle is also the same every time the axial load reaches the yield load. In reality the tangent modulus history deteriorates with cycling and the residual plastic hinge rotation angle changes with the history of the axial displacement applied. The Ikeda model does not take into account this reduction in tangent modulus.

5.3.2 Axial force - plastic hinge moment curves

Figures 5.4 and 5.5 compare the analytical and experimental axial force versus plastic hinge moment interaction curves for specimen 1 and 3, and Figure 5.8 shows the analytical interaction curve for specimen 2.

The following points can be summarized from the comparison:

1. The experimental curves show strain hardening in the later cycles in the form of outward translation of the curve, as shown in the comparison of the analytical and experimental axial force versus plastic hinge moment curves (see Figures 5.4 and 5.5).

This means that the axial load level at the start of zone P2 in Figure 2.1(d), which is the cross point between the elastic and fully plastic axial force versus moment interaction curve, is higher in the experiment compared to the model. This in turn causes the earlier formation of point E, shown in Figure 2.1(a), in the model compared to the experiment.

2. For specimen 1 the slope of experimental yield surfaces in tension is higher than the model which means for the same range of axial load the plastic hinge deformation is smaller than the model. This partly explains the softer analytical hysteresis loops.
3. Figure 5.5(b) shows the effect of local buckling under compressive loads for specimen 3. Each cycle has a loop which has moved closer to the origin of the graph. The experimental loops moved further from the loop for the analytical model which did not allow for local buckling.

5.3.3 Axial force - plastic hinge rotation curves

Figures 5.6 and 5.7 compare the analytical and experimental axial force versus plastic hinge rotation curves for specimen 1 and 3, and Figure 5.9 shows the analytical curves for specimen 2.

The comparison shows the tendency of the maximum plastic hinge rotations in the model to become larger in each cycle than the test results. This partly relates to the deterioration of the tangent modulus history with cycling in the experiment. The geometric axial deformation should be larger to achieve the same total axial deformation to compensate for the smaller contribution from the elastic axial displacement.

5.3.4 Buckling loads and maximum tensile loads


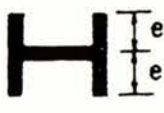
Figure 5.10 compares analytical buckling loads with experimental ones. There are two assumptions that cause the larger values of buckling loads in the model, they are:

1. The specimen is perfectly straight every time the axial load reaches yield load.
2. The tangent modulus history is constant with cyclic loading.

To better represent the experimental results, in the modelling of specimen 3 a minimum plastic hinge rotation angle of 0.0275 is used. This value is chosen to give the same third buckling load of specimen 3 in the model as in the test.

Figure 5.11 compares analytical maximum tensile loads with experimental ones. The analytical maximum tensile loads are smaller than the experimental loads as expected because of the occurrence of strain hardening in the test.

Table 5.1 Theoretical axial force versus moment interaction curves

Sections	Interaction Curve	Limits	M_p
	$\pm m = 1 - \frac{4}{3}p^2$ $\pm m = \frac{4}{3} \pm \frac{4}{3}p$	$ p < \frac{1}{2}$ $ p > \frac{1}{2}$	$\frac{3}{4}\sigma_y A_e$
	$\pm m = 1$ $\pm m = 1 - \left(\frac{\pm pA - A_w}{2A_f} \right)^2$	$ p < \frac{A_w}{A}$ $ p > \frac{A_w}{A}$	$\sigma_y A_f e$

A_f = Cross-sectional area of flanges

A_w = Cross-sectional area of web

$p = P/P_y$

$m = M/M_p$

Table 5.2 Empirical parameters for specimen 1, 2, and 3

Empirical parameters							
β	1.2	p12	0.6188	a2	0.896	e1	0.15
α_t	1.3	b1	0	b2	0.862	e2	0.9
α_c	1.3	c1	0	c2	-1.791	e3	1.2
$^*(\theta p)_{\min}$	0.02755					e4	0

* For specimen 1 and 2, $(\theta p)_{\min}$ is zero.

Table 5.3 Spreadsheet calculation of Ikeda refined physical theory brace model of specimen 3

Strut 3: 150 UC 30.0

kL = 1528 mm	(alpha)t = 1.3	fy = 315 MPa	I = 5580000 mm ⁴	R = 0.005	delta0 = 0 mm
e = 76.19 mm	(alpha)c = 1.3	E = 200 GPa			delta1 = 0 mm
kL/r = 40		A = 3945 mm ²	Al = 1474 mm ²	alpha = 0.5729407	
beta = 1.2	p12 = 0.6188	b1 = 0	c1 = 0	(theta)pmin = 0.02755	
a2 = 0.896	b2 = 0.862	c2 = -1.791		s1 = -0.75	c1 = 0.9
e1 = 0.15	e2 = 0.9	e3 = 1.2	e4 = 0	s2 = -0.3	c2 = 0.9
Py = 1242.675 kN	Mp = 35375.78 kNmm	(LPy)/(AE) = 2.4066 mm		s3 = 0.3	c3 = 0.9
				s4 = 0.75	c4 = 0.9

P (kN)	p = P/Py	kappa	e	Et (GPa)	M (kN mm)	ML/EI	coth (kappa/2)	theta (radian)	h1(kappa)	(delta)e (mm)	(delta)g (mm)	(delta)ty (mm)	(delta)p (mm)	(delta)m (mm)	(delta)po (mm)	(delta)mo (mm)	delta (mm)	(delta)t (mm)
0	0.00000	0.00000	1.00000	200.000	0	0.000000	NA	0.000000	0.12500	0.0000	0.0000	0.7380	0.0000	0.0000	0.0000	0.0000	0.7380	1.4760
-350	-0.28165	1.03108	0.68876	137.752	0	0.000000	NA	0.000000	0.15127	-0.6778	0.0000	0.7380	0.0000	0.0000	0.0000	0.0000	0.0602	0.1204
-700	-0.56330	1.75123	0.47752	95.505	0	0.000000	NA	0.000000	0.23791	-1.3556	0.0000	0.7380	0.0000	0.0000	0.0000	0.0000	-0.6176	-1.2353
-800	-0.64377	2.00299	0.41717	83.434	0	0.000000	NA	0.000000	0.31261	-1.5493	0.0000	0.7380	0.0000	0.0000	0.0000	0.0000	-0.8113	-1.6226
-1000	-0.80472	2.65648	0.29646	59.293	0	0.000000	NA	0.000000	1.27355	-1.9366	0.0000	0.7380	0.0000	0.0000	0.0000	0.0000	-1.1986	-2.3973
-1242.68	-1.00000	4.16322	0.15000	29.999	0	0.000000	NA	0.000000	0.20792	-2.4066	0.0000	0.7380	0.0000	0.0000	0.0000	0.0000	-1.6686	-3.3372
-1242.68	-1.00000	1.47191	1.20000	240.000	0	0.000000	NA	0.000000	0.19068	-2.3078	0.0000	0.7380		-0.0988			-1.6686	-3.3372
-1150	-0.92542	1.42934	1.17763	235.525	-8781	-0.010210	NA	0.016464	0.18544	-2.1568	-0.0768	0.7380	-1.5588	0.0000	0.0000	-0.0988	-3.1533	-6.3065
-800	-0.64377	1.23737	1.09313	218.626	-5790	-0.007252		0.016464	0.16610	-1.5595	-0.0688	0.7380	0.0000	0.0000	-1.5588	-0.0988	-2.5480	-5.0960
-500	-0.40236	1.01234	1.02071	204.141	-3444	-0.004620		0.016464	0.15015	-1.0096	-0.0622	0.7380	0.0000	0.0000	-1.5588	-0.0988	-1.9915	-3.9829
-250	-0.20118	0.73798	0.96035	192.071	-1648	-0.002349		0.016464	0.13735	-0.5207	-0.0569	0.7380	0.0000	0.0000	-1.5588	-0.0988	-1.4972	-2.9945
0	0.00000	0.00000	0.90000	180.000	0	0.000000		0.016464	0.12500	0.0000	-0.0518	0.7380	0.0000	0.0000	-1.5588	-0.0988	-0.9714	-1.9429
100	0.08047	0.49916	0.83965	167.929	575	0.000937	4.089552	0.015360	0.12000	0.2227	-0.0433	0.7380	0.0000	0.0000	-1.5588	-0.0988	-0.7402	-1.4804
300	0.24141	0.93434	0.71894	143.788	1406	0.002678	2.294048	0.013152	0.10894	0.7208	-0.0288	0.7380	0.0000	0.0000	-1.5588	-0.0988	-0.2277	-0.4554
600	0.48283	1.52765	0.53788	107.576	1899	0.004835	1.554423	0.009840	0.08927	1.6518	-0.0132	0.7380	0.0000	0.0000	-1.5588	-0.0988	0.7189	1.4378
900	0.72424	2.29715	0.35682	71.363	1597	0.006127	1.223568	0.006527	0.06523	2.9687	-0.0042	0.7380	0.0000	0.0000	-1.5588	-0.0988	2.0448	4.0896
1100	0.88519	3.12198	0.23611	47.222	1065	0.006173	1.092203	0.004319	0.04677	4.2937	-0.0013	0.7380	0.0000	0.0000	-1.5588	-0.0988	3.3727	6.7454
1207	0.97129	3.83684	0.17153	34.306	722	0.005766	1.044074	0.003138	0.03637	5.3190	-0.0005	0.7380	0.0000	0.0000	-1.5588	-0.0988	4.3988	8.7976
1207	0.97129	3.83684	0.17153	34.306	722	0.005766	1.044074	0.003138	0.03637	5.3190	-0.0005	0.7380	0.0000	0.0000	-1.5588	-0.0988	4.3988	8.7976
1207	0.97129	3.83684	0.17153	34.306	722	0.005766	1.044074	0.003138	0.03637		-0.0005							
1207	0.97129	1.45586	1.19139	238.278	1236	0.001420	1.608244	0.003138	0.09172		-0.0014							
1207	0.97129	1.45586	1.19139	238.278	1236	0.001420	1.608244	0.003138	0.09172	2.2500	-0.0014	0.7380	0.0000	3.0698	-1.5588	-0.0988	4.3988	8.7976
1000	0.80472	1.35385	1.14141	228.283	1044	0.001252	1.696308	0.003138	0.09521	1.9063	-0.0014	0.7380	0.0000	0.0000	-1.5588	2.9710	4.0550	8.1100

P (kN)	$p = P/Py$	kappa	e	Et (GPa)	M (kN mm)	ML/EI	coth (kappa/2)	theta (radian)	h1(kappa)	(delta)e (mm)	(delta)g (mm)	(delta)ty (mm)	(delta)p (mm)	(delta)m (mm)	(delta)po (mm)	(delta)mo (mm)	delta (mm)	(delta)t (mm)
750	0.60354	1.20475	1.08106	216.212	804	0.001018	1.856192	0.003138	0.10026	1.4705	-0.0015	0.7380	0.0000	0.0000	-1.5588	2.9710	3.6191	7.2383
500	0.40236	1.01234	1.02071	204.141	553	0.000742	2.141534	0.003138	0.10653	1.0096	-0.0016	0.7380	0.0000	0.0000	-1.5588	2.9710	3.1582	6.3164
250	0.20118	0.73798	0.96035	192.071	287	0.000409	2.831989	0.003138	0.11452	0.5207	-0.0017	0.7380	0.0000	0.0000	-1.5588	2.9710	2.6691	5.3383
0	0.00000	0.00000	0.90000	180.000	0	0.000000	NA	0.003138	0.12500	0.0000	-0.0019	0.7380	0.0000	0.0000	-1.5588	2.9710	2.1483	4.2966
-250	-0.20118	0.83558	0.74912	149.823	-318	-0.000582	NA	0.003138	0.14123	-0.5888	-0.0021	0.7380	0.0000	0.0000	-1.5588	2.9710	1.5592	3.1185
-500	-0.40236	1.32234	0.59823	119.646	-705	-0.001614	NA	0.003138	0.17387	-1.3105	-0.0026	0.7380	0.0000	0.0000	-1.5588	2.9710	0.8370	1.6741
-750	-0.60354	1.87283	0.44735	89.469	-1305	-0.003993	NA	0.003138	0.26863	-2.2431	-0.0040	0.7380	0.0000	0.0000	-1.5588	2.9710	-0.0970	-0.1940
-1080.2	-0.86925	3.01832	0.24806	49.612	-13902	-0.076734	NA	0.003138	17.14347	-4.1353	-0.2579	0.7380	0.0000	0.0000	-1.5588	2.9710	-2.2430	-4.4860
-1080.2	-0.86925	3.01832	0.24806	49.612	-14797	-0.081675	NA	0.003340	17.14347	-4.1353	-0.2922	0.7380	0.0000	0.0000	-1.5588	2.9710	-2.2773	-4.5546
-1080.2	-0.86925	1.39530	1.16078	232.155	-14797	-0.017454	NA	0.029845	0.18152	-2.0412	-0.2470			-2.0941				
-1080.2	-0.86925	3.01832	0.24806	49.612	-14797	-0.081675	NA	0.003340	17.14347		-0.2922							
-1080.2	-0.86925	1.39530	1.16078	232.155	-14797	-0.017454	NA	0.029845	0.18152		-0.2470							
-960	-0.77253	1.33214	1.13176	226.352	-23955	-0.028980	NA	0.055363	0.17484	-1.8381	-0.8189	0.7380	-1.9403	0.0000	-1.5588	0.8318	-4.5863	-9.1727
-700	-0.56330	1.17045	1.06899	213.798	-16763	-0.021470	NA	0.055363	0.16072	-1.3804	-0.7527	0.7380	0.0000	0.0000	-3.4992	0.8318	-4.0625	-8.1249
-500	-0.40236	1.01234	1.02071	204.141	-11581	-0.015534	NA	0.055363	0.15015	-1.0096	-0.7032	0.7380	0.0000	0.0000	-3.4992	0.8318	-3.6422	-7.2845
-300	-0.24141	0.80339	0.97242	194.485	-6709	-0.009447	NA	0.055363	0.13987	-0.6209	-0.6551	0.7380	0.0000	0.0000	-3.4992	0.8318	-3.2053	-6.4107
-200	-0.16094	0.66426	0.94828	189.657	-4392	-0.006342	NA	0.055363	0.13484	-0.4192	-0.6315	0.7380	0.0000	0.0000	-3.4992	0.8318	-2.9801	-5.9602
0	0.00000	0.00000	0.90000	180.000	0	0.000000	NA	0.055363	0.12500	0.0000	-0.5854	0.7380	0.0000	0.0000	-3.4992	0.8318	-2.5148	-5.0296
200	0.16094	0.73275	0.77929	155.859	3507	0.006161	2.850489	0.047938	0.11465	0.4621	-0.4026	0.7380	0.0000	0.0000	-3.4992	0.8318	-1.8699	-3.7398
400	0.32189	1.12724	0.65859	131.717	5609	0.011660	1.958261	0.040512	0.10283	1.0021	-0.2579	0.7380	0.0000	0.0000	-3.4992	0.8318	-1.1851	-2.3703
600	0.48283	1.52765	0.53788	107.576	6387	0.016259	1.554423	0.033087	0.08927	1.6518	-0.1493	0.7380	0.0000	0.0000	-3.4992	0.8318	-0.4269	-0.8539
800	0.64377	2.00299	0.41717	83.434	6408	0.021031	1.311954	0.027550	0.07376	2.4672	-0.0855	0.7380	0.0000	0.0000	-3.4992	0.8318	0.4523	0.9046
1000	0.80472	2.65648	0.29646	59.293	6884	0.031793	1.150989	0.027550	0.05620	3.5633	-0.0652	0.7380	0.0000	0.0000	-3.4992	0.8318	1.5687	3.1374
1242.675	1.00000	4.16317	0.15000	30.000	0	0.000000	1.031608	0.027550	0.03288	5.7494	-0.0381	0.7380	0.0000	0.0000	-3.4992	0.8318	3.7819	7.5638
1248.246										5.7494	-0.0381	2.8956	0.0000	0.0000	-3.4992	0.8318	5.9395	11.8790
1242.675	1.00000	4.16317	0.15000	30.000	0	0.000000	1.031608	0.027550	0.03288		-0.0381							
1242.675	1.00000	1.47190	1.20000	240.000	0	0.000000	1.595677	0.027550	0.09117		-0.1057							
1248.246	1.00000	1.47190	1.20000	240.000	0	0.000000	1.595677	0.027550	0.09117	2.3078	-0.1057	2.8956	0.0000	3.5092	-3.4992	0.8318	5.9395	11.8790
1000	0.80472	1.35385	1.14141	228.283	0	0.000000	1.696308	0.027550	0.09521	1.9063	-0.1104	2.8956	0.0000	0.0000	-3.4992	4.3410	5.5333	11.0666
800	0.64377	1.23737	1.09313	218.626	0	0.000000	1.817481	0.027550	0.09916	1.5595	-0.1150	2.8956	0.0000	0.0000	-3.4992	4.3410	5.1820	10.3640
600	0.48283	1.09607	1.04485	208.970	0	0.000000	2.003816	0.027550	0.10385	1.1971	-0.1204	2.8956	0.0000	0.0000	-3.4992	4.3410	4.8142	9.6283
400	0.32189	0.91636	0.99657	199.313	0	0.000000	2.333169	0.027550	0.10948	0.8176	-0.1270	2.8956	0.0000	0.0000	-3.4992	4.3410	4.4281	8.8562
200	0.16094	0.66426	0.94828	189.657	0	0.000000	3.120779	0.027550	0.11638	0.4192	-0.1350	2.8956	0.0000	0.0000	-3.4992	4.3410	4.0217	8.0434
0	0.00000	0.00000	0.90000	180.000	0	0.000000	NA	0.027550	0.12500	0.0000	-0.1450	2.8956	0.0000	0.0000	-3.4992	4.3410	3.5925	7.1850

P (kN)	p = P/Py	kappa	e	Et (GPa)	M (kN mm)	ML/EI	coth (kappa/2)	theta (radian)	h1(kappa)	(delta)e (mm)	(delta)g (mm)	(delta)ty (mm)	(delta)p (mm)	(delta)m (mm)	(delta)po (mm)	(delta)mo (mm)	delta (mm)	(delta)t (mm)
-200	-0.16094	0.73275	0.77929	155.859	-2204	-0.003873	NA	0.027550	0.13716	-0.4621	-0.1591	2.8956	0.0000	0.0000	-3.4992	4.3410	3.1163	6.2326
-500	-0.40236	1.32234	0.59823	119.646	-6192	-0.014171	NA	0.027550	0.17387	-1.3105	-0.2016	2.8956	0.0000	0.0000	-3.4992	4.3410	2.2253	4.4506
-800	-0.64377	2.00299	0.41717	83.434	-13136	-0.043113	NA	0.027550	0.31261	-2.4672	-0.3626	2.8956	0.0000	0.0000	-3.4992	4.3410	0.9077	1.8153
-958	-0.77092	2.49559	0.32181	64.362	-24139	-0.102702	NA	0.027550	0.76998	-3.3000	-0.8930	2.8956	0.0000	0.0000	-3.4992	4.3410	-0.4555	-0.9111
-958	-0.77092	2.49559	0.32181	64.362	-24094	-0.102510	NA	0.027499	0.76998	-3.3000	-0.8897	2.8956	0.0000	0.0000	-3.4992	4.3410	-0.4522	-0.9044
-958	-0.77092	1.33104	1.13128	226.255	-24094	-0.029161	NA	0.055819	0.17473	-1.8347	-0.8319			-1.4653				
-958	-0.77092	2.49559	0.32181	64.362	-24094	-0.102510	NA	0.027499	0.76998		-0.8897							
-958	-0.77092	1.33104	1.13128	226.255	-24094	-0.029161	NA	0.055819	0.17473		-0.8319							
-925	-0.74436	1.31254	1.12331	224.662	-26335	-0.032099	NA	0.063509	0.17292	-1.7780	-1.0657	2.8956	-0.5221	0.0000	-3.4992	2.8179	-1.1514	-2.3028
-870	-0.70010	1.28051	1.11003	222.006	-29814	-0.036774	NA	0.077103	0.16990	-1.6826	-1.5433	2.8956	-1.3816	0.0000	-3.4992	2.8179	-2.3932	-4.7864
-635	-0.51099	1.12306	1.05330	210.660	-35376	-0.045985	NA	0.130177	0.15725	-1.2618	-4.0718	2.8956	-2.9222	0.0000	-3.4992	2.8179	-6.0415	-12.0830
-310	-0.24946	0.81565	0.97484	194.968	-16331	-0.022937		0.130177	0.14038	-0.6408	-3.6349	2.8956	0.0000	0.0000	-6.4214	2.8179	-4.9836	-9.9672
0	0.00000	0.00000	0.90000	180.000	0	0.000000		0.130177	0.12500	0.0000	-3.2367	2.8956	0.0000	0.0000	-6.4214	2.8179	-3.9446	-7.8892
200	0.16094	0.73275	0.77929	155.859	6231	0.010947	2.850489	0.112718	0.11465	0.4621	-2.2259	2.8956	0.0000	0.0000	-6.4214	2.8179	-2.4717	-4.9433
400	0.32189	1.12724	0.65859	131.717	9374	0.019488	1.958261	0.095258	0.10283	1.0021	-1.4258	2.8956	0.0000	0.0000	-6.4214	2.8179	-1.1315	-2.2631
600	0.48283	1.52765	0.53788	107.576	9700	0.024692	1.554423	0.077799	0.08927	1.6518	-0.8256	2.8956	0.0000	0.0000	-6.4214	2.8179	0.1182	0.2365
800	0.64377	2.00299	0.41717	83.434	7627	0.025031	1.311954	0.060340	0.07376	2.4672	-0.4103	2.8956	0.0000	0.0000	-6.4214	2.8179	1.3490	2.6980
1000	0.80472	2.65648	0.29646	59.293	3831	0.017692	1.150989	0.042881	0.05620	3.5633	-0.1579	2.8956	0.0000	0.0000	-6.4214	2.8179	2.6975	5.3949
1242.675	1.00000	4.16317	0.15000	30.000	0	0.000000	1.031608	0.027550	0.03288	5.7494	-0.0381	2.8956	0.0000	0.0000	-6.4214	2.8179	5.0034	10.0067
1242.675	1.00000	4.16317	0.15000	30.000	0	0.000000	1.031608	0.027550	0.03288	5.7494	-0.0381	2.8956	0.0000	0.0000	-6.4214	2.8179	5.0034	10.0067
1242.675	1.00000	4.16317	0.15000	30.000	0	0.000000	1.031608	0.027550	0.03288	5.7494	-0.0381	2.8956	0.0000	0.0000	-6.4214	2.8179	5.0034	10.0067
1242.675	1.00000	1.47190	1.20000	240.000	0	0.000000	1.595677	0.027550	0.09117		-0.1057							
1249.091	1.00000	1.47190	1.20000	240.000	0	0.000000	1.595677	0.027550	0.09117	2.3078	-0.1057	5.3807	0.0000	3.5092	-6.4214	2.8179	7.4885	14.9770
1000	0.80472	1.35385	1.14141	228.283	0	0.000000	1.696308	0.027550	0.09521	1.9063	-0.1104	5.3807	0.0000	0.0000	-6.4214	6.3271	7.0823	14.1646
800	0.64377	1.23737	1.09313	218.626	0	0.000000	1.817481	0.027550	0.09916	1.5595	-0.1150	5.3807	0.0000	0.0000	-6.4214	6.3271	6.7310	13.4620
600	0.48283	1.09607	1.04485	208.970	0	0.000000	2.003816	0.027550	0.10385	1.1971	-0.1204	5.3807	0.0000	0.0000	-6.4214	6.3271	6.3632	12.7263
400	0.32189	0.91636	0.99657	199.313	0	0.000000	2.333169	0.027550	0.10948	0.8176	-0.1270	5.3807	0.0000	0.0000	-6.4214	6.3271	5.9771	11.9542
200	0.16094	0.66426	0.94828	189.657	0	0.000000	3.120779	0.027550	0.11638	0.4192	-0.1350	5.3807	0.0000	0.0000	-6.4214	6.3271	5.5707	11.1414
0	0.00000	0.00000	0.90000	180.000	0	0.000000	NA	0.027550	0.12500	0.0000	-0.1450	5.3807	0.0000	0.0000	-6.4214	6.3271	5.1415	10.2830
-200	-0.16094	0.73275	0.77929	155.859	-2204	-0.003873	NA	0.027550	0.13716	-0.4621	-0.1591	5.3807	0.0000	0.0000	-6.4214	6.3271	4.6653	9.3306
-500	-0.40236	1.32234	0.59823	119.646	-6192	-0.014171	NA	0.027550	0.17387	-1.3105	-0.2016	5.3807	0.0000	0.0000	-6.4214	6.3271	3.7743	7.5486
-800	-0.64377	2.00299	0.41717	83.434	-13136	-0.043113	NA	0.027550	0.31261	-2.4672	-0.3626	5.3807	0.0000	0.0000	-6.4214	6.3271	2.4567	4.9133

P (kN)	p = P/Py	kappa	e	Et (GPa)	M (kN mm)	ML/EI	coth (kappa/2)	theta (radian)	h1(kappa)	(delta)e (mm)	(delta)g (mm)	(delta)ty (mm)	(delta)p (mm)	(delta)m (mm)	(delta)po (mm)	(delta)mo (mm)	delta (mm)	(delta)t (mm)
-958	-0.77092	2.49559	0.32181	64.362	-24139	-0.102702	NA	0.027550	0.76998	-3.3000	-0.8930	5.3807	0.0000	0.0000	-6.4214	6.3271	1.0935	2.1869
-958	-0.77092	2.49559	0.32181	64.362	-24094	-0.102510	NA	0.027499	0.76998	-3.3000	-0.8897	5.3807	0.0000	0.0000	-6.4214	6.3271	1.0968	2.1936
-958	-0.77092	1.33104	1.13128	226.255	-24094	-0.029161	NA	0.055819	0.17473	-1.8347	-0.8319			-1.4653				
-958	-0.77092	2.49559	0.32181	64.362	-24094	-0.102510	NA	0.027499	0.76998		-0.8897							
-958	-0.77092	1.33104	1.13128	226.255	-24094	-0.029161	NA	0.055819	0.17473		-0.8319							
-925	-0.74436	1.31254	1.12331	224.662	-26335	-0.032099	NA	0.063509	0.17292	-1.7780	-1.0657	5.3807	-0.5221	0.0000	-6.4214	4.8040	0.3976	0.7952
-870	-0.70010	1.28051	1.11003	222.006	-29814	-0.036774	NA	0.077103	0.16990	-1.6826	-1.5433	5.3807	-1.3816	0.0000	-6.4214	4.8040	-0.8442	-1.6884
-625	-0.50295	1.11546	1.05088	210.177	-35376	-0.046090	NA	0.132479	0.15672	-1.2433	-4.2029	5.3807	-2.9222	0.0000	-6.4214	4.8040	-4.6051	-9.2103
-475	-0.38224	0.98964	1.01467	202.934	-35376	-0.047735	NA	0.178784	0.14885	-0.9620	-7.2701	5.3807	-2.9222	0.0000	-6.4214	4.8040	-7.3910	-14.7820
-255	-0.20520	0.74486	0.96156	192.312	-18268	-0.026012		0.178784	0.13760	-0.5308	-6.7204	5.3807	0.0000	0.0000	-9.3436	4.8040	-6.4100	-12.8200
0	0.00000	0.00000	0.90000	180.000	0	0.000000		0.178784	0.12500	0.0000	-6.1051	5.3807	0.0000	0.0000	-9.3436	4.8040	-5.2640	-10.5279
200	0.16094	0.73275	0.77929	155.859	9309	0.016356	2.850489	0.154806	0.11465	0.4621	-4.1984	5.3807	0.0000	0.0000	-9.3436	4.8040	-2.8952	-5.7904
400	0.32189	1.12724	0.65859	131.717	14298	0.029725	1.958261	0.130827	0.10283	1.0021	-2.6893	5.3807	0.0000	0.0000	-9.3436	4.8040	-0.8461	-1.6921
600	0.48283	1.52765	0.53788	107.576	15308	0.038967	1.554423	0.106849	0.08927	1.6518	-1.5573	5.3807	0.0000	0.0000	-9.3436	4.8040	0.9355	1.8711
800	0.64377	2.00299	0.41717	83.434	12867	0.042230	1.311954	0.082870	0.07376	2.4672	-0.7740	5.3807	0.0000	0.0000	-9.3436	4.8040	2.5344	5.0688
1000	0.80472	2.65648	0.29646	59.293	7831	0.036169	1.150989	0.058892	0.05620	3.5633	-0.2979	5.3807	0.0000	0.0000	-9.3436	4.8040	4.1065	8.2131
1242.675	1.00000	4.16317	0.15000	30.000	497	0.004535	1.031608	0.029797	0.03288	5.7494	-0.0446	5.3807	0.0000	0.0000	-9.3436	4.8040	6.5459	13.0918
1242.675	1.00000	4.16317	0.15000	30.000	0	0.000000	1.031608	0.027550	0.03288	5.7494	-0.0381	5.3807	0.0000	0.0000	-9.3436	4.8040	6.5524	13.1047
1264.521										5.7494	-0.0381	13.8424	0.0000	0.0000	-9.3436	4.8040	15.0140	30.0280
1242.675	1.00000	4.16317	0.15000	30.000	0	0.000000	1.031608	0.027550	0.03288		-0.0381							
1242.675	1.00000	1.47190	1.20000	240.000	0	0.000000	1.595677	0.027550	0.09117		-0.1057							
1264.521	1.00000	1.47190	1.20000	240.000	0	0.000000	1.595677	0.027550	0.09117	2.3078	-0.1057	13.8424	0.0000	3.5092	-9.3436	4.8040	15.0140	30.0280
1000	0.80472	1.35385	1.14141	228.283	0	0.000000	1.696308	0.027550	0.09521	1.9063	-0.1104	13.8424	0.0000	0.0000	-9.3436	8.3132	14.6078	29.2156
800	0.64377	1.23737	1.09313	218.626	0	0.000000	1.817481	0.027550	0.09916	1.5595	-0.1150	13.8424	0.0000	0.0000	-9.3436	8.3132	14.2565	28.5130
600	0.48283	1.09607	1.04485	208.970	0	0.000000	2.003816	0.027550	0.10385	1.1971	-0.1204	13.8424	0.0000	0.0000	-9.3436	8.3132	13.8887	27.7773
400	0.32189	0.91636	0.99657	199.313	0	0.000000	2.333169	0.027550	0.10948	0.8176	-0.1270	13.8424	0.0000	0.0000	-9.3436	8.3132	13.5026	27.0052
200	0.16094	0.66426	0.94828	189.657	0	0.000000	3.120779	0.027550	0.11638	0.4192	-0.1350	13.8424	0.0000	0.0000	-9.3436	8.3132	13.0962	26.1924
0	0.00000	0.00000	0.90000	180.000	0	0.000000	NA	0.027550	0.12500	0.0000	-0.1450	13.8424	0.0000	0.0000	-9.3436	8.3132	12.6670	25.3340
-250	-0.20118	0.83558	0.74912	149.823	-2796	-0.005110	NA	0.027550	0.14123	-0.5888	-0.1638	13.8424	0.0000	0.0000	-9.3436	8.3132	12.0593	24.1187
-500	-0.40236	1.32234	0.59823	119.646	-6192	-0.014171	NA	0.027550	0.17387	-1.3105	-0.2016	13.8424	0.0000	0.0000	-9.3436	8.3132	11.2998	22.5996
-750	-0.60354	1.87283	0.44735	89.469	-11455	-0.035059	NA	0.027550	0.26863	-2.2431	-0.3115	13.8424	0.0000	0.0000	-9.3436	8.3132	10.2573	20.5145
-958	-0.77092	2.49559	0.32181	64.362	-24139	-0.102702	NA	0.027550	0.76998	-3.3000	-0.8930	13.8424	0.0000	0.0000	-9.3436	8.3132	8.6190	17.2379

P (kN)	p = P/Py	kappa	e	Et (GPa)	M (kN mm)	ML/EI	coth (kappa/2)	theta (radian)	h1(kappa)	(delta)e (mm)	(delta)g (mm)	(delta)ty (mm)	(delta)p (mm)	(delta)m (mm)	(delta)po (mm)	(delta)mo (mm)	delta (mm)	(delta)t (mm)
-958	-0.77092	2.49559	0.32181	64.362	-24094	-0.102510	NA	0.027499	0.76998	-3.3000	-0.8897	13.8424	0.0000	0.0000	-9.3436	8.3132	8.6223	17.2446
-958	-0.77092	1.33104	1.13128	226.255	-24094	-0.029161	NA	0.055819	0.17473	-1.8347	-0.8319			-1.4653				
-958	-0.77092	2.49559	0.32181	64.362	-24094	-0.102510	NA	0.027499	0.76998		-0.8897							
-958	-0.77092	1.33104	1.13128	226.255	-24094	-0.029161	NA	0.055819	0.17473		-0.8319							
-769	-0.61883	1.21733	1.08565	217.130	-35373	-0.044612	NA	0.105166	0.16442	-1.5044	-2.7786	13.8424	-2.9222	0.0000	-9.3436	6.7901	4.0836	8.1671
-600	-0.48283	1.09607	1.04485	208.970	-35376	-0.046357	NA	0.138574	0.15540	-1.1971	-4.5597	13.8424	-2.9222	0.0000	-9.3436	6.7901	2.6097	5.2195
-400	-0.32189	0.91636	0.99657	199.313	-35376	-0.048603	NA	0.215085	0.14498	-0.8176	-10.2481	13.8424	-2.9222	0.0000	-9.3436	6.7901	-2.6991	-5.3981
-267	-0.21486	0.76104	0.96446	192.892	-35376	-0.050221	NA	0.329938	0.13820	-0.5549	-22.9882	13.8424	-2.9222	0.0000	-9.3436	6.7901	-15.1764	-30.3529
-225	-0.18106	0.70232	0.95432	190.864	-29584	-0.042445		0.329938	0.13609	-0.4701	-22.6368	13.8424	0.0000	0.0000	-12.2658	6.7901	-14.7403	-29.4806
-175	-0.14083	0.62334	0.94225	188.450	-22799	-0.033130		0.329938	0.13359	-0.3680	-22.2213	13.8424	0.0000	0.0000	-12.2658	6.7901	-14.2227	-28.4455
-125	-0.10059	0.53023	0.93018	186.035	-16134	-0.023749		0.329938	0.13111	-0.2646	-21.8090	13.8424	0.0000	0.0000	-12.2658	6.7901	-13.7070	-27.4139
-50	-0.04024	0.33866	0.91207	182.414	-6363	-0.009552		0.329938	0.12743	-0.1069	-21.1964	13.8424	0.0000	0.0000	-12.2658	6.7901	-12.9367	-25.8734
0	0.00000	0.00000	0.90000	180.000	0	0.000000		0.329938	0.12500	0.0000	-20.7920	13.8424	0.0000	0.0000	-12.2658	6.7901	-12.4254	-24.8509
200	0.16094	0.73275	0.77929	155.859	18884	0.033178	2.850489	0.285687	0.11465	0.4621	-14.2986	13.8424	0.0000	0.0000	-12.2658	6.7901	-5.4699	-10.9397
400	0.32189	1.12724	0.65859	131.717	29611	0.061560	1.958261	0.241436	0.10283	1.0021	-9.1589	13.8424	0.0000	0.0000	-12.2658	6.7901	0.2099	0.4197
600	0.48283	1.52765	0.53788	107.576	32747	0.083357	1.554423	0.197185	0.08927	1.6518	-5.3038	13.8424	0.0000	0.0000	-12.2658	6.7901	4.7145	9.4291
800	0.64377	2.00299	0.41717	83.434	29163	0.095713	1.311954	0.152934	0.07376	2.4672	-2.6359	13.8424	0.0000	0.0000	-12.2658	6.7901	8.1979	16.3959
1000	0.80472	2.65648	0.29646	59.293	20273	0.093627	1.150989	0.108683	0.05620	3.5633	-1.0144	13.8424	0.0000	0.0000	-12.2658	6.7901	10.9155	21.8309
1043.8	0.83996	2.84377	0.27003	54.006	17830	0.090407	1.123606	0.098992	0.05211	3.8630	-0.7803	13.8424	0.0000	0.0000	-12.2658	6.7901	11.4492	22.8985
1043.8	0.83996	2.84377	0.27003	54.006	17731	0.089906	1.123606	0.098596	0.05211	3.8630	-0.7741	13.8424	0.0000	0.0000	-12.2658	6.7901	11.4555	22.9109
1143	0.91979	3.37320	0.21016	42.032	9408	0.061291	1.070993	0.066470	0.04261	4.6673	-0.2877	13.8424	2.6988	0.0000	-12.2658	6.7901	15.4451	30.8902
1242.675	1.00000	4.16317	0.15000	30.000	0	0.000000	1.031608	0.027550	0.03288	5.7494	-0.0381	13.8424	6.3812	0.0000	-12.2658	6.7901	20.4591	40.9182
1272.071										5.7494	-0.0381	16.2183	6.3812	0.0000	-12.2658	6.7901	22.8350	45.6700
1242.675	1.00000	4.16317	0.15000	30.000	0	0.000000	1.031608	0.027550	0.03288		-0.0381							
1242.675	1.00000	1.47190	1.20000	240.000	0	0.000000	1.595677	0.027550	0.09117		-0.1057							
1272.071	1.00000	1.47190	1.20000	240.000	0	0.000000	1.595677	0.027550	0.09117	2.3078	-0.1057	16.2183	6.3812	3.5092	-12.2658	6.7901	22.8350	45.6700
1000	0.80472	1.35385	1.14141	228.283	0	0.000000	1.696308	0.027550	0.09521	1.9063	-0.1104	16.2183	0.0000	0.0000	-5.8846	10.2993	22.4288	44.8576
800	0.64377	1.23737	1.09313	218.626	0	0.000000	1.817481	0.027550	0.09916	1.5595	-0.1150	16.2183	0.0000	0.0000	-5.8846	10.2993	22.0775	44.1550
600	0.48283	1.09607	1.04485	208.970	0	0.000000	2.003816	0.027550	0.10385	1.1971	-0.1204	16.2183	0.0000	0.0000	-5.8846	10.2993	21.7097	43.4193
400	0.32189	0.91636	0.99657	199.313	0	0.000000	2.333169	0.027550	0.10948	0.8176	-0.1270	16.2183	0.0000	0.0000	-5.8846	10.2993	21.3236	42.6472
200	0.16094	0.66426	0.94828	189.657	0	0.000000	3.120779	0.027550	0.11638	0.4192	-0.1350	16.2183	0.0000	0.0000	-5.8846	10.2993	20.9172	41.8344
0	0.00000	0.00000	0.90000	180.000	0	0.000000	NA	0.027550	0.12500	0.0000	-0.1450	16.2183	0.0000	0.0000	-5.8846	10.2993	20.4880	40.9760
-200	-0.16094	0.73275	0.77929	155.859	-2204	-0.003873	NA	0.027550	0.13716	-0.4621	-0.1591	16.2183	0.0000	0.0000	-5.8846	10.2993	20.0118	40.0236
-500	-0.40236	1.32234	0.59823	119.646	-6192	-0.014171	NA	0.027550	0.17387	-1.3105	-0.2016	16.2183	0.0000	0.0000	-5.8846	10.2993	19.1208	38.2416

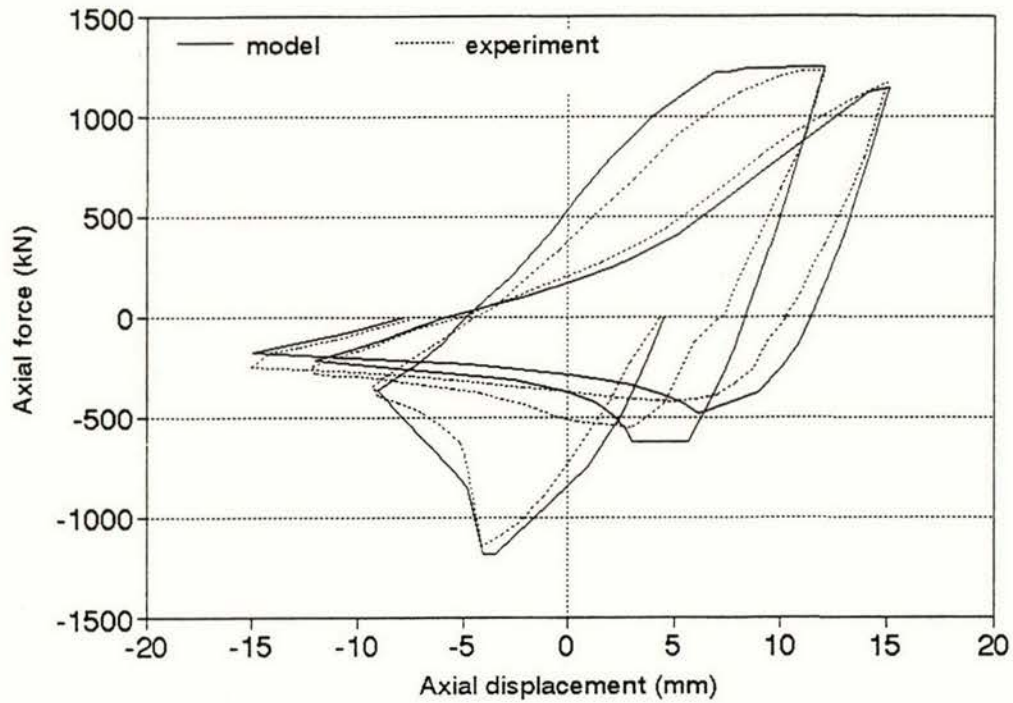
P (kN)	p = P/Py	kappa	e	Et (GPa)	M (kN mm)	ML/EI	coth (kappa/2)	theta (radian)	h1(kappa)	(delta)e (mm)	(delta)g (mm)	(delta)ty (mm)	(delta)p (mm)	(delta)m (mm)	(delta)po (mm)	(delta)mo (mm)	delta (mm)	(delta)t (mm)
-800	-0.64377	2.00299	0.41717	83.434	-13136	-0.043113	NA	0.027550	0.31261	-2.4672	-0.3626	16.2183	0.0000	0.0000	-5.8846	10.2993	17.8032	35.6063
-958	-0.77092	2.49559	0.32181	64.362	-24139	-0.102702	NA	0.027550	0.76998	-3.3000	-0.8930	16.2183	0.0000	0.0000	-5.8846	10.2993	16.4400	32.8799
-958	-0.77092	2.49559	0.32181	64.362	-24094	-0.102510	NA	0.027499	0.76998	-3.3000	-0.8897	16.2183	0.0000	0.0000	-5.8846	10.2993	16.4433	32.8866
-958	-0.77092	1.33104	1.13128	226.255	-24094	-0.029161	NA	0.055819	0.17473	-1.8347	-0.8319			-1.4653				
-958	-0.77092	2.49559	0.32181	64.362	-24094	-0.102510	NA	0.027499	0.76998		-0.8897							
-958	-0.77092	1.33104	1.13128	226.255	-24094	-0.029161	NA	0.055819	0.17473		-0.8319							
-925	-0.74436	1.31254	1.12331	224.662	-26335	-0.032099	NA	0.063509	0.17292	-1.7780	-1.0657	16.2183	-0.5221	0.0000	-5.8846	8.7762	15.7441	31.4882
-870	-0.70010	1.28051	1.11003	222.006	-29814	-0.036774	NA	0.077103	0.16990	-1.6826	-1.5433	16.2183	-1.3816	0.0000	-5.8846	8.7762	14.5023	29.0046
-635	-0.51099	1.12306	1.05330	210.660	-35376	-0.045985	NA	0.130177	0.15725	-1.2618	-4.0718	16.2183	-2.9222	0.0000	-5.8846	8.7762	10.8540	21.7080
-498	-0.40075	1.01055	1.02022	204.045	-35376	-0.047475	NA	0.169856	0.15005	-1.0058	-6.6149	16.2183	-2.9222	0.0000	-5.8846	8.7762	8.5669	17.1338
-256	-0.20601	0.74622	0.96180	192.360	-35376	-0.050359	NA	0.344801	0.13765	-0.5328	-25.0052	16.2183	-2.9222	0.0000	-5.8846	8.7762	-9.3504	-18.7008
-206	-0.16577	0.67363	0.94973	189.946	-35376	-0.050999	NA	0.432418	0.13514	-0.4315	-38.6110	16.2183	-2.9222	0.0000	-5.8846	8.7762	-22.8549	-45.7097
-206																		
-103	-0.08289	0.48269	0.92487	184.973	-17352	-0.025688		0.432418	0.13003	-0.2186	-37.1510	16.2183	0.0000	0.0000	-8.8068	8.7762	-21.1820	-42.3641
0	0.00000	0.00000	0.90000	180.000	0	0.000000		0.432418	0.12500	0.0000	-35.7141	16.2183	0.0000	0.0000	-8.8068	8.7762	-19.5265	-39.0531
100	0.08047	0.49916	0.83965	167.929	14067	0.022939	4.089552	0.403420	0.12000	0.2227	-29.8406	16.2183	0.0000	0.0000	-8.8068	8.7762	-13.4302	-26.8605
150	0.12071	0.62264	0.80947	161.894	20063	0.033935	3.315241	0.388921	0.11737	0.3402	-27.1270	16.2183	0.0000	0.0000	-8.8068	8.7762	-10.5992	-21.1984
200	0.16094	0.73275	0.77929	155.859	25376	0.044584	2.850489	0.374422	0.11465	0.4621	-24.5604	16.2183	0.0000	0.0000	-8.8068	8.7762	-7.9107	-15.8214
250	0.20118	0.83558	0.74912	149.823	30015	0.054860	2.531223	0.359923	0.11185	0.5888	-22.1393	16.2183	0.0000	0.0000	-8.8068	8.7762	-5.3628	-10.7257
275	0.22130	0.88532	0.73403	146.805	32085	0.059849	2.404725	0.352674	0.11041	0.6541	-20.9828	16.2183	0.0000	0.0000	-8.8068	8.7762	-4.1410	-8.2821
319.4	0.25703	0.97203	0.70723	141.446	35357	0.068450	2.217066	0.339799	0.10779	0.7734	-19.0168	16.2183	0.0000	0.0000	-8.8068	8.7762	-2.0558	-4.1116
319.4	0.25703	0.97203	0.70723	141.446	35376	0.068486	2.217066	0.339967	0.10779	0.7734	-19.0357	16.2183	0.0040	0.0000	-8.8068	8.7762	-2.0706	-4.1413
870	0.70010	2.20333	0.37492	74.985	29814	0.108878	1.248289	0.150918	0.06784	2.8099	-2.3609	16.2183	1.7585	0.0000	-8.8068	8.7762	18.3951	36.7901
970	0.78057	2.53991	0.31457	62.914	23251	0.101200	1.171254	0.120884	0.05896	3.3731	-1.3165	16.2183	3.7292	0.0000	-8.8068	8.7762	21.9734	43.9467
1070	0.86105	2.96744	0.25422	50.843	15634	0.084201	1.108448	0.090454	0.04963	4.0566	-0.6205	16.2183	6.0484	0.0000	-8.8068	8.7762	25.6721	51.3442
1175	0.94554	3.58898	0.19084	38.169	6502	0.046644	1.056823	0.055020	0.03950	4.9766	-0.1827	16.2183	9.1355	0.0000	-8.8068	8.7762	30.1171	60.2342
1175										4.9766	-0.1827	16.2183	9.1355	0.0000	-8.8068	8.7762	30.1171	60.2342
1175	0.94554	3.58898	0.19084	38.169	6502	0.046644	1.056823	0.055020	0.03950		-0.1827							
1175	0.94554	1.44111	1.18366	236.732	10562	0.012218	1.620084	0.055020	0.09223		-0.4266							
1176																		
1175	0.94554	1.44111	1.18366	236.732	10562	0.012218	1.620084	0.055020	0.09223	2.1978	-0.4266	16.2183	9.1355	3.0227	-8.8068	8.7762	30.1171	60.2342
1000	0.80472	1.35385	1.14141	228.283	9139	0.010962	1.696308	0.055020	0.09521	1.9063	-0.4404	16.2183	0.0000	0.0000	0.3287	11.7989	29.8117	59.6235
800	0.64377	1.23737	1.09313	218.626	7466	0.009351	1.817481	0.055020	0.09916	1.5595	-0.4587	16.2183	0.0000	0.0000	0.3287	11.7989	29.4467	58.8935
600	0.48283	1.09607	1.04485	208.970	5733	0.007513	2.003816	0.055020	0.10385	1.1971	-0.4804	16.2183	0.0000	0.0000	0.3287	11.7989	29.0627	58.1253
400	0.32189	0.91636	0.99657	199.313	3926	0.005394	2.333169	0.055020	0.10948	0.8176	-0.5064	16.2183	0.0000	0.0000	0.3287	11.7989	28.6571	57.3141
200	0.16094	0.66426	0.94828	189.657	2025	0.002924	3.120779	0.055020	0.11638	0.4192	-0.5383	16.2183	0.0000	0.0000	0.3287	11.7989	28.2268	56.4535

P (kN)	p = P/Py	kappa	e	Et (GPa)	M (kN mm)	ML/EI	coth (kappa/2)	theta (radian)	h1(kappa)	(delta)e (mm)	(delta)g (mm)	(delta)ty (mm)	(delta)p (mm)	(delta)m (mm)	(delta)po (mm)	(delta)mo (mm)	delta (mm)	(delta)t (mm)
0	0.00000	0.00000	0.90000	180.000	0	0.000000	NA	0.055020	0.12500	0.0000	-0.5782	16.2183	0.0000	0.0000	0.3287	11.7989	27.7677	55.5354
-200	-0.16094	0.73275	0.77929	155.859	-4402	-0.007735	NA	0.055020	0.13716	-0.4621	-0.6344	16.2183	0.0000	0.0000	0.3287	11.7989	27.2494	54.4987
-500	-0.40236	1.32234	0.59823	119.646	-12365	-0.028301	NA	0.055020	0.17387	-1.3105	-0.8042	16.2183	0.0000	0.0000	0.3287	11.7989	26.2311	52.4622
-800	-0.64377	2.00299	0.41717	83.434	-26234	-0.086100	NA	0.055020	0.31261	-2.4672	-1.4460	16.2183	0.0000	0.0000	0.3287	11.7989	24.4326	48.8653
-853	-0.68642	2.15245	0.38518	77.037	-30890	-0.109802	NA	0.055020	0.38510	-2.7232	-1.7813	16.2183	0.0000	0.0000	0.3287	11.7989	23.8414	47.6827
-853	-0.68642	2.15245	0.38518	77.037	-30825	-0.109571	NA	0.054904	0.38510	-2.7232	-1.7738	16.2183	0.0000	0.0000	0.3287	11.7989	23.8488	47.6977
-853	-0.68642	1.27029	1.10593	221.185	-30825	-0.038162	NA	0.081523	0.16898	-1.6529	-1.7160			-1.0703				
-853	-0.68642	2.15245	0.38518	77.037	-30825	-0.109571	NA	0.054904	0.38510		-1.7738							
-853	-0.68642	1.27029	1.10593	221.185	-30825	-0.038162	NA	0.081523	0.16898		-1.7160							
-760	-0.61158	1.21140	1.08348	216.695	-35376	-0.044704	NA	0.106572	0.16394	-1.4884	-2.8450	16.2183	-1.2778	0.0000	0.3287	10.6707	21.6065	43.2131
-640	-0.51502	1.12683	1.05451	210.901	-35376	-0.045932	NA	0.129053	0.15752	-1.2709	-4.0086	16.2183	-1.2778	0.0000	0.3287	10.6707	20.6604	41.3208
-527	-0.42409	1.03601	1.02723	205.445	-35376	-0.047152	NA	0.159719	0.15156	-1.0607	-5.9078	16.2183	-1.2778	0.0000	0.3287	10.6707	18.9714	37.9428
-410	-0.32993	0.92663	0.99898	199.796	-35376	-0.048485	NA	0.209472	0.14549	-0.8370	-9.7547	16.2183	-1.2778	0.0000	0.3287	10.6707	15.3482	30.6964
-290	-0.23337	0.79086	0.97001	194.002	-35376	-0.049933	NA	0.302513	0.13937	-0.6009	-19.4879	16.2183	-1.2778	0.0000	0.3287	10.6707	5.8510	11.7021
-171	-0.13761	0.61649	0.94128	188.256	-35376	-0.051457	NA	0.524298	0.13339	-0.3598	-56.0293	16.2183	-1.2778	0.0000	0.3287	10.6707	-30.4491	-60.8983
-171																		
-85	-0.06840	0.43953	0.92052	184.104	-17303	-0.025737		0.524298	0.12914	-0.1808	-54.2444	16.2183	0.0000	0.0000	-0.9491	10.6707	-28.4854	-56.9707
0	0.00000	0.00000	0.90000	180.000	0	0.000000		0.524298	0.12500	0.0000	-52.5037	16.2183	0.0000	0.0000	-0.9491	10.6707	-26.5638	-53.1275
																	-26.5638	-53.1275
236.1	0.18999	0.80751	0.75750	151.501	35411	0.064005	2.609902	0.441287	0.11264	0.5531	-33.5153	16.2183	0.0000	0.0000	-0.9491	10.6707	-7.0223	-14.0446
236.1	0.18999	0.80751	0.75750	151.501	35376	0.063941	2.609902	0.440871	0.11264	0.5531	-33.4521	16.2183	0.0000	0.0000	-0.9491	10.6707	-6.9591	-13.9182
460	0.37017	1.24350	0.62237	124.475	35376	0.077824	1.810465	0.254166	0.09896	1.1836	-9.7678	16.2183	0.0000	0.0000	-0.9491	10.6707	17.3557	34.7114
680	0.54721	1.70462	0.48960	97.919	35376	0.098930	1.444515	0.195219	0.08331	1.9536	-4.8515	16.2183	0.0000	0.0000	-0.9491	10.6707	23.0420	46.0840
910	0.73229	2.32967	0.35078	70.156	27315	0.106617	1.215645	0.138818	0.06434	3.0234	-1.8946	16.2183	2.5144	0.0000	-0.9491	10.6707	29.5831	59.1662
1130	0.90933	3.29305	0.21800	43.601	10558	0.066307	1.077146	0.070928	0.04387	4.5497	-0.3372	16.2183	7.7012	0.0000	-0.9491	10.6707	37.8536	75.7071
																	75.7071	
1130										4.5497	-0.3372	16.2183	7.7012	0.0000	-0.9491	10.6707	37.8536	75.7071
1130	0.90933	3.29305	0.21800	43.601	10558	0.066307	1.077146	0.070928	0.04387		-0.3372							
1130	0.90933	1.41977	1.17280	234.560	16106	0.018802	1.637719	0.070928	0.09296		-0.7146							
1131																		
1130	0.90933	1.41977	1.17280	234.560	16106	0.018802	1.637719	0.070928	0.09296	2.1239	-0.7146	16.2183	7.7012	2.8032	-0.9491	10.6707	37.8536	75.7071
1000	0.80472	1.35385	1.14141	228.283	14431	0.017310	1.696308	0.070928	0.09521	1.9063	-0.7319	16.2183	0.0000	0.0000	6.7521	13.4739	37.6187	75.2373
800	0.64377	1.23737	1.09313	218.626	11789	0.014766	1.817481	0.070928	0.09916	1.5595	-0.7623	16.2183	0.0000	0.0000	6.7521	13.4739	37.2416	74.4831
600	0.48283	1.09607	1.04485	208.970	9053	0.011864	2.003816	0.070928	0.10385	1.1971	-0.7983	16.2183	0.0000	0.0000	6.7521	13.4739	36.8431	73.6863
400	0.32189	0.91636	0.99657	199.313	6200	0.008518	2.333169	0.070928	0.10948	0.8176	-0.8416	16.2183	0.0000	0.0000	6.7521	13.4739	36.4203	72.8406
200	0.16094	0.66426	0.94828	189.657	3197	0.004616	3.120779	0.070928	0.11638	0.4192	-0.8946	16.2183	0.0000	0.0000	6.7521	13.4739	35.9689	71.9377
0	0.00000	0.00000	0.90000	180.000	0	0.000000	NA	0.070928	0.12500	0.0000	-0.9609	16.2183	0.0000	0.0000	6.7521	13.4739	35.4834	70.9668

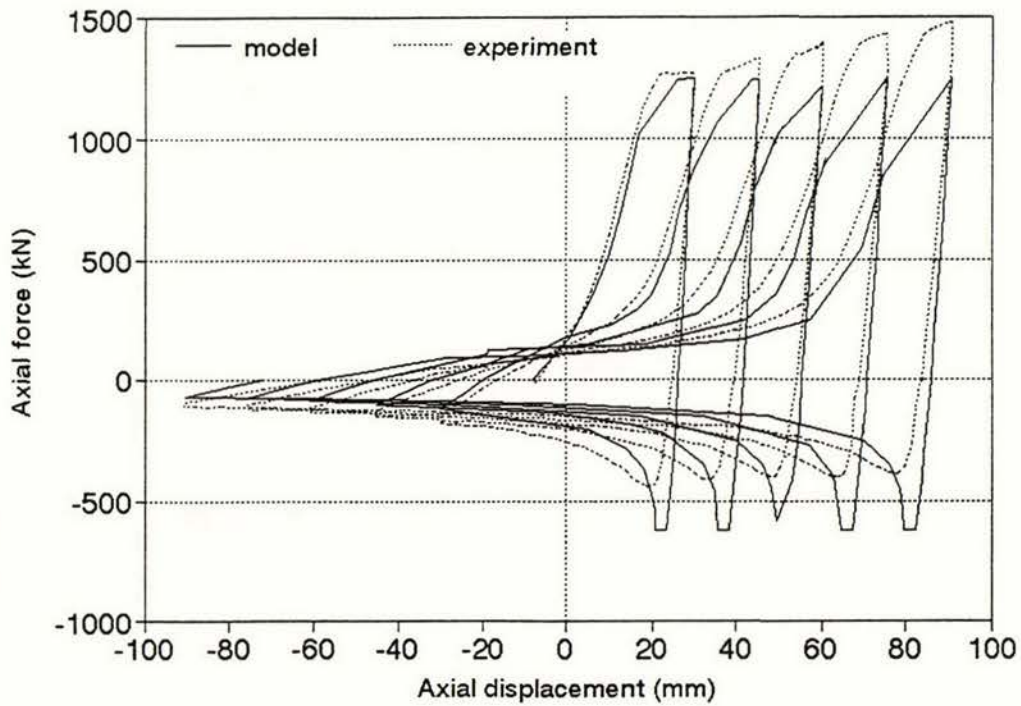
P (kN)	p = P/Py	kappa	e	Et (GPa)	M (kN mm)	ML/EI	coth (kappa/2)	theta (radian)	h1(kappa)	(delta)e (mm)	(delta)g (mm)	(delta)ty (mm)	(delta)p (mm)	(delta)m (mm)	(delta)po (mm)	(delta)mo (mm)	delta (mm)	(delta)t (mm)
-250	-0.20118	0.83558	0.74912	149.823	-7197	-0.013155	NA	0.070928	0.14123	-0.5888	-1.0856	16.2183	0.0000	0.0000	6.7521	13.4739	34.7699	69.5397
-500	-0.40236	1.32234	0.59823	119.646	-15941	-0.036483	NA	0.070928	0.17387	-1.3105	-1.3365	16.2183	0.0000	0.0000	6.7521	13.4739	33.7972	67.5944
-750	-0.60354	1.87283	0.44735	89.469	-29491	-0.090261	NA	0.070928	0.26863	-2.2431	-2.0650	16.2183	0.0000	0.0000	6.7521	13.4739	32.1362	64.2723
-800	-0.64377	2.00299	0.41717	83.434	-33818	-0.110993	NA	0.070928	0.31261	-2.4672	-2.4030	16.2183	0.0000	0.0000	6.7521	13.4739	31.5740	63.1480
-800	-0.64377	2.00299	0.41717	83.434	-33781	-0.110872	NA	0.070850	0.31261	-2.4672	-2.3978	16.2183	0.0000	0.0000	6.7521	13.4739	31.5792	63.1585
-800	-0.64377	1.23737	1.09313	218.626	-33781	-0.042312	NA	0.096064	0.16610	-1.5595	-2.3421			-0.9077				
-800	-0.64377	2.00299	0.41717	83.434	-33781	-0.110872	NA	0.070850	0.31261		-2.3978							
-800	-0.64377	1.23737	1.09313	218.626	-33781	-0.042312	NA	0.096064	0.16610		-2.3421							
-500	-0.40236	1.01234	1.02071	204.141	-35376	-0.047453	NA	0.169119	0.15015	-1.0096	-6.5621	16.2183	-0.4673	0.0000	6.7521	12.5105	27.4418	54.8837
-300	-0.24141	0.80339	0.97242	194.485	-35376	-0.049809	NA	0.291905	0.13987	-0.6209	-18.2111	16.2183	-0.4673	0.0000	6.7521	12.5105	16.1816	32.3633
-200	-0.16094	0.66426	0.94828	189.657	-35376	-0.051077	NA	0.445881	0.13484	-0.4192	-40.9618	16.2183	-0.4673	0.0000	6.7521	12.5105	-6.3674	-12.7348
-150.7	-0.12127	0.58026	0.93638	187.276	-35376	-0.051726	NA	0.597171	0.13239	-0.3179	-72.1376	16.2183	-0.4673	0.0000	6.7521	12.5105	-37.4419	-74.8838
-75	-0.06035	0.42846	0.85473	170.947	-17376	-0.027833		0.597171	0.12893	-0.1656	-70.2559	16.2183	0.0000	0.0000	6.2848	12.5105	-35.4079	-70.8159
0	0.00000	0.00000	0.90000	180.000	0	0.000000		0.597171	0.12500	0.0000	-68.1131	16.2183	0.0000	0.0000	6.2848	12.5105	-33.0995	-66.1991
197	0.15853	0.72639	0.78110	156.221	35387	0.062029	2.873354	0.518280	0.11482	0.4546	-47.1268	16.2183	0.0000	0.0000	6.2848	12.5105	-11.6586	-23.3171
197	0.15853	0.65951	0.94756	189.512	35376	0.051116	3.141685	0.514552	0.11650	0.4131	-47.1297	16.2183	0.0000	0.0000	6.2848	12.5105	-11.7031	-23.4062
400	0.32189	1.12724	0.65859	131.717	35376	0.073545	1.958261	0.283078	0.10283	1.0021	-12.5907	16.2183	0.0000	0.0000	6.2848	12.5105	23.4250	46.8499
600	0.48283	1.52765	0.53788	107.576	35376	0.090050	1.554423	0.210805	0.08927	1.6518	-6.0619	16.2183	0.0000	0.0000	6.2848	12.5105	30.6035	61.2070
800	0.64377	2.00299	0.41717	83.434	33781	0.110872	1.311954	0.172792	0.07376	2.4672	-3.3649	16.2183	0.5195	0.0000	6.2848	12.5105	34.6354	69.2709
850	0.68401	2.14362	0.38699	77.399	31000	0.109678	1.265594	0.157058	0.06955	2.7082	-2.6216	16.2183	1.3944	0.0000	6.2848	12.5105	36.4945	72.9891
970	0.78057	2.53991	0.31457	62.914	23251	0.101200	1.171254	0.120884	0.05896	3.3731	-1.3165	16.2183	3.7292	0.0000	6.2848	12.5105	40.7993	81.5987
970										3.3731	-1.3165	16.2183	3.7292	0.0000	6.2848	12.5105	40.7993	81.5987
970	0.78057	2.53991	0.31457	62.914	23251	0.101200	1.171254	0.120884	0.05896		-1.3165							
970	0.78057	2.53991	0.31457	62.914	23251	0.101200	1.171254	0.120884	0.05896		-1.3165							
970	0.78057	2.53991	0.31457	62.914	23251	0.101200	1.171254	0.120884	0.05896	3.3731	-1.3165	16.2183	3.7292	0.0000	6.2848	12.5105	40.7993	81.5987
900	0.72424	1.29817	1.11727	223.455	28231	0.034596	1.751145	0.120884	0.09710	1.7348	-2.1682	16.2183	0.0000	0.0000	10.0140	12.5105	38.3093	76.6186
800	0.64377	1.23737	1.09313	218.626	25366	0.031772	1.817481	0.120884	0.09916	1.5595	-2.2142	16.2183	0.0000	0.0000	10.0140	12.5105	38.0881	76.1763
600	0.48283	1.09607	1.04485	208.970	19480	0.025527	2.003816	0.120884	0.10385	1.1971	-2.3188	16.2183	0.0000	0.0000	10.0140	12.5105	37.6211	75.2422
400	0.32189	0.91636	0.99657	199.313	13341	0.018329	2.333169	0.120884	0.10948	0.8176	-2.4446	16.2183	0.0000	0.0000	10.0140	12.5105	37.1157	74.2314
200	0.16094	0.66426	0.94828	189.657	6880	0.009933	3.120779	0.120884	0.11638	0.4192	-2.5987	16.2183	0.0000	0.0000	10.0140	12.5105	36.5633	73.1266
0	0.00000	0.00000	0.90000	180.000	0	0.000000	NA	0.120884	0.12500	0.0000	-2.7911	16.2183	0.0000	0.0000	10.0140	12.5105	35.9517	71.9033

Table 5.4 Numerical integration for plastic hinge axial displacement

P* (kN)	p = P*/Py	kappa	e	Et (GPa)	M (kN mm)	g(kappa)	theta	theta dM(P*)/P*	f(P*)	
-1080.2	-0.8693	1.3953	1.1608	232	14797	1.7099	0.02984	-2.4626	-0.003145	-0.003145
-1074.2	-0.8644	1.3923	1.1593	232	15291	1.7189	0.03104	-2.5417	-0.003271	-0.013084
-1068.2	-0.8596	1.3893	1.1579	232	15782	1.7279	0.03225	-2.6199	-0.003398	-0.006796
-1062.2	-0.8547	1.3862	1.1564	231	16268	1.7371	0.03346	-2.6972	-0.003526	-0.014103
-1056.2	-0.8499	1.3832	1.1550	231	16751	1.7464	0.03468	-2.7736	-0.003654	-0.007309
-1050.2	-0.8451	1.3801	1.1535	231	17229	1.7557	0.03591	-2.8491	-0.003784	-0.015135
-1044.1	-0.8402	1.3770	1.1521	230	17704	1.7652	0.03714	-2.9236	-0.003914	-0.007828
-1038.1	-0.8354	1.3739	1.1506	230	18176	1.7748	0.03839	-2.9972	-0.004045	-0.016180
-1032.1	-0.8306	1.3708	1.1492	230	18643	1.7845	0.03964	-3.0699	-0.004177	-0.008354
-1026.1	-0.8257	1.3676	1.1477	230	19107	1.7943	0.04090	-3.1416	-0.004310	-0.017239
-1020.1	-0.8209	1.3645	1.1463	229	19566	1.8043	0.04217	-3.2124	-0.004444	-0.008887
-1014.1	-0.8161	1.3613	1.1448	229	20022	1.8143	0.04345	-3.2823	-0.004578	-0.018313
-1008.1	-0.8112	1.3581	1.1434	229	20474	1.8245	0.04473	-3.3512	-0.004714	-0.009428
-1002.1	-0.8064	1.3550	1.1419	228	20923	1.8348	0.04603	-3.4191	-0.004850	-0.019402
-996.1	-0.8015	1.3517	1.1405	228	21367	1.8452	0.04733	-3.4860	-0.004988	-0.009976
-990.1	-0.7967	1.3485	1.1390	228	21808	1.8557	0.04865	-3.5520	-0.005126	-0.020505
-984.0	-0.7919	1.3453	1.1376	228	22245	1.8664	0.04997	-3.6170	-0.005266	-0.010532
-978.0	-0.7870	1.3420	1.1361	227	22678	1.8772	0.05130	-3.6810	-0.005406	-0.021625
-972.0	-0.7822	1.3387	1.1347	227	23107	1.8881	0.05265	-3.7440	-0.005548	-0.011096
-966.0	-0.7774	1.3354	1.1332	227	23533	1.8992	0.05400	-3.8060	-0.005690	-0.022762
-960.0	-0.7725	1.3321	1.1318	226	23955	1.9104	0.05536	-3.8670	-0.005834	-0.005834
									int f(P*) =	-0.535955
									(delta)p =	-1.940318

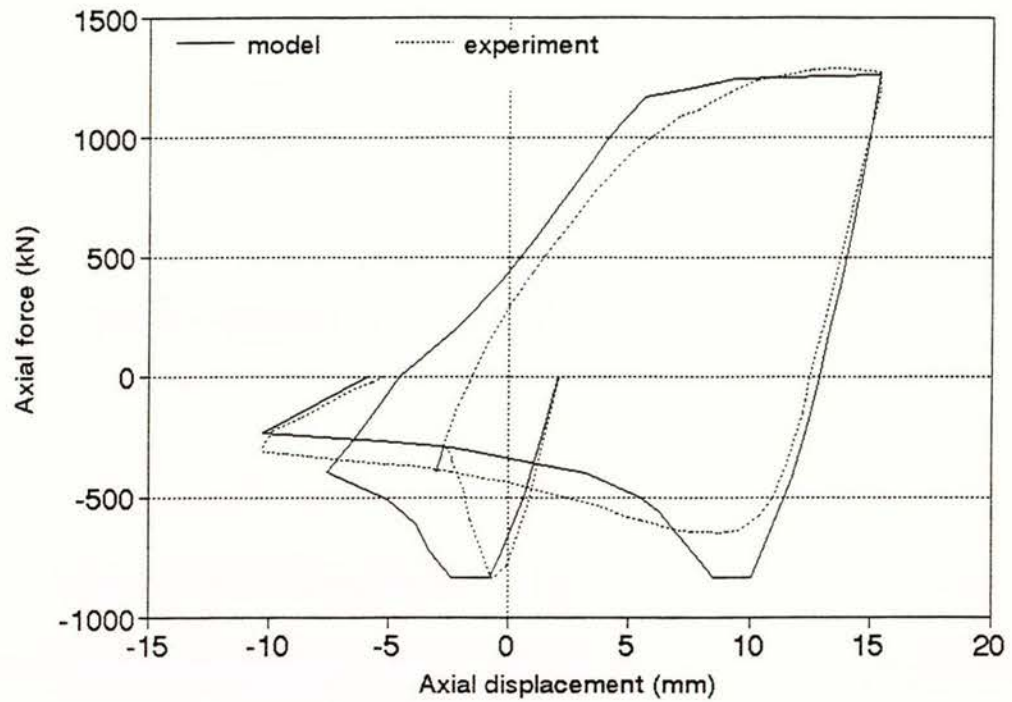


(a) Hysteresis loops for cycle 4 to 6

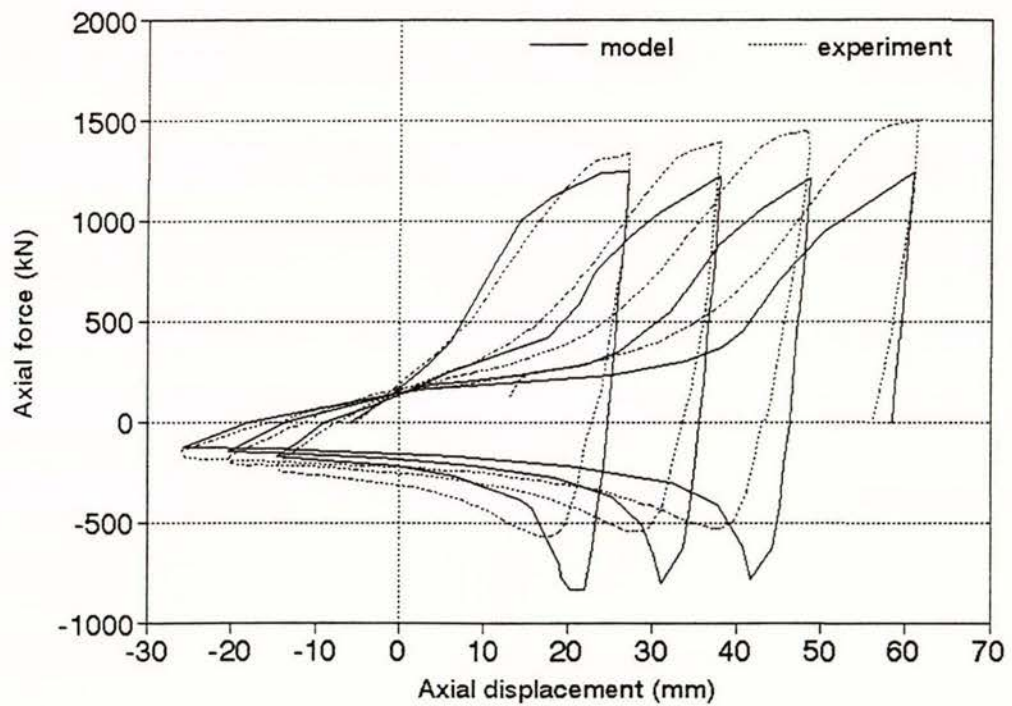


(b) Hysteresis loops for cycle 7 to 11

Figure 5.1 Comparison of analytical and experimental axial force - axial displacement curves for specimen 1

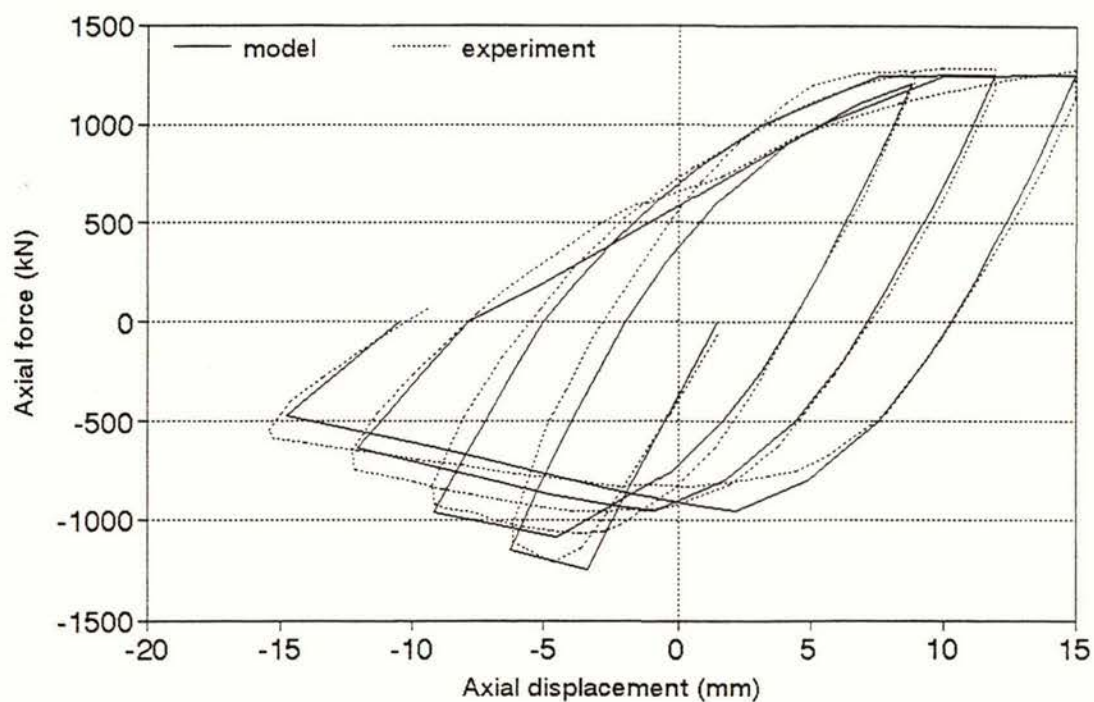


(a) Hysteresis loops for cycle 4 to 5

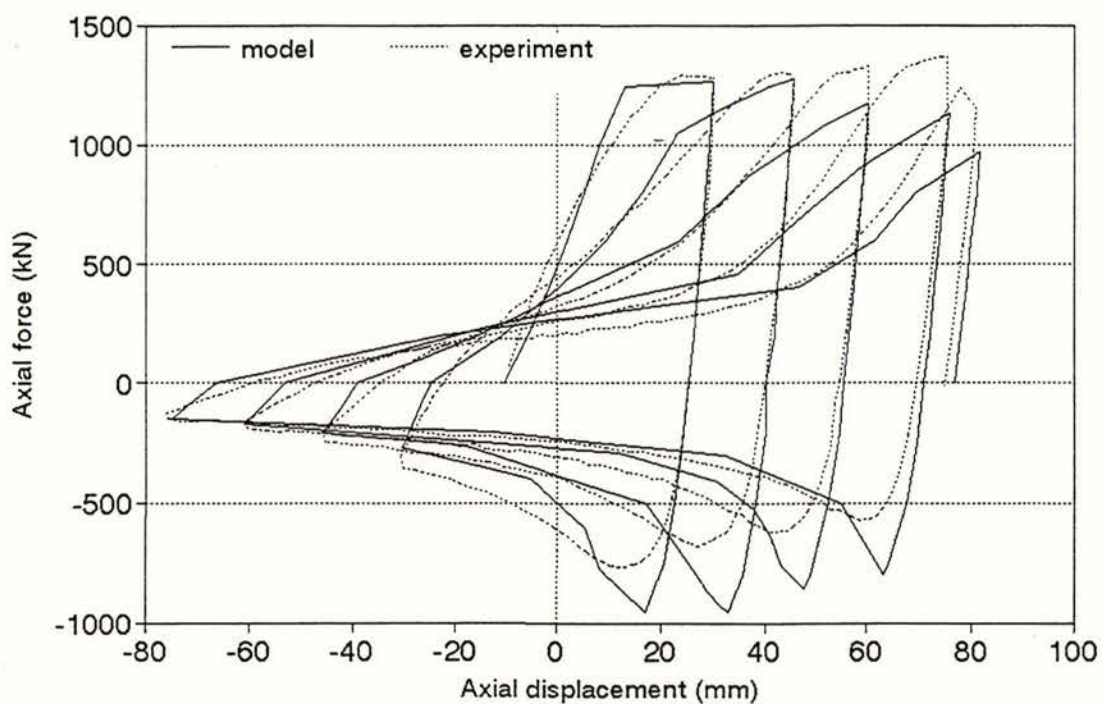


(b) Hysteresis loops for cycle 6 to 9

Figure 5.2 Comparison of analytical and experimental axial force-axial displacement curves for specimen 2

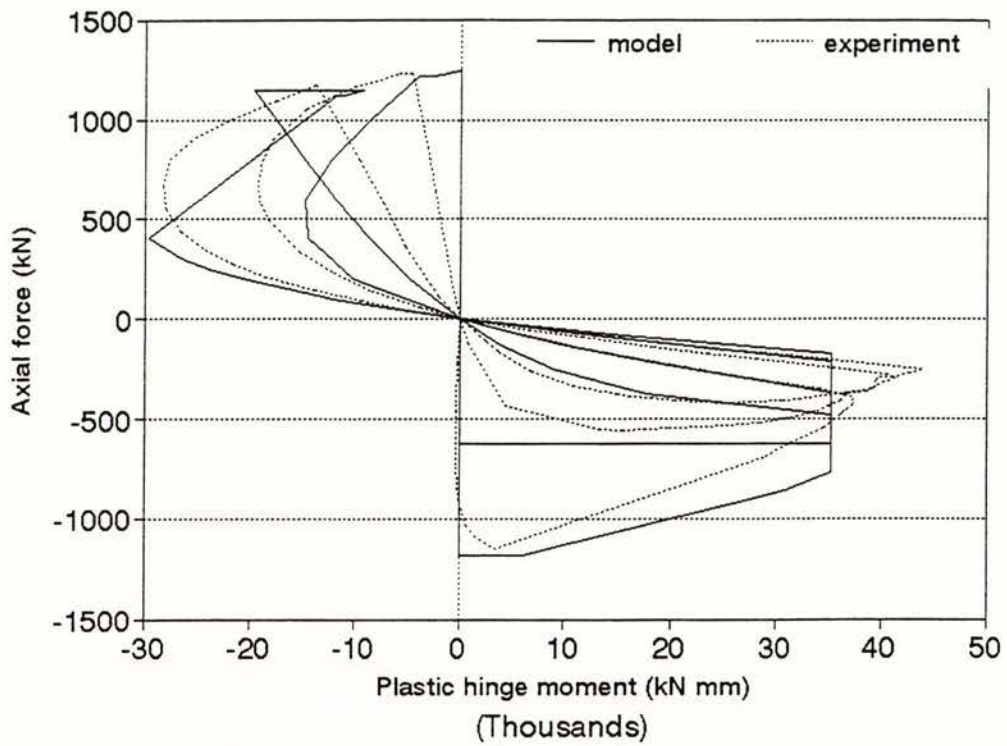


(a) Hysteresis loops for cycle 3 to 6

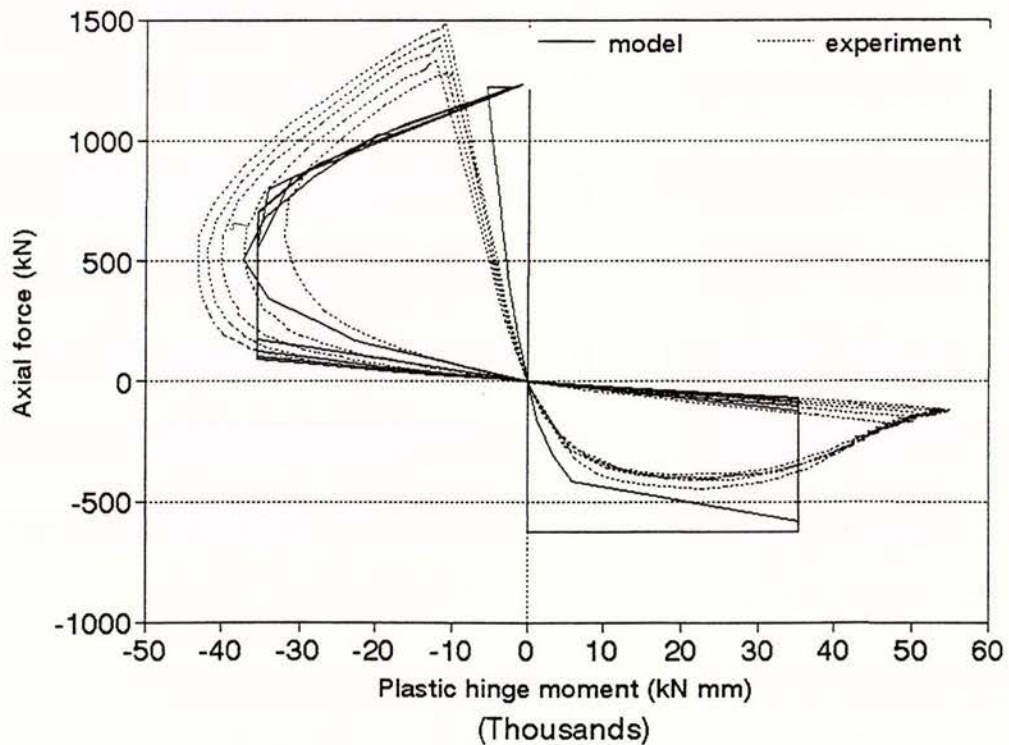


(b) Hysteresis loops for cycle 7 to 11

Figure 5.3 Comparison of analytical and experimental axial force-axial displacement curves for specimen 3

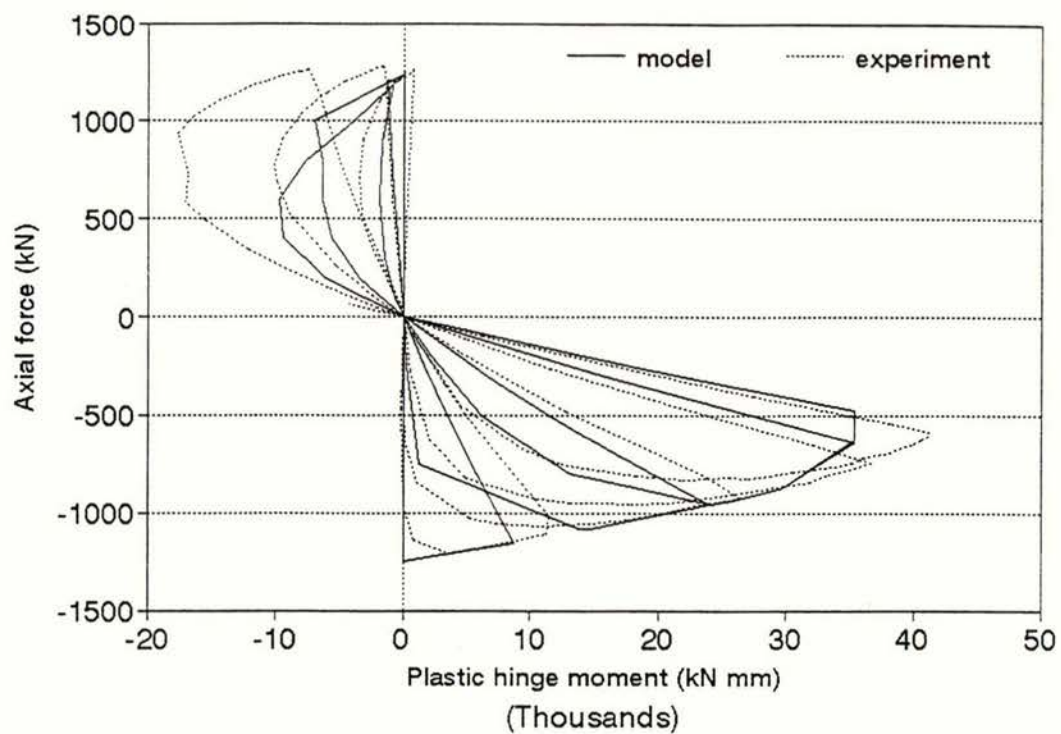


(a) Axial force - plastic hinge moment interaction curves for cycle 4 to 6

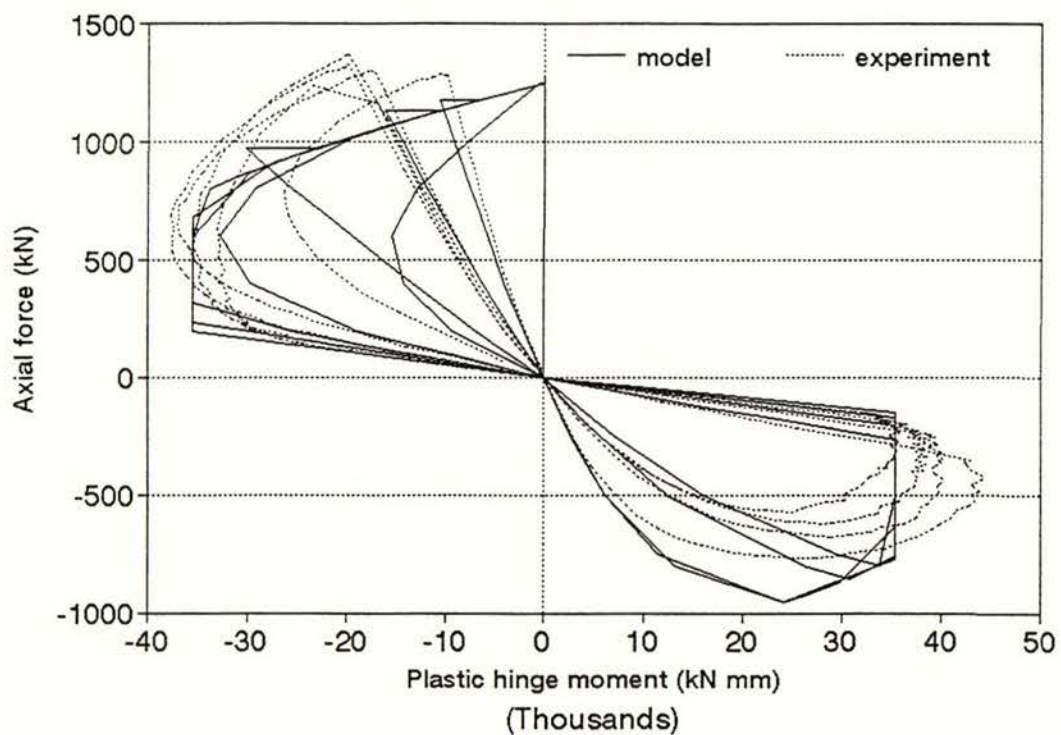


(b) Axial force - plastic hinge moment interaction curves for cycle 7 to 11

Figure 5.4 Comparison of analytical and experimental axial force - plastic hinge moment interaction curves for specimen 1

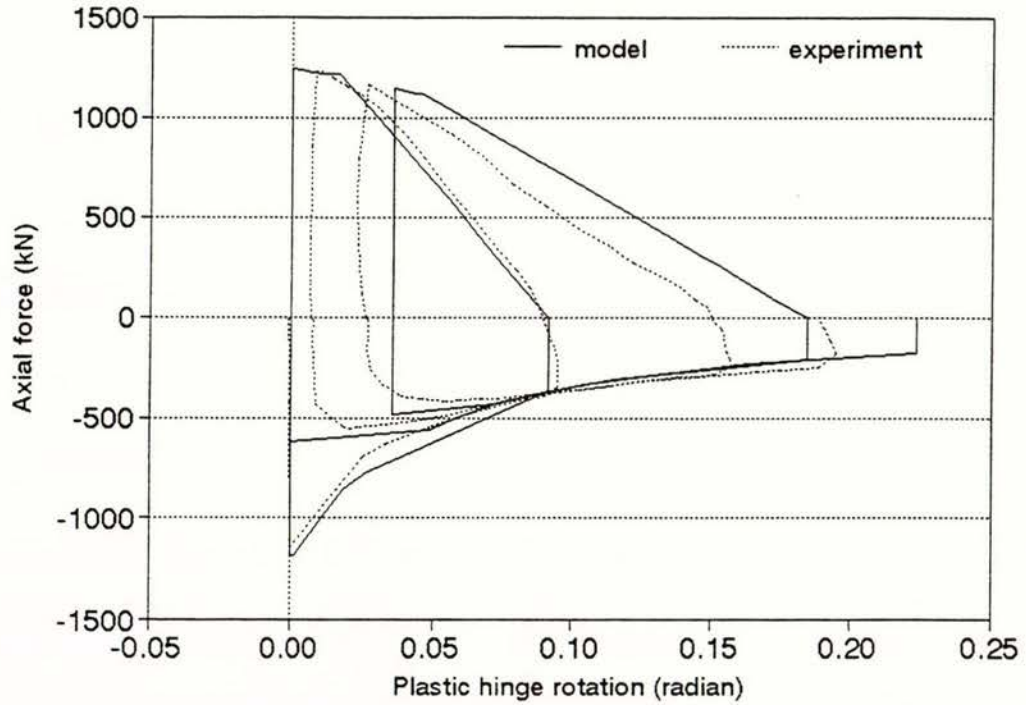


(a) Axial force - plastic hinge moment interaction curves for cycle 3 to 6

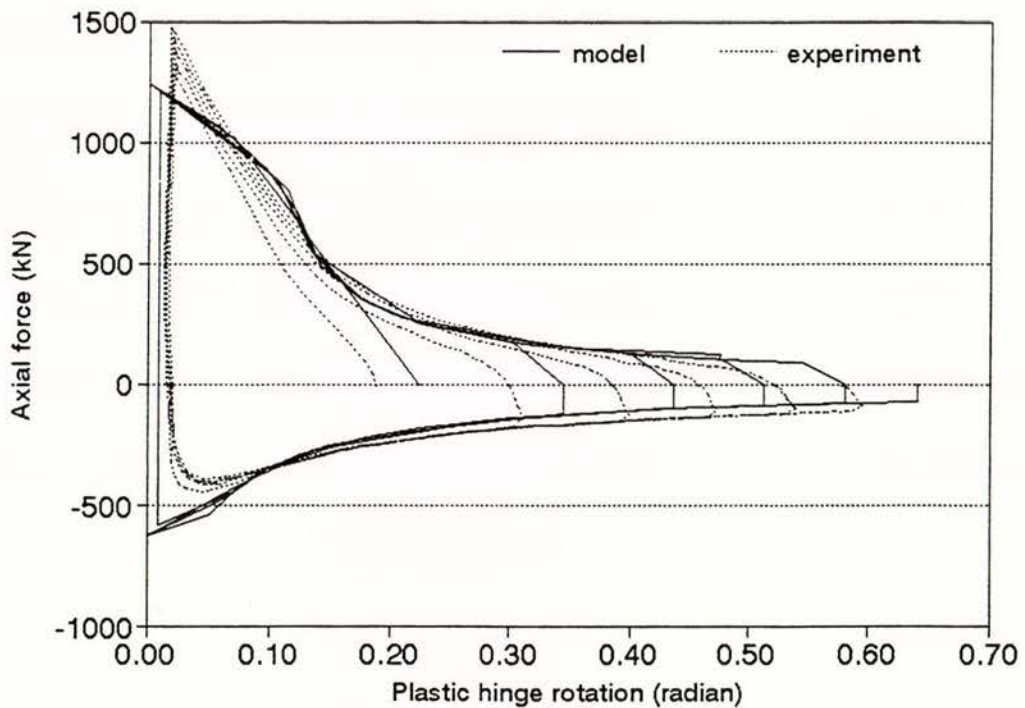


(b) Axial force - plastic hinge moment interaction curves for cycle 7 to 11

Figure 5.5 Comparison of analytical and experimental axial force - plastic hinge moment interaction curves for specimen 3

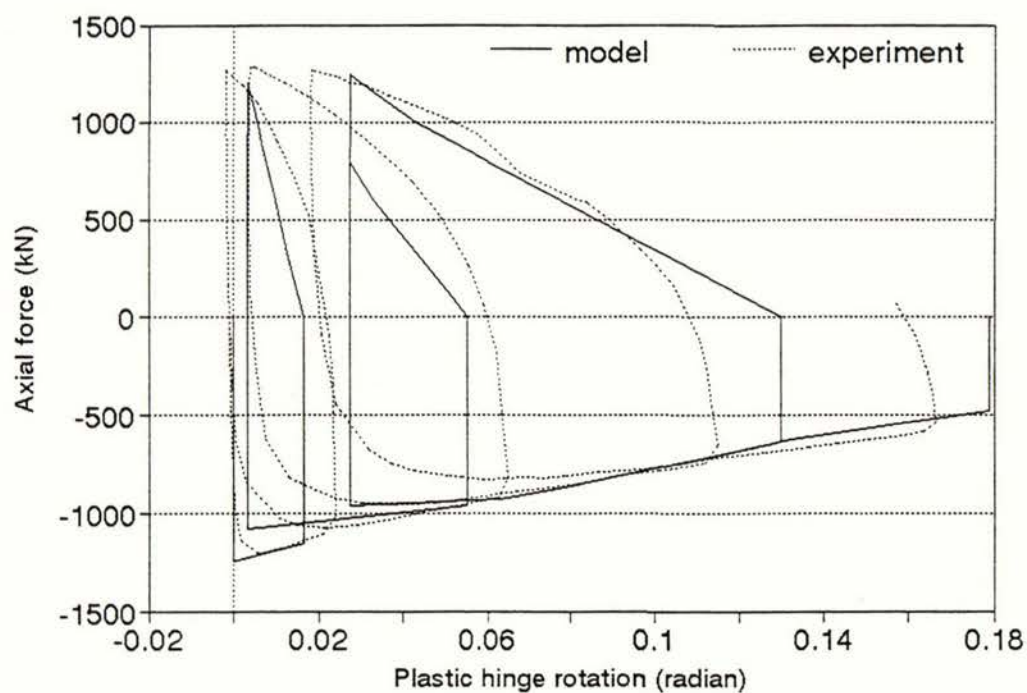


(a) Axial force - plastic hinge rotation curves for cycle 4 to 6

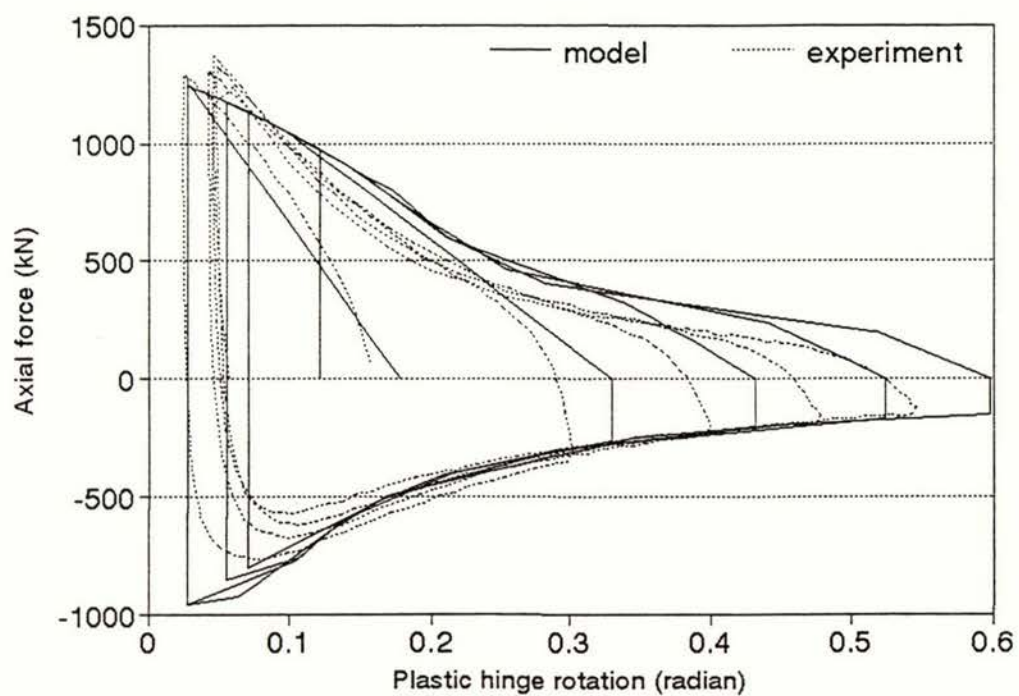


(b) Axial force - plastic hinge rotation curves for cycle 7 to 11

Figure 5.6 Comparison of analytical and experimental axial force - plastic hinge rotation curves for specimen 1



(a) Axial force - plastic hinge rotation curves for cycle 3 to 6



(b) Axial force - plastic hinge rotation curves for cycle 7 to 11

Figure 5.7 Comparison of analytical and experimental axial force - plastic hinge rotation curves for specimen 3

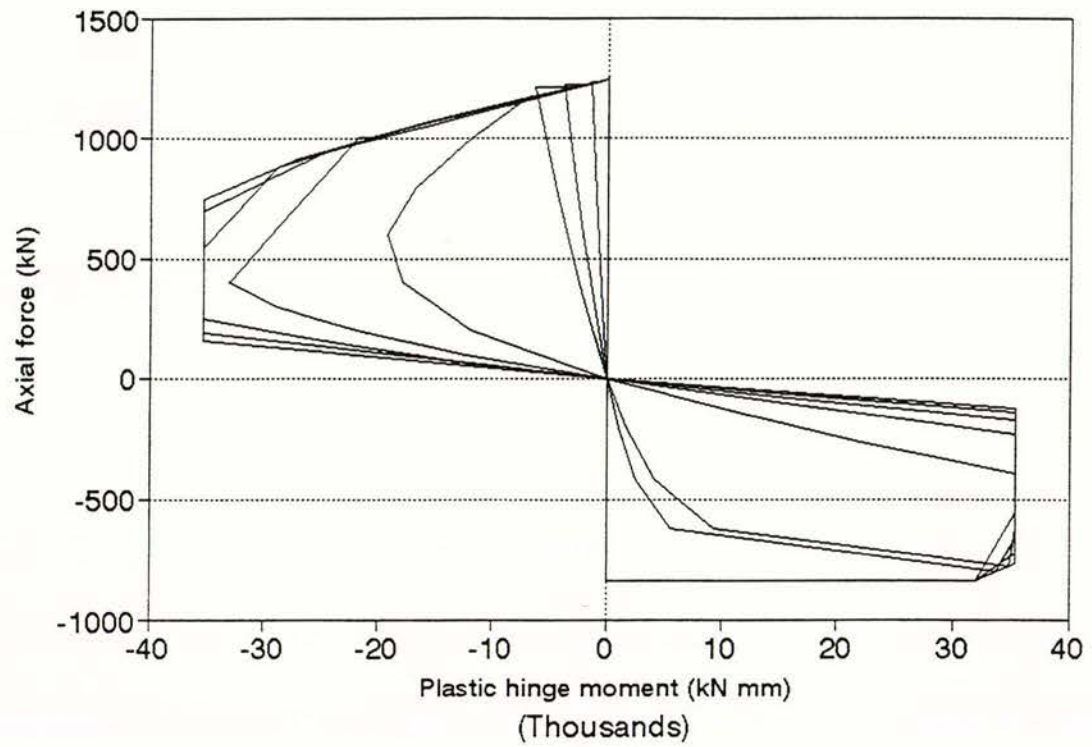


Figure 5.8 Analytical axial force - plastic hinge moment curves for specimen 2

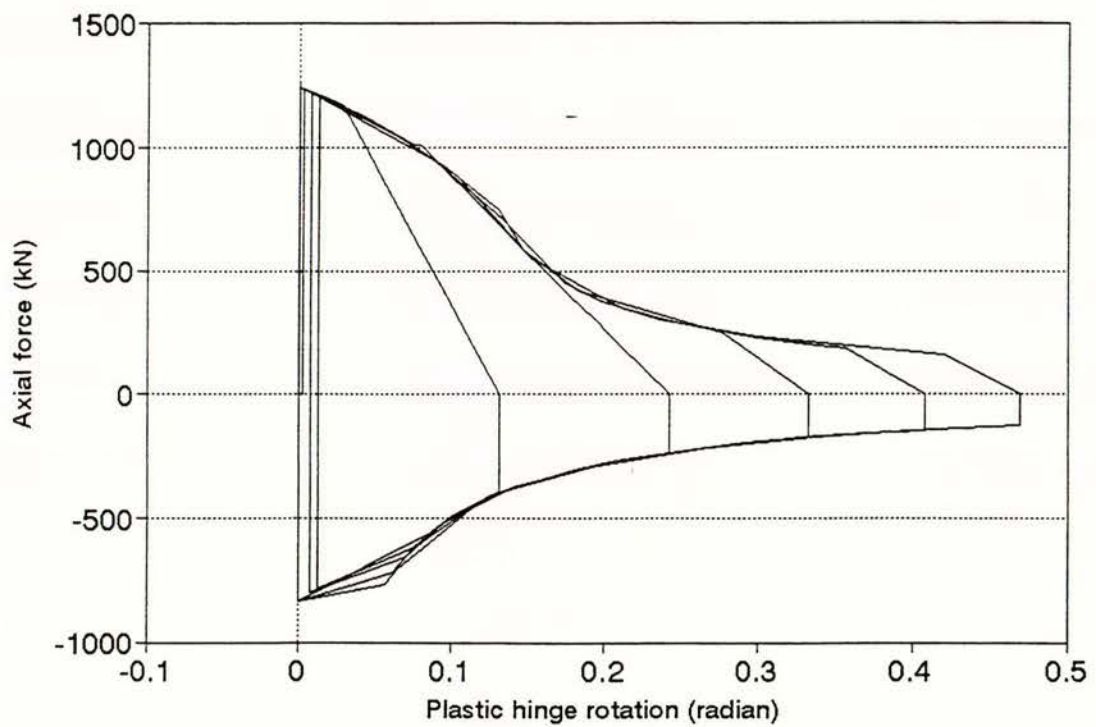


Figure 5.9 Analytical axial force - plastic hinge rotation curves for specimen 2

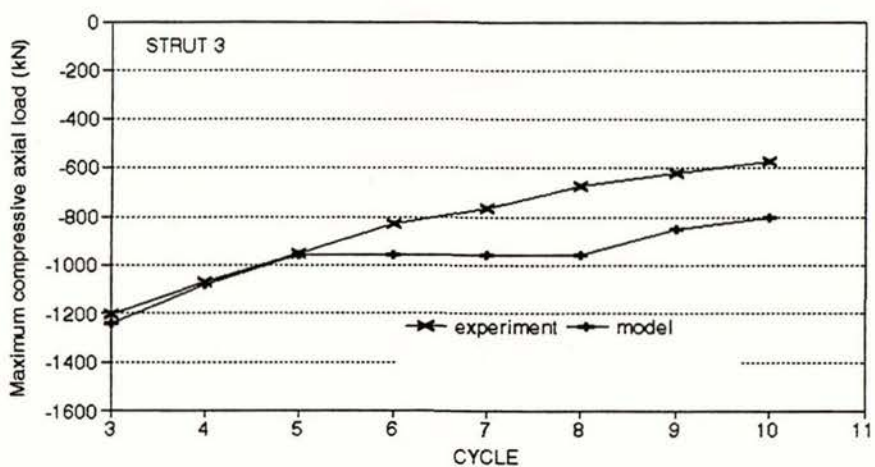
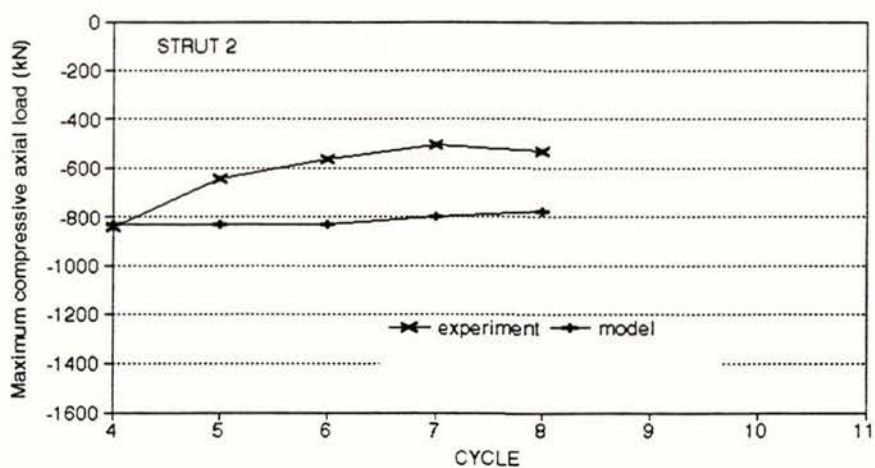
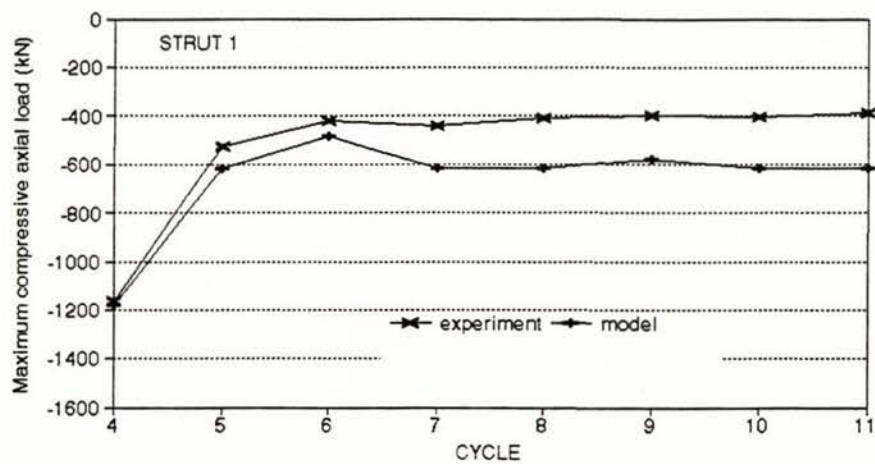


Figure 5.10 Comparisons of analytical and experimental buckling loads

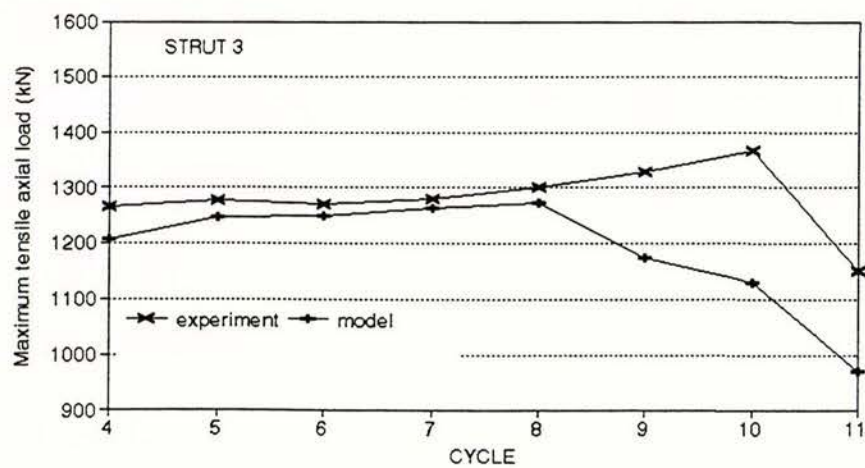
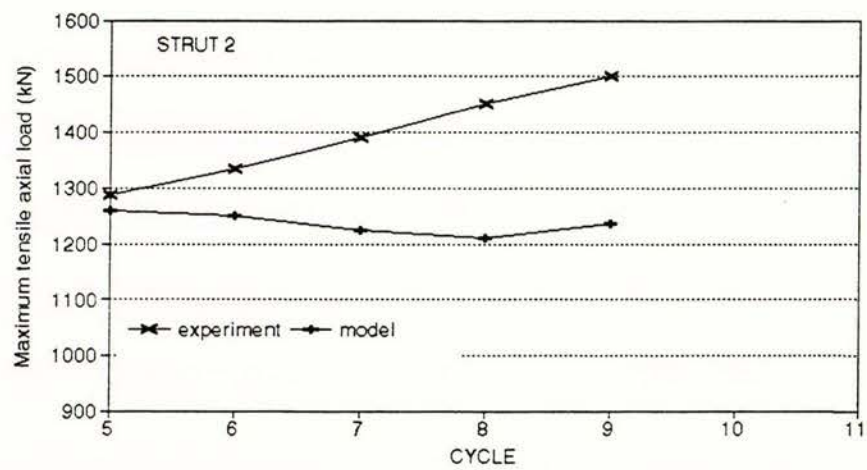
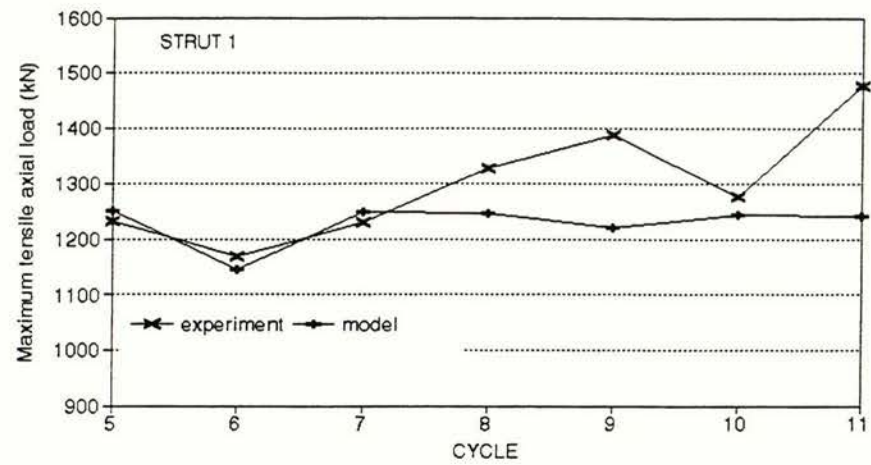


Figure 5.11 Comparison of analytical and experimental maximum tensile loads

CHAPTER 6

SUMMARY, CONCLUSIONS, AND RECOMMENDATIONS

6.1 SUMMARY

Chapter 1 reviews previous researches that are grouped into experimental and analytical studies. From the experimental study, the general characteristics of the hysteretic responses of tube and angle specimen were identified, and also general parameters of the hysteretic responses of wide-flange, built-up, circular tube and square tube specimens. The development of the analytical study through the stages of the purely theoretical model, the phenomenological model, and the refined physical theory brace model was also reviewed.

The features and procedures of the phenomenological model and the refined physical theory brace model were reviewed in Chapter 2. For the refined physical theory brace model (the Ikeda model), the basic equations and empirical formulas used were described. In addition, the method of calculation from zone to zone was introduced.

Chapter 3 describes the experimental programme including the test set-up, instrumentation, loading history and specimen selection. For specimen selection a statistical study based on geometric parameters of the specimen cross section was used.

Chapter 4 discusses the test results for material properties, overall behaviour of the UC specimen and the inelastic behaviour under cyclic loading.

Chapter 5 describes the data preparation for the Ikeda model and compares the analytical results with the experimental results. An additional parameter, i.e. the minimum plastic hinge rotation, was introduced for specimen 3 to better represent the decrease of buckling load even after yielding

6.2 CONCLUSIONS

The conclusions from this study were drawn from the observed and measured test results and the comparison of analytical with experimental results.

The main conclusions from the test results are as follows:

1. The conclusion from previous tests that stockier members generate fuller loops than the more slender ones is confirmed.

2. In slender members the occurrence of local buckling was delayed compared to the stockier ones.
3. The effect of fixed - fixed end conditions can be taken into account by the effective member length and effective lateral displacement that are half the actual values.
4. The residual plastic hinge rotation and the residual lateral displacement did not disappear even after applying the yield load in tension.

The following conclusions were drawn from the comparison of analytical with experimental results:

1. The refined physical theory brace model from Ikeda can best represent hysteresis loops of brace member for several reasons. It includes the effect of tangent modulus variation with load and load reversal, and the degradation of plastic hinge rotations in Zone EL2 but the model does not allow for the degradation of tangent modulus over a number of inelastic cycles.
2. The model simulates the hysteresis loops of braces better in range of small axial displacements but when the axial displacement was increased to cause substantial plastic elongation in tension and compression, the model was unable to include the effects of strain hardening and local buckling.

6.3 RECOMMENDATION FOR FUTURE RESEARCH

To improve the available analytical model, it is necessary to have a model of cyclic stress - strain relationship which is simple enough to be differentiated to give the tangent modulus value.

It is also necessary to identify the parameters for local buckling and fracture of brace member and to model these phenomena for the analytical model.

The analytical model could be improved by allowing for strain hardening or strain softening. This model needs to be included in a dynamic inelastic frame analysis program.

Accurate cyclic stress-strain relationships giving the tangent modulus variation with stress are required for the variety of steel sections currently in use.

REFERENCES

- 1 Black, R.G., Wenger, W.A.B. and Popov, E.P., "Inelastic Buckling of Steel Strut under Cyclic Load Reversals", Report No. UCB/EERC-80/40, Earthquake Engineering Research Centre, University of California, Berkeley, CA., October 1980.
- 2 Jain, A.K., Goel, S.C., Hanson, R.D., "Hysteretic Cycles of Axially Loaded Members", Journal of Structural Division, Proceeding of ASCE, Vol.106, No. ST8, August 1980.
- 3 Nilforoushan, R., "Seismic Behaviour of Multi-Story K-Braced Frame Structures", University of Michigan Research Report UMEE 73R9, Ann Arbor, November 1973.
- 4 Nonaka, T., "An Elastic-Plastic Analysis of a Bar under Repeated Axial Loading", Int. J. Solids Structures, 1973, Vol.9, pp 569-580, Pergamon Press. Printed in Great Britain.
- 5 Nonaka, T., "Approximation of Yield Condition for the Hysteresis Behaviour of a Bar Under Repeated Axial Loading", Int. J. Solids Structures, 1977, Vol. 13, pp 637-643, Pergamon Press. Printed in Great Britain.
- 6 Ikeda, K., and Mahin, S.A., and Dermitzakis, S.N., "Phenomenological Modelling of Steel Braces under Cyclic Loading", Report No. UCB/EERC-84/09, Earthquake Engineering Research Centre, University of California, Berkeley, CA., May 1984.
- 7 Ikeda, K., and Mahin, S.A., "A Refined Physical Theory Model for Predicting the Seismic Behaviour of Braced Steel Frames", Report No. UCB/EERC-84/12, Earthquake Engineering Research Centre, University of California, Berkeley, CA., July 1984.
- 8 Timoshenko, S.P. and Gere, J.M., "Theory of Elastic Stability", Second Edition, McGraw-Hill Book Co., New York, N.Y., 1961.
- 9 "Test Methods for Compression Members", ASTM Special Technical Publication No. 419, American Society for Testing and Materials, 1967.

- 10 Galambos, T.V., "Guide to Stability Design Criteria for Metal Structures", Fourth Edition, Wiley, 1988, Appendix B.
- 11 Gugerli, H. and Goel, S.C., "Inelastic Cyclic Behaviour of Steel Bracing Member", Report No. UMEE 82R1, Department of Civil Engineering, The University of Michigan, Ann Arbor, Michigan, January 1982.
- 12 Zayas, V.A., Popov, E.P., and Mahin, S.A., "Cyclic Inelastic Buckling of Tubular Steel Braces", EERC report No. 80-16, Earthquake Engineering Research Centre, University of California, Berkeley, June 1980.
- 13 Chen, W.F., and Han, D.J., "Plasticity for Structural Engineers", Springer-Verlag, New York, 1988.
- 14 Chen, W.F., and Atsuta, T., "Theory of Beam-Columns Volume 1: In-Plane Behavior and Design", Mc Graw-Hill, 1976.

APPENDIX A

POINT HINGE MODEL

The refined physical theory brace model⁽⁷⁾ was based on point hinge model^(4,5,11) of the brace member as shown in Figure A1. In the point hinge model plastic deformation is assumed to be concentrated in the plastic hinge whereas outside the plastic hinge the member is always elastic (with the exception at tensile yield condition).

The refined physical theory model combines this basic model with adjusted theoretical relationships for material properties and member geometries to better represent the experimental data.

The differential equation for the lateral deflection $\bar{\Delta}$ of an elastic beam-column segment without lateral load is given by

$$\bar{\Delta}^{iv}(x) - \frac{P}{EI} \bar{\Delta}'' = 0 \quad (\text{A1})$$

The general solution of this fourth order differential equation is

$$\bar{\Delta}(x) = q_1 \sinh(Kx) + q_2 \cosh(Kx) \quad (\text{A2})$$

where q_1 and q_2 are constants and

$$K^2 = P/EI \quad (\text{A3})$$

The boundary conditions are

$$\bar{\Delta}(0) = 0 \quad \text{or} \quad \bar{\Delta}(L) = 0; \quad (\text{A4a,b})$$

$$\bar{\Delta}(L/2) = \Delta \quad \text{or} \quad \bar{\Delta}'(L/2 - 0) = \theta/2 \quad (\text{A5a,b})$$

After imposing the boundary conditions (A4a) and (A5b), the expression for the deflected shape of the left brace segment becomes

$$\bar{\Delta}(x) = \frac{\theta}{2} \frac{\sinh(Kx)}{K \cosh(\frac{KL}{2})} \quad (\text{A6})$$

The relationship between the plastic hinge moment and the plastic hinge rotation can be derived from the equilibrium of the half bar.

$$\begin{aligned}
 M &= -P \bar{\Delta}(L/2) = -P \frac{\sinh(KL/2)}{K \cosh(KL/2)} \frac{\theta}{2} \\
 &= -\frac{EI}{L^2} (KL)^2 \frac{\tanh(KL/2)}{K} \frac{\theta}{2} \\
 &= -\frac{\kappa}{2} \tanh(\kappa/2) \frac{EI}{L} \theta
 \end{aligned} \tag{A7}$$

$$\text{where } \kappa^2 = \frac{|P|L^2}{EI} \tag{A8}$$

Deflection $\bar{\Delta}$ in the transverse direction reduces the relative displacement δ by the amount

$$\begin{aligned}
 \delta_g &= - \int_0^{L/2} \{ \bar{\Delta}^i(x) \}^2 dx \\
 &= - \int_0^{L/2} \left\{ \frac{\theta}{2} \frac{\cosh(Kx)}{\cosh(KL/2)} \right\}^2 dx \\
 &= - \frac{\frac{\sinh \kappa}{\kappa} + 1}{16 \cosh^2(\kappa/2)} \theta^2 L
 \end{aligned} \tag{A9}$$

The plastic hinge moment from equation (A7) is substituted for the rotation angle in (A9) to avoid numerical difficulty at $P = P_{cr}$ ($\kappa = \pi$). This substitution gives an alternate expression for geometric shortening,

$$\delta_g = - \frac{\frac{\sinh \kappa}{\kappa} + 1}{4 \kappa^2 \sinh^2(\kappa/2)} \left(\frac{ML}{EI} \right)^2 L \tag{A10}$$

When the axial force is compressive, P is negative, and the above hyperbolic functions have to be replaced by its corresponding trigonometric functions.

Due to the presence of axial force, plastic deformation occurs in axial direction as well as in bending in the plastic hinge. Their relationship is provided by the flow rule associated with the yield condition. In geometric terms, the flow rule states that when the state of stress is represented by a point on the yield surface, the plastic flow vector is in the direction of the outward normal to the yield surface at the corresponding stress point. This is shown in Figure A2. It follows that

$$\frac{d\delta_p}{d\theta} = -\frac{dM}{dP} \quad (\text{A11})$$

$$\int d\delta_p = -\int \frac{dM}{dP} d\theta \quad (\text{A12})$$

$$\delta_p = -\int \frac{dM}{dP} \frac{d\theta}{dP} dP \quad (\text{A13})$$

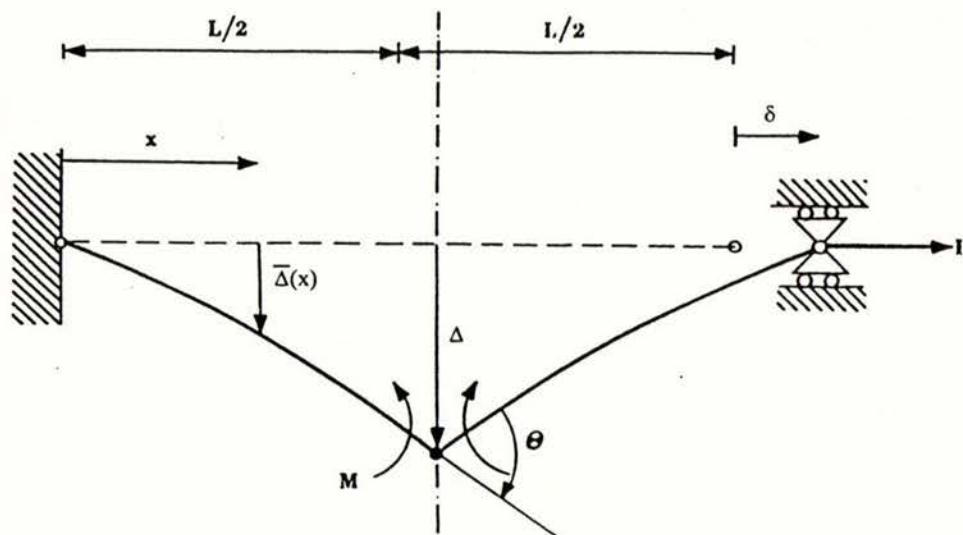


Figure A1 Point hinge model⁽¹¹⁾

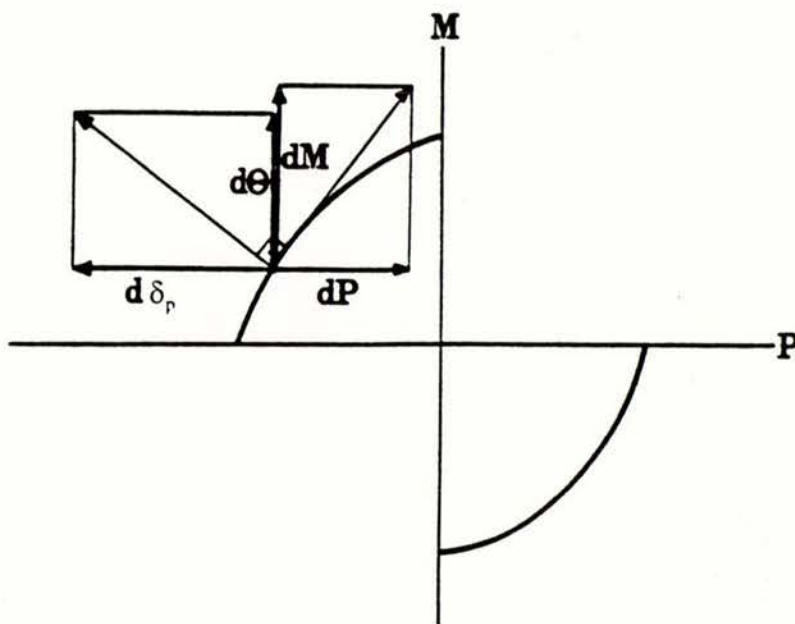


Figure A2 Flow rule associated with yield surface